Electropolishing of Niobium in Sulfuric Acid-Methanol Electrolytes: Development of Hydrofluoric Acid-Free Electrolytes

By

Xin Zhao

Dissertation submitted to the Faculty of the Virginia Polytechnic Institute and State University in partial fulfillment of the requirements for the degree of

Doctor of Philosophy

In

Materials Science and Engineering

Sean G. Corcoran, Chair

Michael J. Kelley, Co-Chair

William T. Reynolds Jr.

Alex O. Aning

Marc A. Edwards

July 16, 2009

Blacksburg, Virginia

Keywords: niobium, electropolishing, sulfuric acid-methanol, hydrofluoric acid-free

Electropolishing of Niobium in Sulfuric Acid-Methanol Electrolytes: Development of Hydrofluoric Acid-Free Electrolytes

Xin Zhao

Abstract

Niobium (Nb) has the highest superconducting transition temperature (9.2 K) of the pure metals, which makes it the most used material for the construction of superconducting radio frequency (SRF) accelerators. The performance of the accelerator is critically dependent upon the quality of Nb surface. Electropolishing (EP) in hydrofluoric acid (HF)-containing electrolytes is the currently accepted treatment process. The presence of HF is necessary for the removal of the passive oxide surface film formed in aqueous electrolytes. But HF is hazardous and must be contained without human exposure and eliminated in an environmentally appropriate manner.

In the present dissertation project, HF-Free EP of Nb was performed in sulfuric acid-methanol electrolytes. Sulfuric concentrations of 0.1 M, 0.5 M, 1 M, 2 M, and 3 M were used. Cyclic voltammetry and potential hold experiments were performed in cells of both two-electrode and three-electrode setups to evaluate the electrochemical process. The influence of electrolyte concentration, temperature, and EP duration was investigated. At room temperature, both the corrosion rate and the surface quality obtained were

comparable to those currently obtained with HF-based processing. With decreasing temperature, the mean current level decreased and the surface quality improved substantially. For a desired average material removal of 100 μm, nanometer scale surface roughness was obtained under multiple conditions.

Mechanism of EP was also investigated by electrochemical impedance spectroscopy (EIS). The EIS diagram indicates the presence of a compact film during EP at mass transport controlled limiting current and a film-free surface during EP at ohmic controlled current. Transfer from a film-free surface to an anodic film precipitation with decreasing temperature was also observed. Microsmoothing is only achieved under mass transport control. Nb^{5+} ions are determined to be the mass transport limiting species.

To my wife;

Yan Yang

Acknowledgement

I would like to express my sincere appreciation to my advisor Prof. Sean Corcoran for teaching me how to approach and solve problems encountered during my PhD program. My appreciation also goes to my co-advisor, Prof. Michael Kelley in William & Mary College, for his guidance and support on experiments.

I would like to thank my committee members, Prof. Bill Reynolds, Prof. Alex Aning, and Prof. Marc Edwards, for many valuable discussions and suggestions. I would also like to thank my lab-mate Mr. Davis Eichelberger for sharing many practical experience in an electrochemical laboratory, and the Materials Science and Engineering family at Virginia Tech for making everyday a good day.

Thank Dr. Charlie Reece, Dr. Hui Tian, Dr. Gigi Ciovati, and Dr. Xin Zhao in Thomas Jefferson National Accelerator Facility for providing me niobium samples and sharing data of niobium electropolishing. I am grateful to Steve McCartney, Jerry Hunter, and John McIntosh for their kind help on the niobium characterization.

Thanks to Department of Energy (DOE) for the support of this project.

I would like to thank all my friends here in Blacksburg for making my life colorful.

A heart felt acknowledgement to my parents, Guoquan Zhao and Shumin Zheng, for their love and support throughout my life and education.

The deepest appreciation goes to my dear wife, Yan Yang, for her love, company, and support. Also to my lovely daughter, Kate, who gives me the most happiness and the biggest power. The life with them is a gift.

Index

Figure List

Table List

Chapter 1

Introduction

1.1 Application of niobium surface finish

1.1.1 Niobium superconducting radio frequency accelerator cavity

Nb is a famous superconductor that has been used as the superconducting radio frequency (SRF) accelerator cavity material for many years. There are many attractive features of Nb such as having the highest transition temperature (T_c = 9.2 K) of all elemental metals, sufficiently high critical magnetic field (H_c > 2 K Oe) to maintain SRF accelerator in superconducting phase, and good metallurgical properties for fabrications and service loads [1,2]. Compared to copper cavities, Nb SRF cavities—for example, those installed on the Continues Electron Beam Accelerators Facility (CEBAF) at Thomas Jefferson National Laboratory (Jefferson Lab)—consume about five orders of magnitude less energy and also obtain five times higher efficiency in converting AC power into beam power [3]. The lower power requirement enables Nb cavities to be operated at a higher acceleration gradient. Another important advantage of the Nb SRF cavity is the suppression on disruptive effect. Because of their capability to provide higher energy and

lower wall loss, Nb SRF cavities are affordable for a design of shorter and larger hole and, therefore, impose less disruption [4, 5].

SRF technology was first employed at Stanford University in 1974 [6]. Today, SRF technology is widely used. The SRF machines in the United States include the CEBAF at the Jefferson Lab, the Cornell Electron Positron Storage Ring (CESR) at Cornell University, the Tevatron in the Fermi National Accelerator Laboratory, and the Spallation Neutron Source (SNS) at Oak Ridge National Laboratory (ORNL). World-famous SRF machines include TRISTAN at the High Energy Accelerator Research Organization (KEK) in Japan, Hadron-Elektron-Ringanlage (HERA) in the Deutsches Electronen-Synchrotron Laboratory (DESY), and the Large Electron Positron Collider (LEP) in Counseil Eutopéene pour la Rechérche Nucleaire (CERN) in Switzerland. The largest and most important project ever undertaken is the International Linear Collider (ILC), which is planned to stretch approximately 35 km in length and consume 20,000 nine-cell Nb SRF cavities and 2,500 cryomodules.

1.1.2 Impaction of surface quality on performance of SRF cavity

Nb metal superconductivity is a nanometer-scale and near-surface phenomenon because of the shallow RF penetration (e.g., 36 nm at 1.5 GHz) [5]. The performance of niobium SRF cavities is characterized by the quality factor Q_0 defined as [7]:

$$Q_0 = \omega \times \frac{EnergyStored}{PowerDissipated} \tag{1.1}$$

where ω is the frequency of the RF field. The interior surface chemistry and topography of the cavity strongly impact the performance of the SRF cavity [8, 9]. The surface limitations that may reduce the Q_0 value (Q-drop) include residual surface resistance, thermo breakdown (quench), high field emission, and electron multipacting [7, 10].

Residual surface resistance is temperature-independent resistance and limits the superconductivity of SRF cavity. Thermo breakdown—"quench"—occurs when the temperature of the good superconductor outside the "defects" (submillimeter sized regions with high RF loss) exceeds the transition temperature. The quench area expands and larger region becomes a normal conductor. Filed emission is also common for the Q-drop. In a high electric field, electrons from local spots are drawn out of the surface and accelerated in RF fields. The electrons gain energy to produce heat and bremsstrahlung when impacting on the opposing surface, resulting in an exponential decrease of Q value with increasing field. These three limitations are caused by surface defects and imperfection including sharp edges, metal scratches, and surface contaminations. Multipacting is mainly caused by cavity geometries and is no longer an issue due to the successful shape modification [7, 10].

1.1.3 Techniques of Nb surface finish

The preparation of an Nb SRF cavity requires the removal of surface damages and contaminations mentioned above. Due to the pillbox-like shape of the cavity, chemical or electrochemical etching is the most efficient technique for Nb surface finish. Etching to a depth of 100 to 200 μm is believed to be enough to remove the mechanically damaged

layer [7]. Two widely practiced etching techniques are buffered chemical polishing (BCP) and electropolishing (EP) [9]. A BCP process is usually performed in a typical solution of 1:1:1 or 1:1:2 (volume ratio) HNO_3 (69%), HF (49%), and H_3PO_4 (85%). In the practical fabrication—in Jefferson Lab, for example—the BCP solution flows end-to-end through the cavity at approximate 10^oC. The process is performed for a time sufficient to remove the layer containing mechanical damage and contaminations. BCP commonly results in Nb dissolution at a rate of 10 μm/min and a final surface roughness of 2 to 5 micron [1, 11].

The final surface finish is EP [11-14]. Cavity fabrication by EP is also known as "Siemens method" because it was Siemens Company that firstly employed EP to treat SRF cavity surface in the 1970s [14]. Researchers in KEK further developed this technique and claimed that the improved SRF cavity performance—such as the higher acceleration gradient—would be achieved by EP over BCP [15]. This discovery has been confirmed by other laboratories that were also investigating this process [16]. The currently accepted EP process for Nb surface treatment is performed in a solution of HF (49%) and sulfuric acid electrolyte (98%) at volume ratio of 1:8 to 1:10. During the EP, the Nb cavity is polarized anodically in an electrolytic cell at temperature of 30^oC to 40^oC. The cathode is an aluminum rod with high purity. The area ratio of anode and cathode is 10:1.The applied voltage is usually from 12 to 25 V and causes a current density of 30 to 100 mA/cm^2 [15]. EP results in a corrosion rate—around 0.5 μm/min—that is lower than BCP but with a much better surface finish, especially at a microscopic scale [2, 10, 11]. It has been accepted widely that the best EP condition occurs under the voltage within the

range of limiting current plateau and that parameters such as electrolyte concentration, electrolyte temperature, and viscosity strongly impact the surface finish [2, 11, 17, 18].

1.2 Motivation of this dissertation

1.2.1 hydrofluoric acid-based system

Nb performs a large negative free energy and is highly reactive toward oxygen [19-21]. In an aqueous electrolyte, it is easy for Nb to react with water molecules to form non-soluble niobium pentoxide (Nb_2O_5) by the reaction [11, 19]:

$$2Nb + 5H_2O \rightarrow Nb_2O_5 + 10H^+ + 10e^- . \quad (1.2)$$

The thickness of oxide layer with Nb_2O_5 is about 2 to 6 nm [1, 10, 22-25]. Suboxides such as NbO_2, NbO, and Nb_2O are observed to form between the Nb_2O_5 outer layer and the underlying Nb surface [21, 24-30]. In additional to its negligible solubility in water, Nb_2O_5 is difficult to dissolve in majority of acids as well. The oxides form a stable protective film on metal surface, thus prevent further polishing of the metal surface during EP in aqueous electrolytes [30-34].

Hydrofluoric acid (HF) has good ability to destabilize Nb_2O_5 with the following reactions to form soluble niobium fluorides and niobium oxifluorides [10]:

$$Nb_2O_5 + 14HF \rightarrow 2H_6NbO_2F_7 + H_2O \quad (1.3)$$

$$Nb_2O_5 + 12HF \rightarrow 2HNbF_6 + 5H_2O \quad (1.4)$$

$$Nb_2O_5 + 10HF \rightarrow 2NbF_5 + 5H_2O \quad (1.5)$$

$$Nb_2O_5 + 10HF \rightarrow 2H_6NbOF_5 + 3H_2O \quad (1.6)$$

$$HNbF_6 + HF \rightarrow H_2NbF_7 . \quad (1.7)$$

The presence of HF is necessary in practical electrolytes for EP processes of Nb. However, finish of a one single-cell cavity (e.g., the 1.5GHz single-cell cavity in Jefferson Lab) needs a minimum 1 liter of HF that must be contained without human exposure and must be eliminated in an environmentally appropriate manner. At present, about 300 five- to nine-cell cavities are processed per year in Jefferson Lab. This is a manageable concern. However, ILC will require the operations capable of processing over 20,000 nine-cell cavities per year. The tremendous cost of managing large amounts of HF demands the development of HF-free electrolytes.

1.2.2 Sulfuric acid-methanol electrolytes

As far as present author is aware, no results for HF-free EP processes of Nb have been reported in the literature. Methanol is sometimes used as a solvent instead of water [35-41]. Piotrowski et al report the successful EP of tantalum (Ta) and Titanium (Ti) by sulfuric acid-methanol electrolytes [42-44]. The nature of sulfuric acid-methanol electrolytes is still under investigation. Table 1.1 shows some detail of the sulfuric acid-methanol system. The kinetic viscosity of solutions increases with increasing sulfuric acid concentration [44]. They studied the EP processes by using steady state measurement and impedance spectroscopy. The best surface finish was obtained under mass transport limiting current. The value of limiting current decreased as the concentration increased and the temperature decreased [42, 44]. The observed current decrease with increasing concentration is suggested to be due to the corresponding

decrease in solubility of metal ions [44]. Compact film was characterized to explain the mass transport mechanism [42, 44]. One of the advantages of methanol-based electrolyte is the much-decreased water content; therefore, the formation of Nb_2O_5 is expected to be avoided. Piowtroski observed the current decrease by adding water into the methanol-based electrolyte—when the water content in a 3 M sulfuric acid-methanol electrolyte increased from 0.02wt% to 5wt%, the current during Ti EP decreased approximately 75 percent (about 0.8 A/cm^2 to 0.2 A/cm^2). When the water content reached 10wt%, the Ti anode became passive [44]. It is important to use sulfuric acid with a weight ratio as high as possible and prevent it from water condensing from air. On the other hand, Nb has a very close chemical property to Ta, so it is promising to electropolish Nb in the methanol-based electrolyte.

Table 1.1: Parameters of 3 M sulfuric acid-methanol electrolyte at 25^{o}C [42, 44].

Concentration	**Kinetic viscosity**	**Conductivity**	**Saturation concentration**	
3 M	0.029 cm^2s^{-1}	0.049 $\Omega^{-1}cm^{-1}$	Ta^{5+}: 3.8 mol l^{-1}	Ti^{4+}: 2.9 mol l^{-1}

The primary motivation for this dissertation project is to develop a methanol-based electrolyte as a replacement of HF-based system for Nb surface finish. EP parameters—such as electrolyte concentration, flow rate, and temperature—strongly influence the surface finish [2, 11, 42-45]. Very recently, Tian et al. electropolished Nb in a solution of 1:9 HF/ H_2SO_4 (volume ratio) and claim dependence of anodic current on electrolyte concentration and temperature [2, 11]. However, the exact function of each individual

factor is still unknown. Furthermore, evaluation of electropolished Nb surface at both macroscopic and microscopic scales—especially of the grain boundary elimination—is also seldom mentioned in the literature. In this dissertation project, surface finish by methanol-based EP is characterized at both microscopic and macroscopic scale. The influence of EP parameters is discussed. Mass transport mechanism during EP at limiting current is also investigated.

1.3 Organization of this dissertation

Following this introduction, there are five chapters entitled:

Chapater 2. Methods and experimental procedures.

Chapater 3. Electropolishing of niobium: Two-electrode setup.

Chapater 4. Electropolishing of niobium: Three-electrode setup.

Chapater 5. Electrochemical impedance spectroscopy: Toward an understanding of electropolishing mechanism in sulfuric acid-methanol electrolyte.

Chapater 6. Conclusions and suggestions for future work.

In chapter 2, the fundamental of EP is introduced and the experimental apparatus is then described. Because cyclic voltammetry, potential hold, scanning electron microscopy (SEM), and optical stylus profilometry are the experimental methods employed in both chapter 3 and chapter 4, they are briefly demonstrated in this chapter. Finally, the mathematical method for advanced surface characterization is explained.

In chapter 3, two-electrode setup electropolishing of Nb in the 0.1 M sulfuric acid-methanol electrolytes is introduced. Also presented are potential hold experiments at low temperature (-30^{o}C) in the 1 M and 2 M sulfuric acid-methanol electrolytes. Surface finish is shown to depend upon concentration, EP duration, and temperature. Electrochemical results are correlated with surface characterization. To describe the microscopic profile suppression, the relationship between root mean square of roughness and length scale is calculated.

In chapter 4, EP process in three-electrode electrochemical cell is first presented. Two-electrode cell and three-electrode cell are compared by monitoring the surface potential to a reference. The same electrochemical experiments and surface characterization as those performed in chapter 3 are repeated for comparison of two-electrode and three-electrode setups. Experimental conditions are optimized to obtain a better surface finish.

In chapter 5, the mechanism of mass transport during the EP at limiting current is investigated by electrochemical impedance spectroscopy (EIS). The influences of electrolyte concentration and temperature on mass transport mechanism are discussed. Also discussed is the mass transport limiting specie.

Conclusions about the methanol-based EP of Nb and suggestions for future work are given in chapter 6.

References

1. H. Tian, C. Reece, M. Kelley, S. Wang, L. Plucinski, and K. Smith, Appl. Surf. Sci. **253**, 1236 (2006).
2. H. Tian, M. Kelley, C. Reece, and S. Corcoran, J. Electrochem. Soc. **V155**, D563 (2008).
3. J. R. Delayen, and K. W. Shepard, Appl. Phys. Lett. **57**, 51 (1990).
4. http://www.Ins.cornell.edu/public/CESR/SRF/BasicSRF/SRFBas.html
5. C. Reece, Proceeding of the 3rd workshop of RF superconductivity, Argonne, IL, p545 (1987).
6. H. Padamsee, J. Knobloch, and T. Hays, RF superconductivity for accelerators, Wiley, New York, (1998).
7. H. Padamsee, Supercond. Sci. Technol. **14**, R28 (2001).
8. P. Kneisel, Proceeding of the 9th workshop of RF superconductivity, Sante Fe, NM, p328 (1999).
9. R. Ballantimi, R. Parodi, Proceeding of the 9th workshop of RF superconductivity, Sante Fe, NM, p211 (1999).
10. P. Kneisel, IEEE Trans. on Appl. Supercond. **9**, 1023 (1999).
11. H. Tian, Surface study of niobium for superconducting radio frequency (SRF) accelerators, PhD thesis, College of William and Mary (2008).
12. International linear collider (ILC) reference design report (2007), http://www.inearcollider.org.
13. H. Tian, G. Ribeil, M. Kelley, and C. Reece, Proceeding of 13th international workshop of RF superconductivity, Beijing, China (2007).

14. H. Diepers, O. Schmidt, H. Martens, and F. Sun, Phys. Lett. **37(A)**, 139 (1971).
15. K. Satio, Y. Kojina, T. Furuya, S. Mitsunobu, S. Noguchi, K. Hosoyama, T. Nalazato, T. Tajima, K. Asano, K. Inoue, Y. Lino, H. Nomura, and K. Takeuchi, Proceeding of 4th of RF superconductivity, KEK, Tsukuba, Japan, p635 (1989).
16. E. Kato, S. Noguchi, M. Ono, K. Satio, T. Sjishido, H. Safa, J. Knobloch, and L. Lije, Proceeding of 9th of RF superconductivity, Santa Fe, NM, p328 (1999).
17. F. Eozénou, A. Aspart, C. Antoine, and B. Maliki, CARE Report 06-10-SRF-Eu contract # RII3-CT-2003-506395 (2006).
18. C. Boffo, P. Bauer, T. Reid, and R. Geng, Proceeding of 12th workshop of RF superconductivity, Ithaca, NY, p8 (2005).
19. Arsova, A. Prusi, T. Grcev, and L. Arsov, J. Serb. Chem, Soc. **71**, 177 (2006).
20. Q. Ma, and R. Rosenberg, Proceeding of the 2001 particle accelerator conference, Piscataway, NJ, 2, p1050 (2001).
21. A. Dacca, G. Gemme, L. Mattera, and R. Parodi, Appl. Surf. Sci. **126**, 219 (1998).
22. J. Halbritter, Surf. Interf. Anal. **12**, 354 (1998).
23. Q. Ma, and R. Rosenberg, Appl. Surf. Sci. **206**, 209 (2003).
24. Q. Ma, and R. Rosenberg, J. Appl. Phys. **96**, 7675 (2004).
25. M. Grindner, and J. Halbritter, J. Appl. Phys. **51**, 397 (1980).
26. A. Dacca, G. Gemme, L. Mattera, and R. Parodi, Surf. Sci. Spec. **5**, 332 (1998).
27. J. Halbritter, Appl. Phys. A **43**, 1 (1987).
28. J. Halbritter, Solid State Commun. **34**, 675 (1980).
29. A. Darlinski, and J. Halbritter, J. Vac. Sci. Technol. A **5**, 1235 (1987).
30. H. Hahn, and J. Halama, J. Appl. Phys. **47**, 4629 (1976).

31. P. Kneisel, K. Satio, and P. Parodi, Proceeding of 8th workshop of RF superconductivity, Abano Terme, Italy, p463 (1997).
32. C. Alkine, and L. Nart, Electrochim. Acta **33**, 1015 (1988).
33. F. Juliao, J. Chagas, H. Cesar, N. Dias, F. Decker, and U. Gomes, Electrochim. Acta **36**, 1297 (1991).
34. Y. Li, and L Young, Electrochem. Soc. **147**, 1344 (2000).
35. D. Gabe, Metallography **5**, 415 (1972).
36. D. Gabe, Corros. Sci. **13**, 175 (1973).
37. J. Tousek, Corros. Sci. **15**, 113 (1975).
38. J. Tousek, Electrochim. Acta **22**, 47 (1977).
39. S. Rambert, R. Sautebin, and D. Landolt, Oberflache/Surface **22**, 46 (1981).
40. H. Heinrich, and H. Feller, Metalloberflache **38**, 192 and 267 (1984).
41. L. Berlouis, and D. Schiffrin, Trans. Inst. Met. Finish **63**, 52 (1985).
42. O. Piotrowski, C. Madore, and D. Landolt, Electrochim. Acta **44**, 3389 (1999).
43. O. Piotrowski, C. Madore, and D. Landolt, Plat. Surf. Finish. **85**, 115 (1998).
44. O. Piotrowski, C. Madore, and D. Landolt, J. Electrochem. Soc. **145**, 2362 (1998).
45. H. Figour, and P. Jacquet, French Patent, No.707526, (1930).

Chapter 2

Methods and experimental procedures

2.1 Electropolishing fundamentals

Electropolishing (EP) is a process in which a metallic surface is made smoothed by anodic dissolution [1]. The discovery of EP goes back to the beginning of the 20th century [2, 3]. Jacquet was the first to investigate EP systematically and received a patent in the 1930s [4]. Today, EP is a well-developed method divided into various research branches such as the practical applications including medical device fabrication and mechanical-deformation-free preparation of metals for imaging in transmission electron microscopy (TEM), and the fundamental researches including the mechanism investigation and quantitative simulation. The literature on EP is extensive [5-10].

2.1.1 Macrosmoothing and microsmoothing

In the literature, EP regimes are commonly referred to as anodic leveling and brightening, or macrosmoothing and microsmoothing [1, 11]. This dissertation uses the later terminology where macrosmoothing will refer to the elimination of roughness with

heights over 1 μm, and microsmoothing to the elimination of roughness under 1 μm. However, the distinction of macrosmoothing and microsmoothing based on roughness is just a simplification. The value of 1 μm is not a criterion. There is no simple correlation between profile heights measured by mechanical means such as profilometry and that corresponding to optical brightness testing [12].

It is thought that different mechanisms are suitable for macrosmoothing and microsmoothing [1, 13-16]. Macrosmoothing results from the higher current leading to the higher local dissolution rate on peaks. This is under an ohmic control (or voltage control). Theoretical prediction of local macrosmoothing rate based on the Nernst diffusion layer model is in good agreement with experimental results. Following section (2.2.2) is a detailed description of the model.

Microsmoothing on the other hand results from the suppression of the influence of surface defects and crystallographic orientation on the dissolution process [1]. Microsmoothing is the final finish of EP. The mechanism of microsmoothing is rather complex [5, 17-18]. It is accepted that microsmoothing occurs under mass transport limiting current with the presence of an anodic film on the metal surface [6-8, 19-32]. About the nature of anodic film, some researchers favor a thin compact salt film consisting of an oxide contaminated with significant amounts of anions from solution [31], and others favor a highly viscous and anhydrous film [33-35]. Only the metal ion is mobile in the anodic salt film [14]. The extensive discussion of the salt film is in chapter 5. One performing EP usually wants to achieve both macrosmoothing and

microsmoothing, but in practice it is possible to only achieve macrosmoothing without microsmoothing and vice versa [9, 14-16].

2.1.2 Nernst diffusion layer

Figure 2.1 is a schematic diagram of the Nernst diffusion layer model under ideal conditions [1]. The macrosmoothing rate is equal to the difference in dissolution rate between peaks and valleys of a rough surface. The difference in dissolution is determined by the local current distribution along the surface profile [1]. An arbitrary two-dimension surface profile is treated as a Fourier sine series [36]. The corresponding parameters are: the initial profile height ε_0, the wavelength λ, and the diffusion layer thickness δ. When $\delta \gg \varepsilon_0$, the interface between the diffusion layer and the bulk electrolyte will be flat. The difference in distance from the metal surface to the interface—for example in figure 2.1, AB < CD—results in a difference in resistance, that is, $R_{AB} < R_{CD}$. The current density at point A (peak) is larger than that at point C (valley); resulting in the reduction of peak heights typically > 1 μm. If $\varepsilon_0 \gg \delta$, the diffusion layer will follow the surface profile in a perfect way as shown by the broken line in figure 2.1. In this case, there is no difference in resistance along the surface, in figure 2.1 for example, AB' = CD' => $R_{AB'} = R_{CD'}$. The current density is uniform, i.e. no profile flattening. The wavelength λ also contributes to the macrosmoothing rate. Wagner and McGeough conclude that the larger the ratio of λ/ε_0, the smaller the smoothing rate [36, 37].

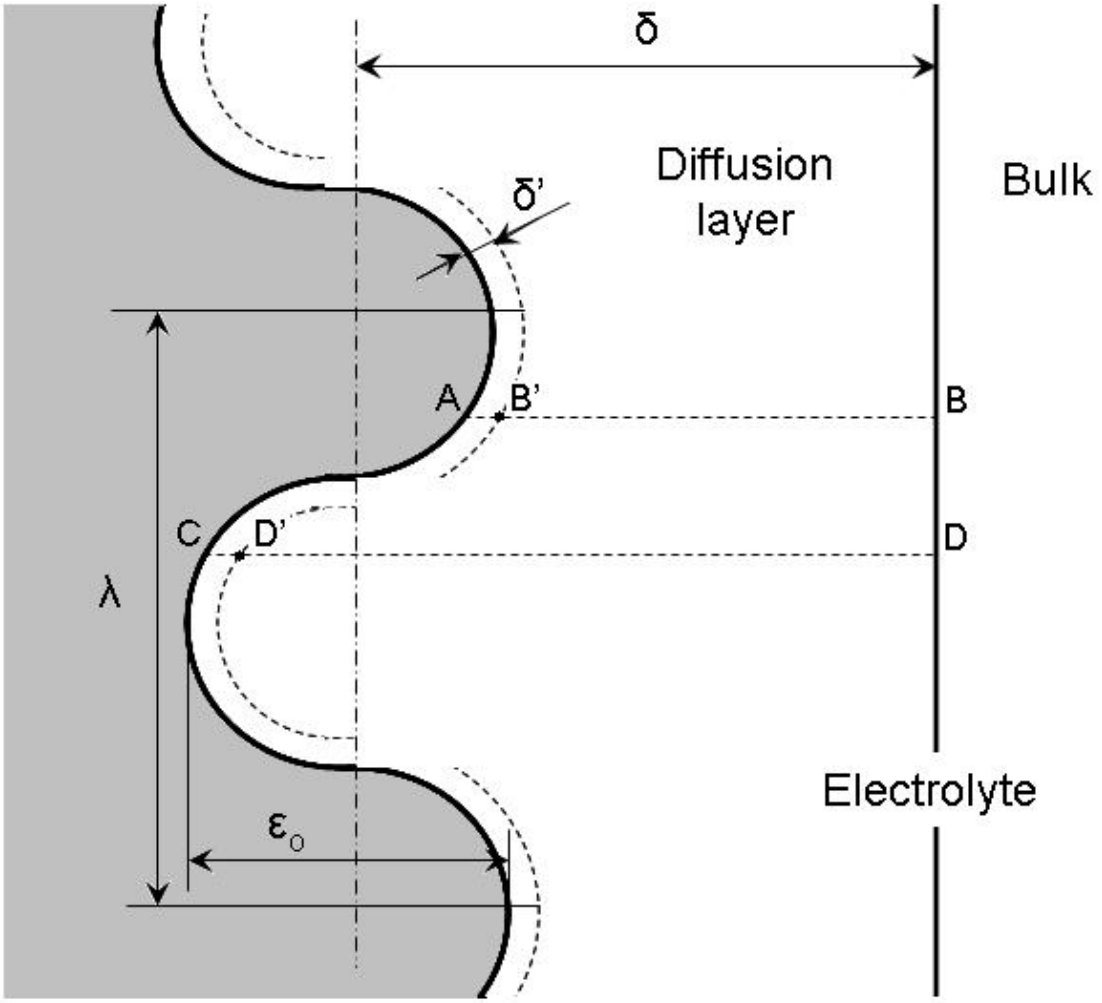

Figure 2.1: Schematic diagram of the Nernst diffusion layer model [1].

2.1.3 Mass transport mechanism

Mass transport is the only condition that leads to microsmoothing. Figure 2.2 summarizes the three possible mass transport mechanisms proposed in the literature [1]. Mechanism 1—salt precipitation—considers rate limiting diffusion of cations (M^+) of the dissolving metal from the anode to the electrolyte. During EP within the limiting current region a

salt film presents on the anodic surface where the concentration of M^+ in the salt film is equal to the saturation concentration. The anions (A^-) from the electrolyte also accumulate within the anodic film to maintain the electro-neutrality. Extensive discussions of the relationship between salt film precipitation and microsmoothing is presented in chapter 5. Mechanism 2—acceptor anion limited—is limited by the transport of acceptor anions (A^-) to the metal surface. Mechanism 3—hydrogen limited—considers the diffusion of water from the electrolyte to the anode as the rate limiting process. Regardless of the mechanisms, mass transport of the dissolved metal ions is the limiting factor responsible for the shift from surface etching to microsmoothing [6-8, 21-25]. In all these EP cases, the estimation of the surface concentration of the dissolving metal ions at the limiting current yields values in reasonable agreement with the saturation concentration.

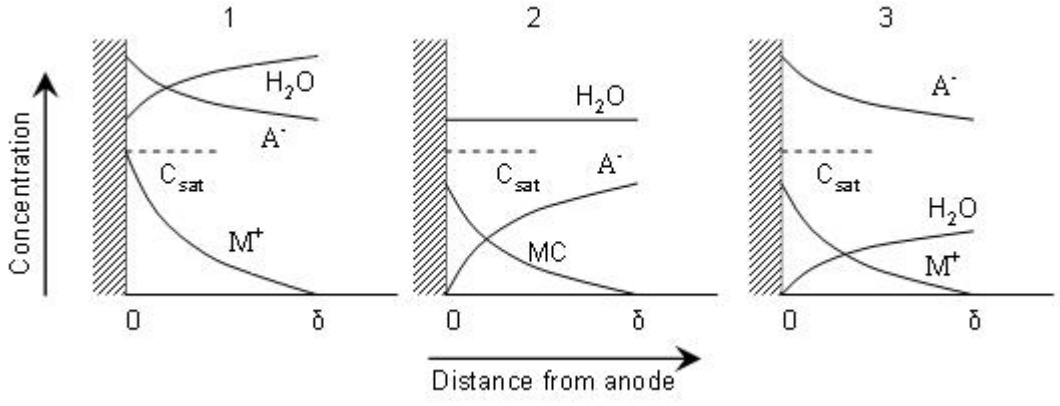

Figure 2.2: Schematic diagram of three mass transport mechanisms involving (1) salt film, (2) acceptor, and (3) water as transport species. C_{sat} is the saturation concentration and δ is the thickness of Nernst diffusion layer [1].

2.2 Electrochemical apparatus and procedures

2.2.1 Potentiostat instrumentation

A potentiostat is an instrument that provides the control of the potential difference between the working electrode and the reference electrode [38]. The potentiostat implements this control by applying current into the cell between the working electrode and the counter electrode until the desired potential between the working electrode and the reference electrode is reached. Figure 2.3 shows the schematic diagram of a potentiostat with computer control. The amplifier compares the desired potential with the measured cell potential and then drives the current into the cell to equalize the two potentials. The electrometer measures the potential difference between the working electrode and the reference electrode, and then sends the signal to the amplifier for comparison. The I/E converter obtains the cell current by measuring the voltage drop across the measurement resistor, R_m.

In an electrochemical cell for EP, the working electrode is the electrode to be polished [1]. A well-working reference electrode should have a constant electrochemical potential. A saturated mercury/mercurous sulfate electrode (MSE), which has an electrode potential of 0.615 versus the standard hydrogen electrode (SHE) [26, 27], is used as the reference electrode in this dissertation work. The counter electrode completes the cell circuit. Platinum is always employed as the counter electrode due to its catalysis for hydrogen bubble formation and inertness to dissolution [26, 27].

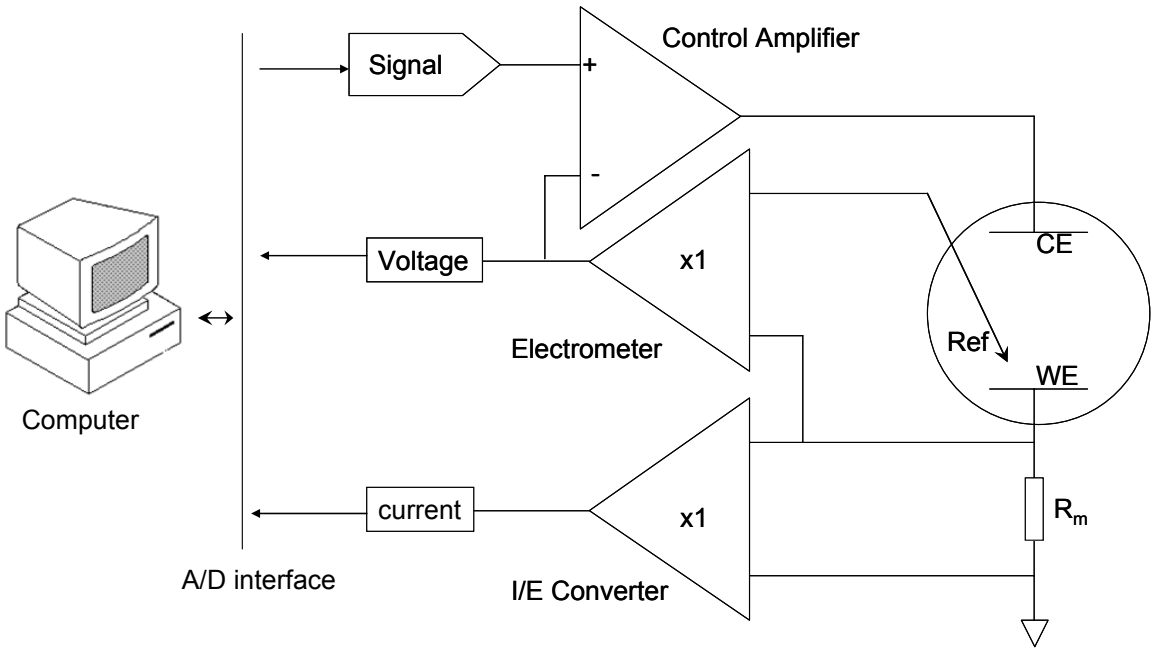

Figure 2.3: Schematic diagram of a potentiostat.

2.2.2 Anodic polarization scan

Polarization is measured as overpotential, i.e. as a change in potential from the equilibrium half-cell electrode potential or the corrosion potential [26, 27]. During an anodic polarization scan the potential on the working electrode is varied linearly with the time and the change in current is recorded. Figure 2.4 shows a typical anodic polarization curve [39]. The polarization scan progresses from negative potential to positive potential follows the blue curve from point 1 to point 2. In region B, the active region, metal oxidation is the dominant reaction. When the potential increases above the passivation potential (point C), the current will decrease rapidly to region E, the passive region. When the potential reaches a sufficiently positive value (point F), the current will increase rapidly to region G, the transpassive region. Experimental polarization curve may show some—but not necessarily all—of the features described in figure 2.4.

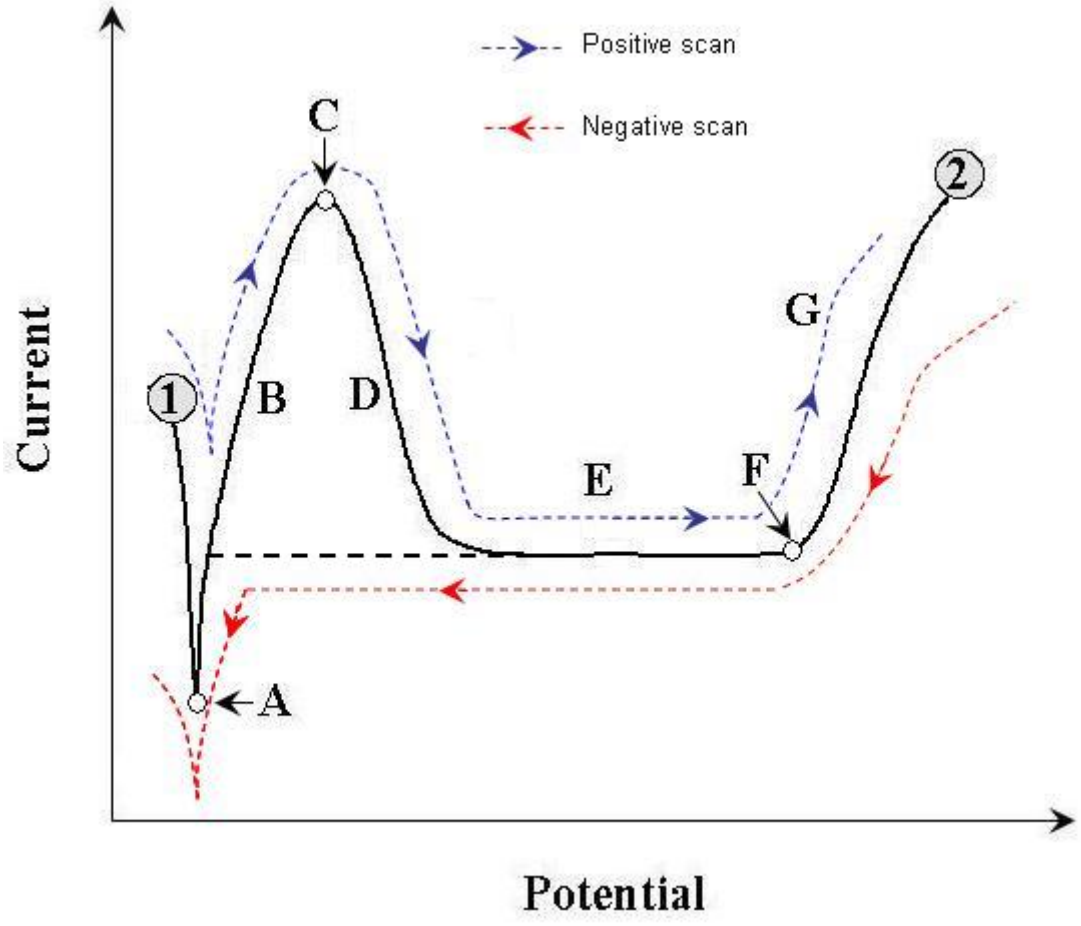

Figure 2.4: Schematic diagram of an anodic polarization.

The experimental polarization scans used in this dissertation project are performed with the negative scan direction as shown by the red curve in figure 2.4. Figure 2.5 shows the anodic polarization curve measured on the Nb working electrode in a 2 M sulfuric acid-methanol electrolyte at room temperature. The curve was measured from 9 to 0 V (versus the MSE reference) at a rate of -10 mV/s. The current minimum at the beginning of the scan (region I) is related to the formation and thinning of an anodic film [6]. The negative voltage scan provides more reproducible current response as the formation of a salt film

during a positive scan is highly scan rate dependent [6]. Region II on the curve presents a limiting current plateau corresponding to the mass transport control. Notice that the current does not decrease with decreasing voltage since metal dissolution is mass transport controlled but not voltage controlled. Microsmoothing is only observed in region II. Region III presents a linear relationship between current and voltage representing an ohmic resistance limited current. Surface etching of Nb happens in this region.

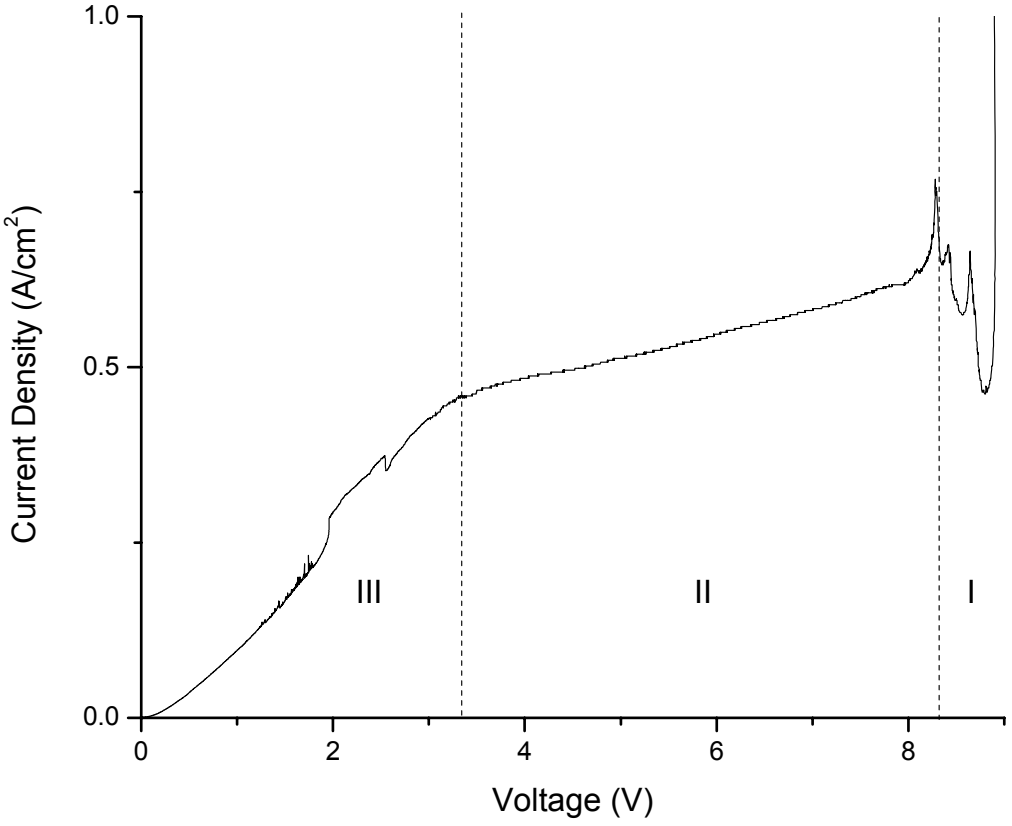

Figure 2.5: Practical anodic polarization curve measured on Nb working electrode in a 2 M sulfuric acid-methanol electrolyte at room temperature.

2.3 Surface characterization

2.3.1 Scanning electron microscopy (SEM) and surface orientation mapping

SEM is a powerful technique that uses electrons rather than light to form images of objects. Literature about principle and application of SEM is easy to be found [40, 41]. An SEM image is commonly captured by detecting the secondary electrons which are sensitive to surface profile heights but not to grain orientations. For a flat surface, one only obtains a uniform contrast as shown in figure 2.6 (a). This Nb surface was obtained by EP in a 0.5 M sulfuric acid-methanol electrolyte at -30^{o}C for 30 min. Note the black points correspond to contaminations on the Nb surface. The surface roughness was measured to be approximately 300 nm/mm by profilometry (section 2.3.2).

Backscattered electrons provide different information than secondary electrons. Backscattered electrons contain the surface orientation information. A Robinson backscatter detector (RBSD) was used in the present study. Figure 2.6 (b) shows the surface orientation contrast on the same surface as shown in figure 2.6 (a). The white contrast corresponds to the orientation close to the direction perpendicular to the RBSD while the dark contrast to the orientation parallel to the RBSD. In order to achieve the surface orientation contrast, the surface must be extremely flat to avoid the surface height contrast. In figure 2.7, the SEM images were obtained by using (a) secondary electrons and (b) backscattered electrons scanning across an Nb surface polished in a 0.1 M sulfuric acid-methanol electrolyte at room temperature for 30 min. The surface roughness

is approximately 1 μm/mm and the surface profile completely masks the grain orientation contrast.

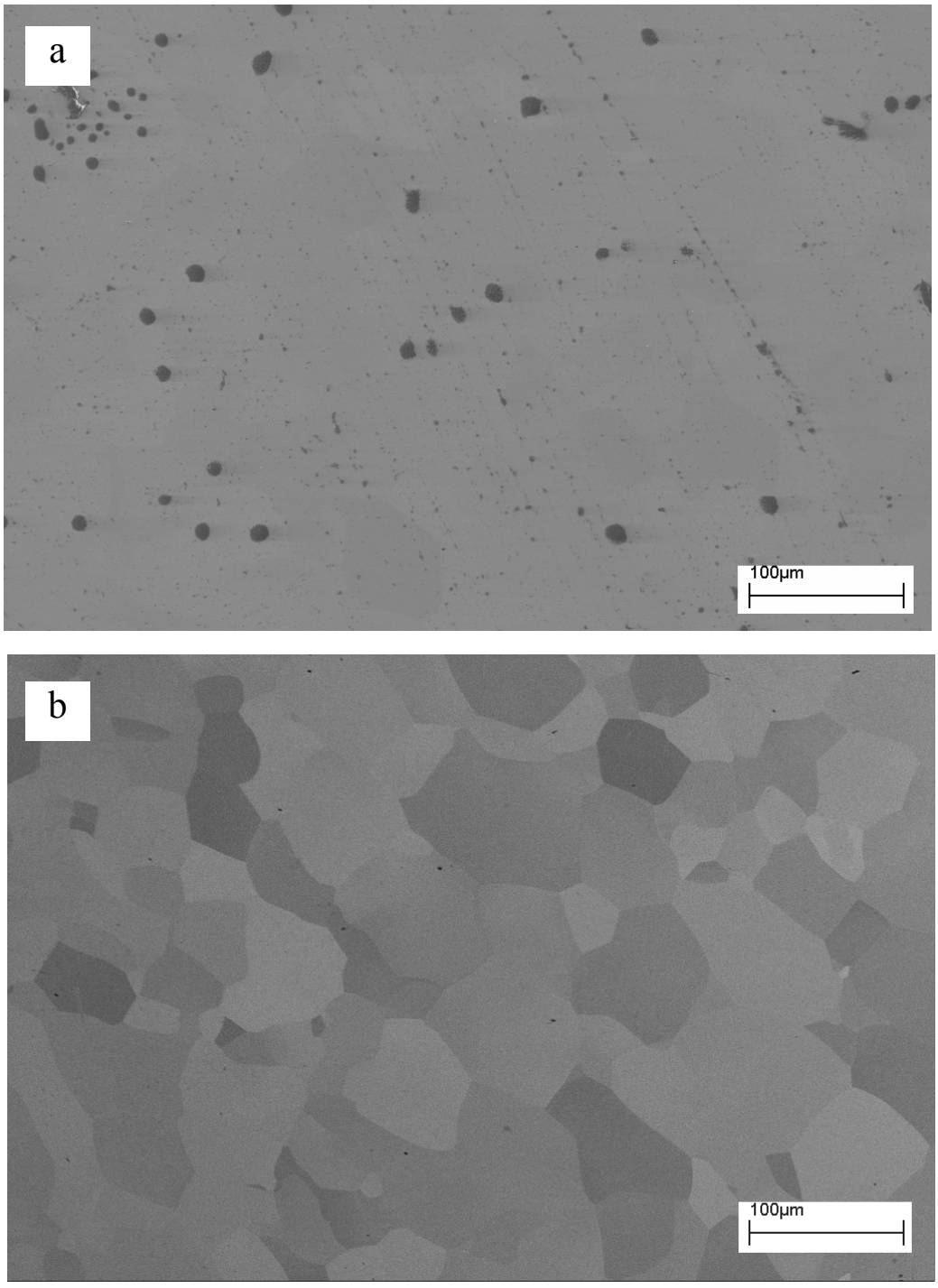

Figure 2.6: SEM images of Nb surfaces captured by using (a) secondary electron and (b) RBSD. The Nb surface is electropolished in a 0.5 M sulfuric acid-methanol electrolyte at -30^{o}C for 30 min.

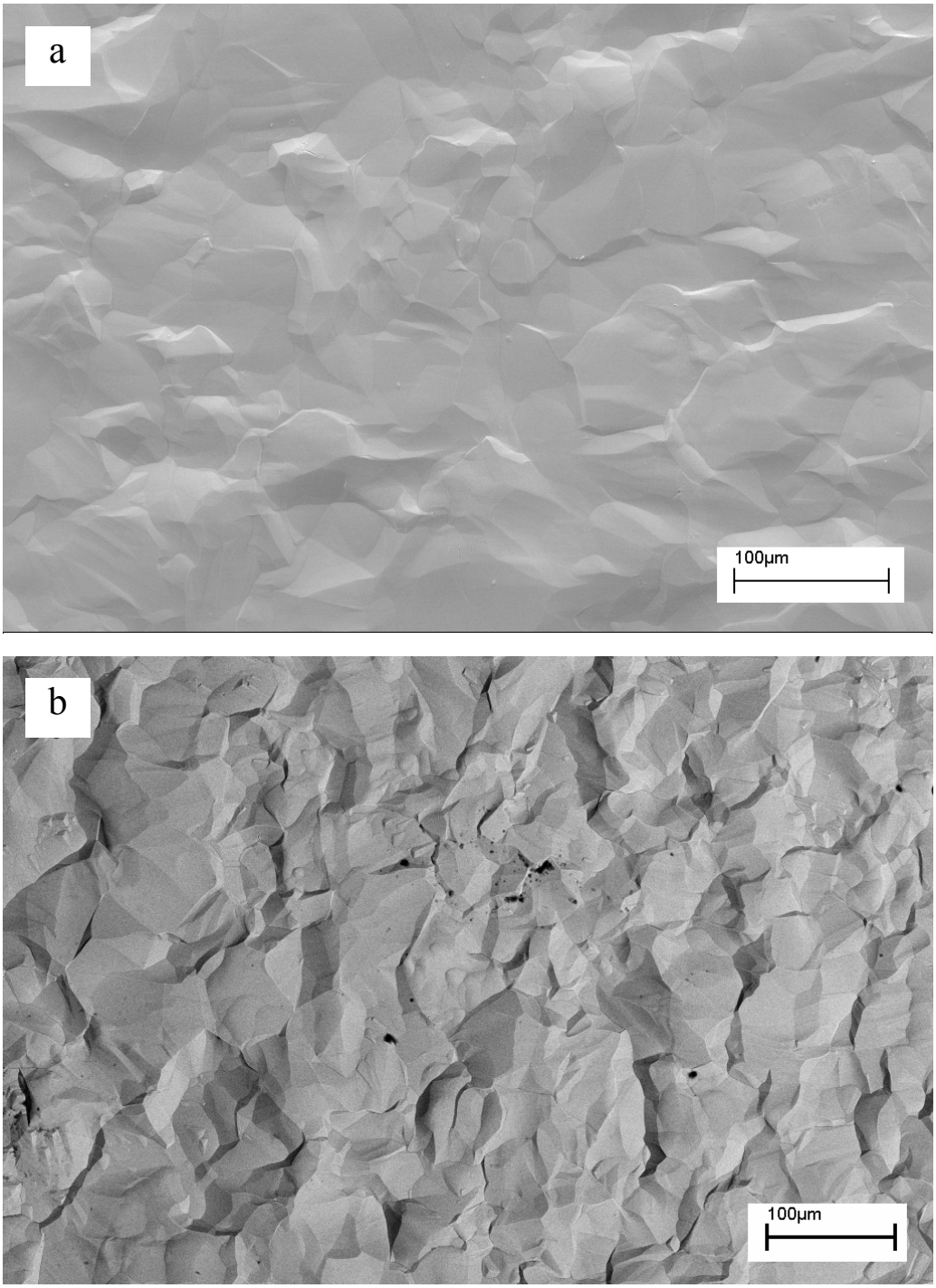

Figure 2.7: SEM images of Nb surfaces captured by using (a) secondary electron and (b) RBSD. The Nb surface is electropolished in a 0.1 M sulfuric acid-methanol electrolyte at room temperature for 30 min.

2.3.2 Stylus profilometry

Profilometry is a method used to measure the profile of a surface, in order to quantify its roughness. The surface roughness values discussed in this dissertation were measured by contact profilometry. A diamond stylus scans laterally across a sample surface under a specified force for a specified distance. The stylus detects small variations in vertical displacement as a function of lateral position. A typical profilometer is sensitive to vertical height variations ranging from 10 nm to 1 mm. Scan speed, contact force, and stylus radius all affect the lateral resolution. A typical stylus radius ranges from 5 to 25 μm, but a very sharp stylus with radius of 0.1 μm is also available [42]. The profilometer used in this dissertation was Alfa-step 500, KLA-TENCOR. The scan length was 1 mm. The scan rate was 100 Hz. The contact force was 13.5 mg. The stylus radius was about 5 μm. The lateral resolution was 1 μm.

2.3.3 Variable length scale analysis

Typically a single value of root mean square roughness is calculated from a profilometry trace. While it is useful to many applications, a single value does not convey information of topographic features along the length scale. For example, figure 2.8 shows SEM images of two Nb surfaces electropolished in different electrolytes. Though they have identical macroscopic surface roughness (approximately 300 nm/mm) many different small scale features can be observed. A surface characterization method is needed to provide roughness over a micro- to macroscopic lateral scale.

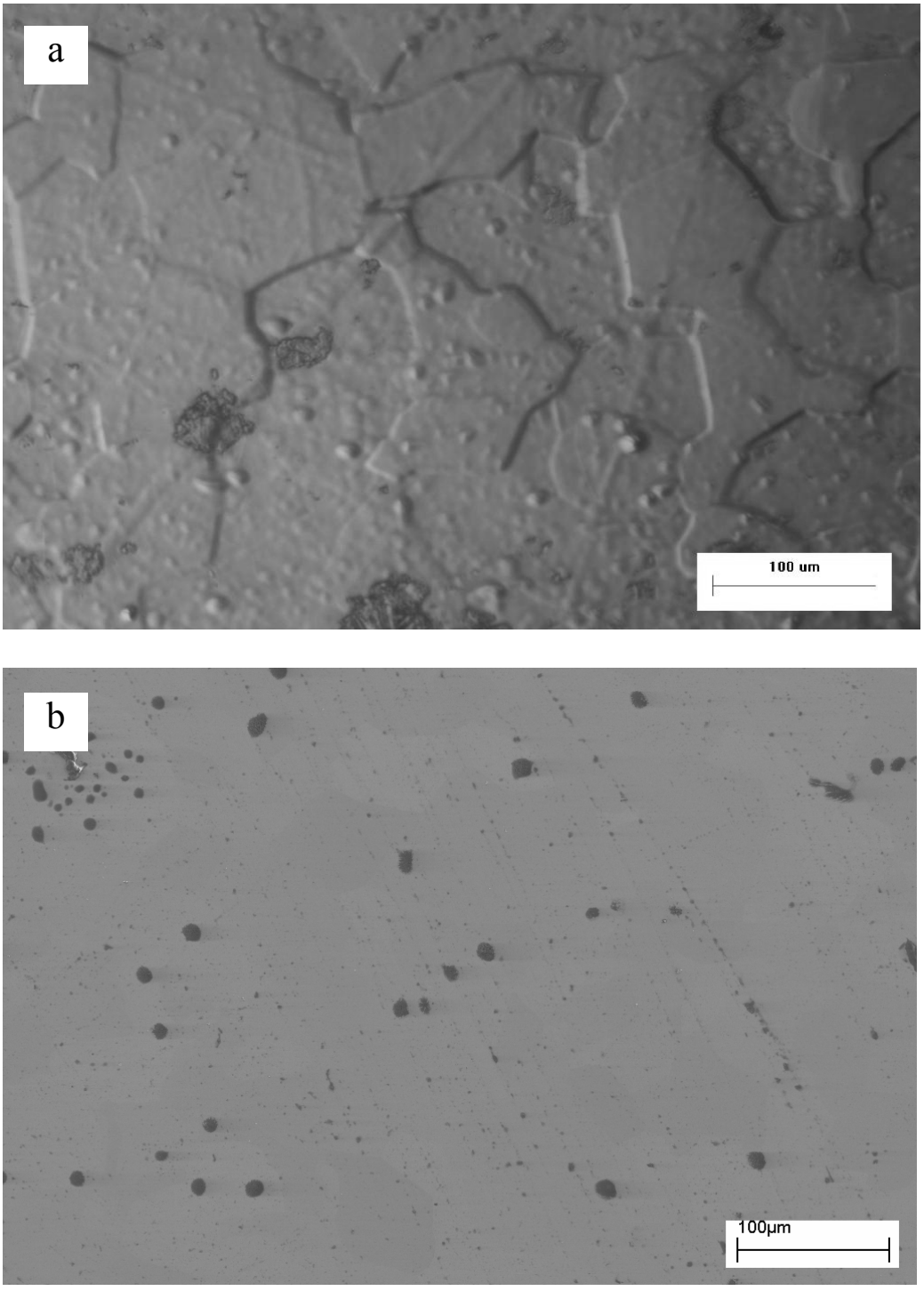

Figure 2.8: SEM images of Nb surfaces electropolished in (a) HF-based electrolyte (b) methanol-based electrolyte.

Chauvy et al developed a variable length scale analysis for surface topography [43]. Using a profile measurement, the variable length scale is performed by: 1) defining intervals of length ε, starting from a small fraction of the entire measurement length—for example, 5 lateral points—and up to the entire profile length; 2) finding the baseline in each interval by performing a linear square fit on the data in ε and then calculating the roughness; 3) moving ε along the profile length point by point and repeat 2); 4) calculating the average roughness; 5) repeating 2) to 4) for each increasing length of ε. There are many parameters that can be used to characterize the roughness. The root mean square roughness (R_{rms}) averaged over the number of intervals of length ε (n_ε) is examined in this dissertation.

The R_{rms} would be defined as [43]:

$$R_{rms} = \frac{1}{n_\varepsilon}\sum_{i=1}^{n_\varepsilon}\sqrt{\frac{1}{p_\varepsilon}\sum_{j=1}^{p_\varepsilon} h_j^2} \tag{2.1}$$

where p_ε is the number of points in the length ε, h_j is the j-th height calculated relative to the fitted profile line within the i-th interval. Figure 2.9 shows the curves of R_{rms} versus length scale calculated by equation 2.1 for the raw Nb surface, the mechanically polished (600 grit emery paper) Nb surface, and the electropolished Nb surface, respectively. R_{rms} of the raw surface shows an almost constant value along the whole length scale. The curve of the mechanically polished surface shows a much decreased roughness value along the whole length scale. Figure 2.10 shows the optical image of the mechanically polished Nb surface for comparison to the length scale data. In contrast, R_{rms} of the electropolished surface decreases with decreasing length scale. The electropolishing produces a smoother surface below approximately 700 nm lateral scale but also produces

large scale surface waviness [43]. Furthermore, the linear fit of the surface profile over the entire scan length gives the straightforward observation of the elimination of the grain-grain height variations as shown in figure 2.11. The profile of the raw surface shows the grain structures. Mechanical polishing removes the grain height difference but leaves a rough Nb surface. EP results in a much flatter surface at the microscopic scale, but waviness at larger length scales. This is identical to the observation by R_{rms}. One thing should be noted that the surface curvature is not available in the surface profiles due to the linear fit.

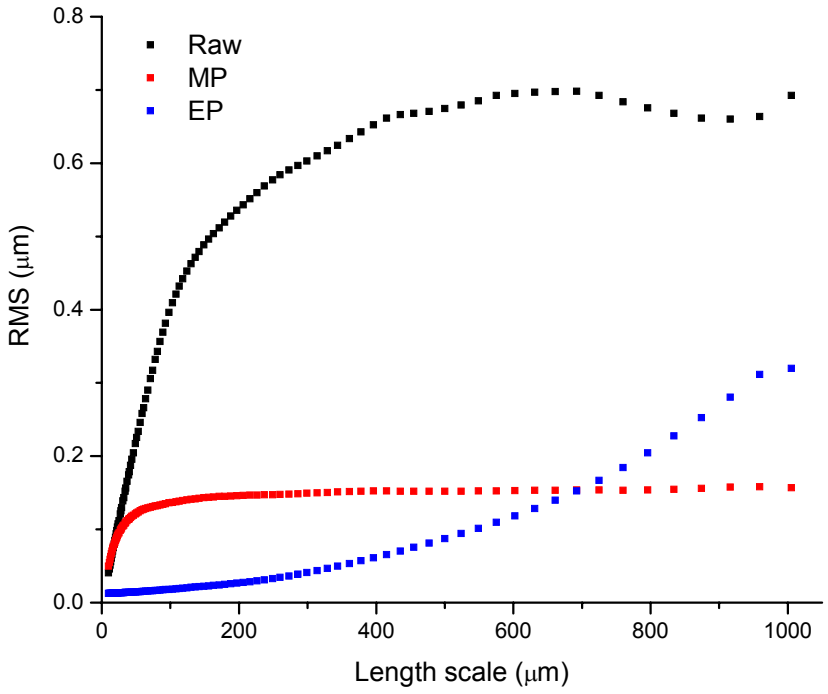

Figure 2.9: R_{rms} as a function of length scale of the raw surface (Raw), the mechanically polished (MP) surface, and the electropolished (EP) surface. EP was performed in a 0.5 M sulfuric acid-methanol electrolyte at -30°C for 30 min.

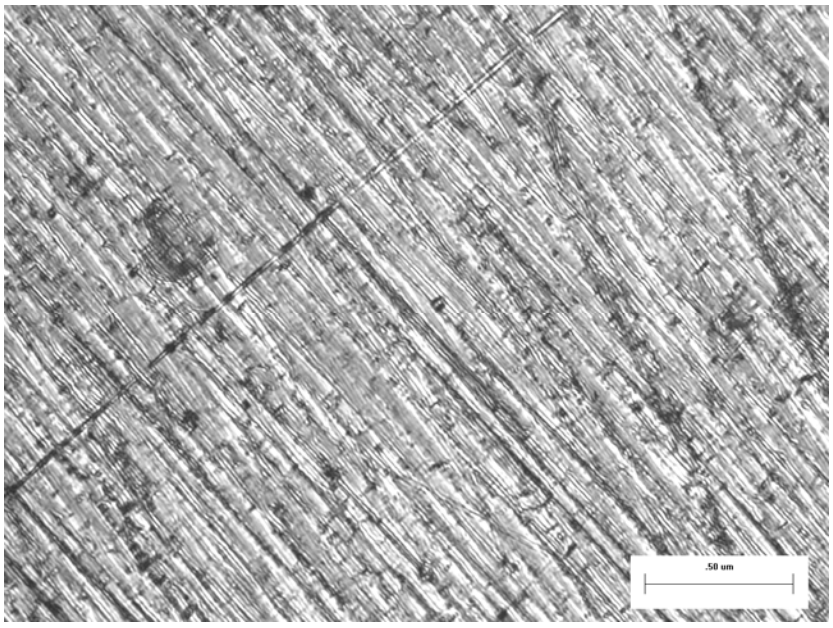

Figure 2.10: The optical imaged of the mechanically polished Nb surface.

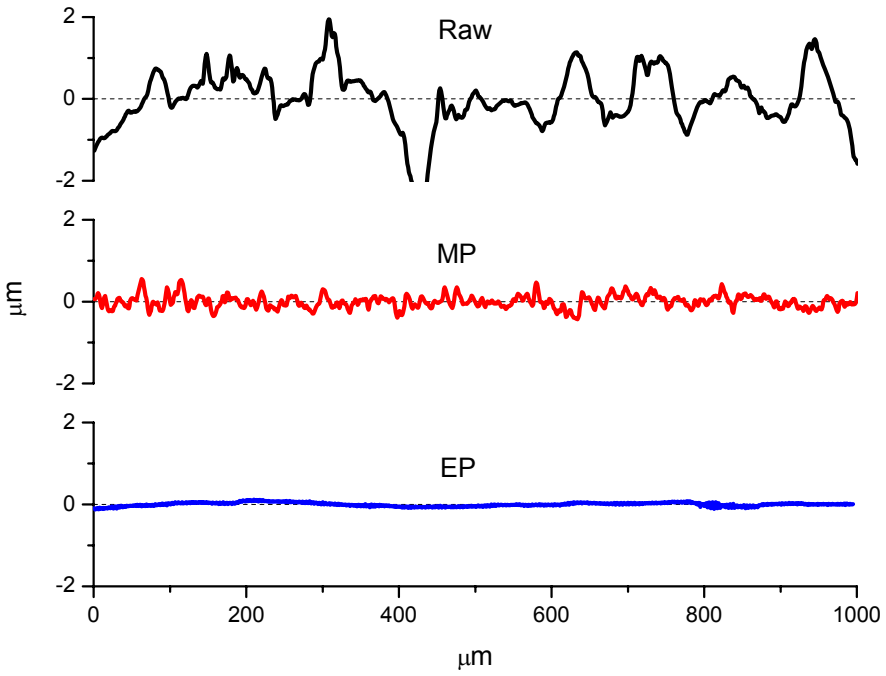

Figure 2.11: Surface profiles of the raw surface (Raw), the mechanically polished (MP) surface, and the electropolished (EP) surface in a 0.5 M sulfuric acid-methanol electrolyte at -30^{o}C for 30 min.

Figure 2.12 shows a comparison of surfaces with identical macroscopic roughness value (approximately 300 nm/mm) shown in figure 2.8. Notice that the comparison here is not to compare the polishing techniques, but to show that the surfaces having identical macroscopic roughness may have various small scale features. The HF-based EP was performed in a 1:9 HF/H_2SO_4 electrolyte and the sample was provided by Fermi National Lab as a typical one. The methanol-based EP was performed in a 0.5 M sulfuric acid-methanol electrolyte at -30^{o}C for 30 min. The R_{rms} of each surface starts with a rather low value and then increases with increasing length scale that agrees with the conclusion made above. But the R_{rms} of surface electropolished in the HF-based electrolyte is much larger than that in methanol-based electrolyte over microscopic length scales. This is related to the grain boundaries still observed on the SEM images (figure 2.8) and the surface profiles (figure 2.12 (b)).

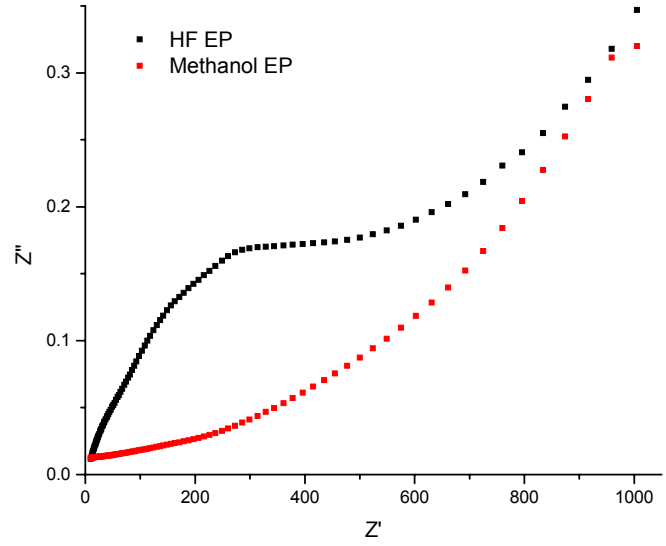

(a)

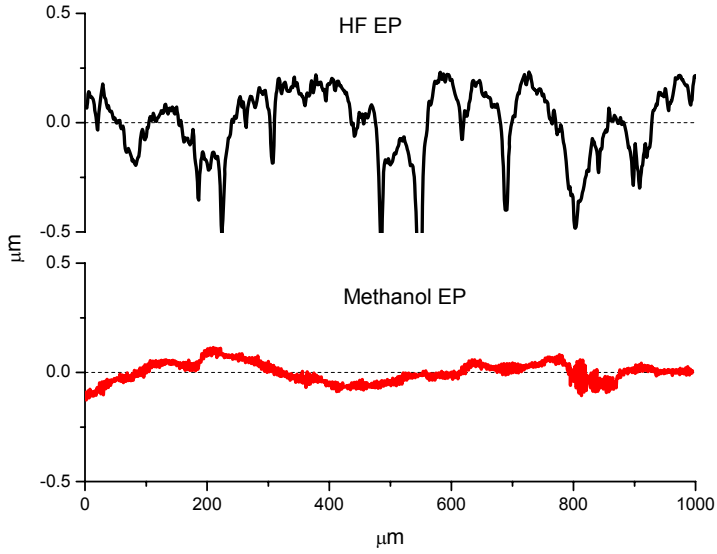

(b)

Figure 2.12: (a) R_{rms} as a function of length scale and (b) surface profiles of Nb surfaces electropolished in the HF-based electrolyte and the methanol-based electrolyte.

References

1.D. Landolt, Electrochim. Acta **32**, 1 (1987).

2. A. Kutzelnigg, Metalloberflache **3**, 867 (1951).

3. R. Weiner, Metalloberflache **27**, 441 (1973).

4. H. Figour and P. A. Jacquet, French Patent No. 707526 (1930).

5. P. Jacquet, Nature **135**, 1076 (1935).

6. O. Piotrowski, C. Madore, and D. Landolt, Electrochim. Acta **44**, 3389 (1999).

7. O. Piotrowski, C. Madore, and D. Landolt, Plat. Surf. Finish. **85**, 115 (1998).

8. O. Piotrowski, C. Madore, and D. Landolt, J. Electrochem. Soc. **145**, 2362 (1998).

9. H. Tian, M. Kelley, C. Reece, and S. Corcoran, J. Electrchem. Soc. **155**, D563 (2008).

10. W. Elmore, J. Appl. Phys. **10**, 724 (1939); **11**, 639 (1940).

11. J. Edwards, J. Electrodeposition Techn. Sco. **28**, 133 (1952).

12. R. Young, and E. Teague, Passivity of Metals, The Electrochemical Society, Princeton, NJ (1978).

13. R. Grimn, and D. Landolt, Corros. Sci. **36**, 1847 (1994).

14. M. Matlosz, Electrochim. Acta **40**, 393 (1995).

15. R. Grimn, A. West, and D. Landolt, J. Electrochem. Soc. **139**, 1622 (1992).

16. R. Grimn, and D. Landolt, Corros. Sci. **36**, 1847 (1994).

17. P. Jacquet, Tans. Electrochem. Soc. **69**, 639 (1936).

18. P. Jacquet, Metal Finishing **47**, **48** and **83** (1949).

19. D. Landolt, R. Muller, and C. Tobias, J. Electrochem. Soc. **116**, 384 (1969).

20. M. Datta, and D. Landolt, J. Electrochem. Soc. **122**, 1446 (1975).

21. D. Landolt, R. Muller, and C. Tobias, J. Electrochem. Soc. **116**, 1384 (1968).

22. D. Landolt, R. Muller, and C. Tobias, Fundamentals of Electrochemical Machining, The Electrochemical Soc. Princeton, NJ (1971).

23. M. Datta and D. Landolt, J. Electrochem. Soc. **122**, 1466 (1975).

24. M. Datta and D. Landolt, J. Appl. Electrochem. **7**, 247 (1977).

25. M. Datta and D. Landolt, Electrochim. Acta **25**, 1263 (1980).

26. D. Jones, Principle and prevention of corrosion, 2nd Edition, Prentice Hall, Upper Saddle River, NJ (1996).

27. A. Bard, and L. Faulkner, Electrochemical methods: Fundamentals and Applications, John Wiley and Sons Inc. (1994).

28. T. Hoar, and J. Mowart, Nature **165**, 64 (1950).

29. T. Hoar, and T. Farthing, Nature **169**, 324 (1952).

30. T. Hoar, Modern aspects of electrochemistry, Vol 2, Butterworths, Landon (1959).

31. T. Hoar, D. Mears, and G. Rothwell, Corros. Sci. **5**, 279 (1965).

32. T. Hoar, Corros. Sci. **7**, 341 (1967).

33. S. Glarum, and J. Marshall, J. Electrochem. Soc. **132**, 2872 (1985).

34. M. Movak, A. Reddy, and H. Wroblowa, J. Electrochem. Soc. **117**, 733 (1970).

35. M. Turner, and P. Brook, Electrodep. Surf. Treatment **2**, 245 (1973).

36. J. McGeough, Principles of electrochemical machining, Chapman and Halls, Landon, (1974).

37. J. Wargner, J. Electrochem. Soc. **101**, 225 (1954).

38. http://www.gamry.com/App_Notes/Potentiostat_Primer.htm.

39. http://www.solartronanalytical.com/technicalsupport/technicalnotes/technote33.htm.

40. J. Vickerman, Surface Analysis: The Principal Techniques, John Wiley (1997).

41. A Shwartz, M. Kumar, and B. Adams, Electron backscatter diffraction in materials science, Kluwer Academic, New York, NY (2000).

42. C. Poo, and B. Bhushan, wear **190 (1)**, 76 (1995).

43. P. Chauvy, C. Madore, and D. Landolt, Surf. Coat. Technol. **110**, 48 (1998).

Chapter 3

Electropolishing of niobium: Two-electrode setup

3.1 Introduction

In the present chapter, current-voltage behavior of Nb working electrode in the 0.1 M sulfuric acid-methanol electrolyte is studied by voltammetry. Potential hold experiments at low temperature (−30^{o}C) in the 1 M and 2 M sulfuric acid-methanol electrolytes are conducted. The surface quality of electropolished Nb is characterized as a function of EP duration and temperature. Electrochemical results are correlated with surface characterization. It is proved that the surface qualities obtained in some experimental conditions are comparable to and even better than those obtained by HF-based methods.

3.2 Experimental Procedures

Sample preparation

Polycrystalline Nb plates were embedded in epoxy cylinder with a diameter of 10 mm. The areas of working electrodes were 0.2 to 0.4 cm^2. The Nb plates were cut from the

high-RRR-grade fine grain Nb sheet stock used to make standard SRF cavities. The stock has a purity of 99.9999% according to the manufacture (Wah Chang, USA). The Nb working electrodes in epoxy were fabricated as follows: a nut with a Teflon separator was pasted on one side of the plate; the plate was then embedded in epoxy by silica mold; after the epoxy healed, the separator was removed; a hole was then left to have the inside of the nut exposed. Figure 3.1 shows an Nb working electrode and a schematic diagram of the cross-section. The surface for polishing is exposed on one end of the cylinder and a thread rod connects with the nut through the hole on the opposite. It is easy to load the working electrode in the cell and apply potential on it via the thread rod during an electrochemical experiment. It is also easy to push the Nb plate out for other measurements. Before each electrochemical experiment, the working electrodes were mechanically polished by 600 grit emery paper, rinsed in methanol, and dried in air. All the Nb working electrodes were conserved in a dry keeper (SANPIA, USA).

Electrolytes preparation

Electrolytes were prepared by sulfuric acid (Certified ACS plus, 98%, Fisher Chemical) and methanol (HPLC grade, 99.9%, Fisher Chemical). To obtain the least of water content, a very low sulfuric acid concentration of 0.1 M in the methanol solution was prepared. The water content in the 0.1 M electrolyte was calculated from the weight ratio to be smaller than 0.05wt%. The detail of calculation is introduced in Appendix A. The water content is much smaller than that in the mixture of HF (49%) and sulfuric acid (96.8%) (1:9 volume ratio), which was estimated to be about 6wt%. It is also smaller than that in the electrolyte of 3 M sulfuric acid-methanol, which was measured to be 0.2wt%

by Piotrowski et al [1]. Concentrations of 1 M and 2 M were also prepared, and the maximum water contents were calculated to be 0.21wt% and 0.49wt%, respectively.

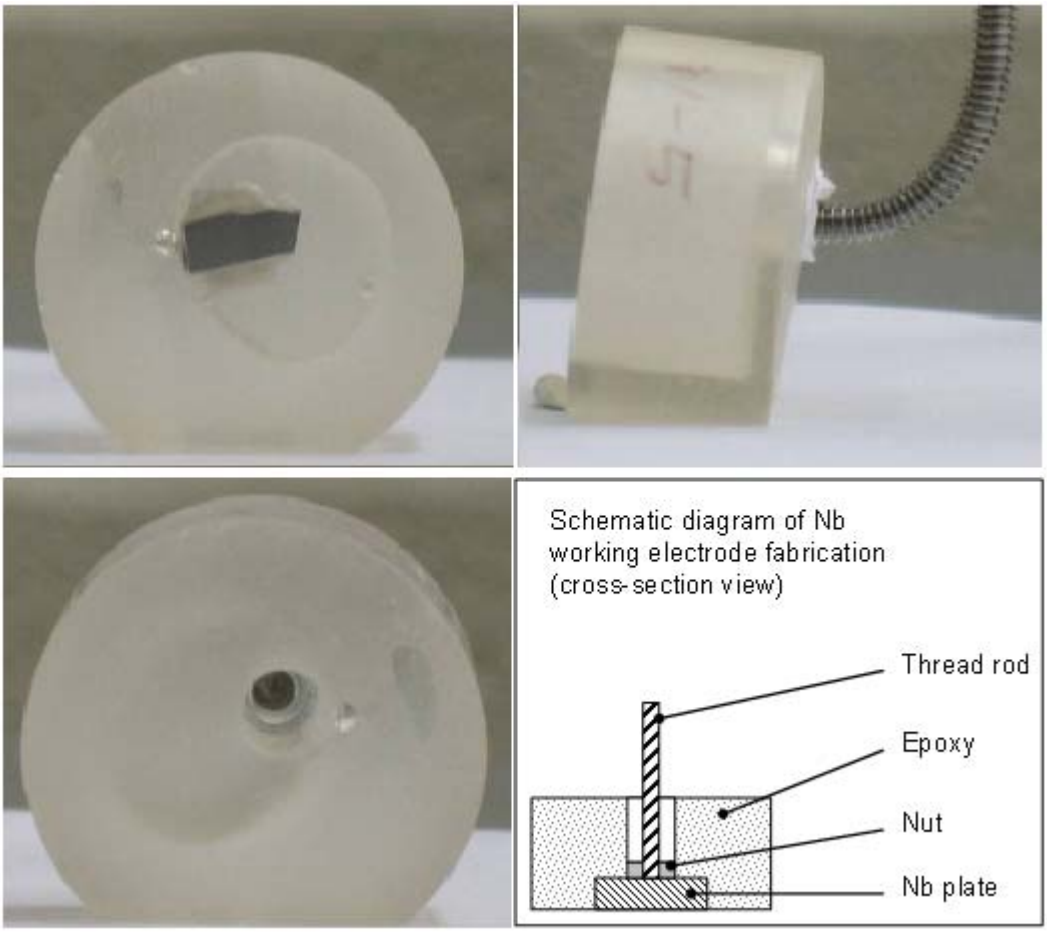

Figure 3.1: Nb working electrode-front (up-left), back (down-left), connection with a thread rod at back (up-right), and a schematic diagram of the cross-section (down-right).

Electrochemical experiments

All the electrochemical experiments were performed in a two-electrode electrochemical cell. A platinum foil was used as the counter electrode parallel to the working electrode. The two-electrode setup was used to follow the practical cavity treatment [2-4]. The volume of electrolyte in the cell was about 300 ml. Every experiment was performed in

fresh prepared electrolyte. A potentiostat (Model 273, EG&G, Princeton Applied Research) was used to measure the current-voltage (C-V) data [1, 5, 6]. By a pre-amplifying circuit shown in figure 3.2, the potential output from the potentiostat was amplified by the factor of $(R_1+R_2)/R_2$. All the voltage values in the present chapter refer to those magnified and measured between working and counter electrodes. The voltage was scanned from 26 to 0 V at a rate of -10 mV/s, and the negative scan direction is for the reproducible limited current [1]. EP processes were performed under conditions of various durations and temperatures. The current transient (C-t) curves were tracked simultaneously. To control the electrolyte temperature, the cell was placed in a reservoir of ethanol whose temperature was controlled by a chiller. A thermometer was used to monitor the electrolyte temperature. The cell was sealed by a Teflon cover to avoid water condensing from atmosphere into electrolytes. Figure 3.3 shows a schematic diagram of the low temperature experiment setup. After EP, every Nb working electrode was conserved in the dry keeper again until no more weight loss was measured. The net weight loss was recorded for the corrosion rate calculation.

Surface characterization

Surface topographies of the electropolished Nb working electrodes were characterized by scanning electron microscopy (SEM, Leo (Zeiss) 1550). A Robinson backscatter detector (RBSD) was used to detect the backscattered electrons for surface orientation contrast [2, 7]. A profilometry (Alfa-step 500, KLA-TENCOR) was also performed to study the surface roughness [11]. Details of the surface characterization have been demonstrated in chapter 2. On each surface, the roughness was measured at five different places at least,

and the average roughness with standard deviation was calculated. To investigate the grain boundary elimination, the relationship between root mean square roughness (R_{rms}) and various length intervals was studied.

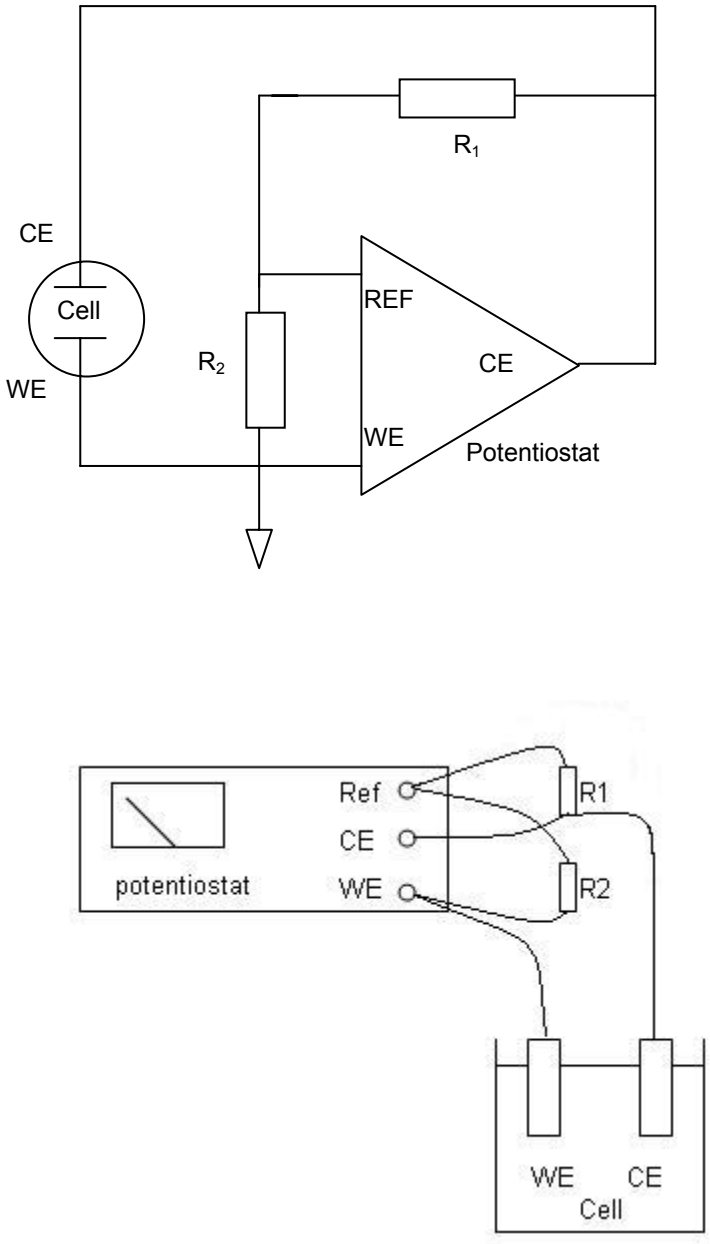

Figure 3.2: Schematic diagram (upper) and practical circuit setup (lower) of the two-electrode setup measurement circuit.

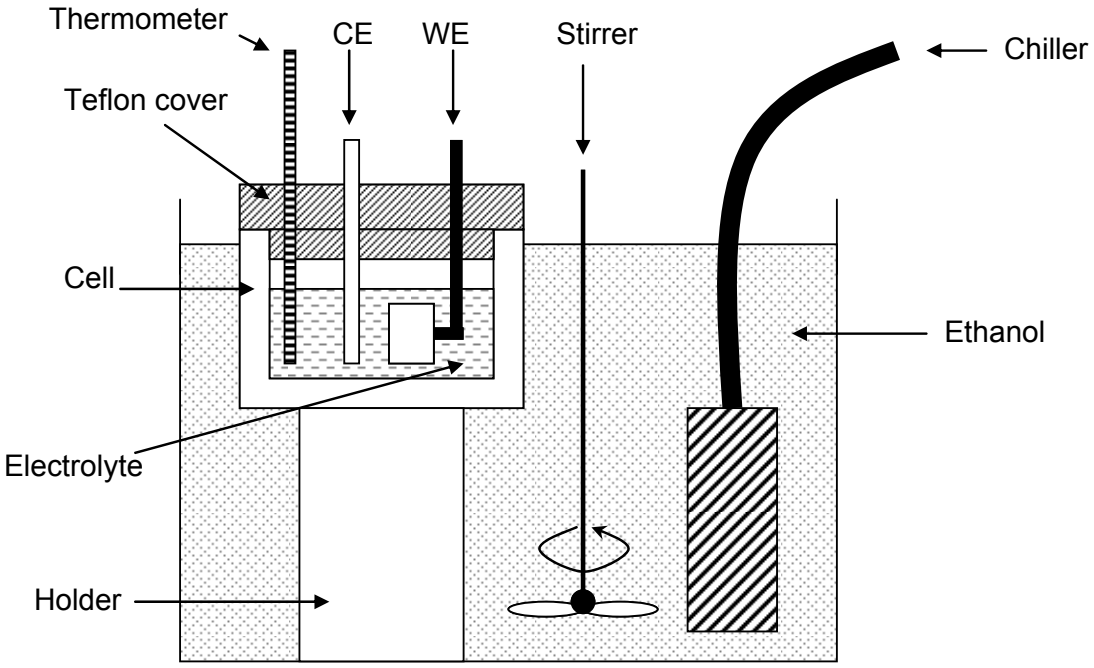

Figure 3.3: Schematic diagram of the cell setup for low temperature experiments.

3.3 Results and discussion

3.3.1 EP in the 0.1 M sulfuric acid-methanol electrolyte

Electrochemical experiments

Figure 3.4 shows the C-V curves measured in the 0.1 M sulfuric acid-methanol electrolyte at room temperature, 0^{o}C, -10^{o}C, and -30^{o}C. The C-V curve measured at each temperature shows no limiting current plateau but a linear relationship between current and voltage. A linear C-V curve indicates an ohmic resistance limited current [8, 9]. The electrolyte resistance is temperature-dependent, i.e. the current decreases with decreasing

temperature under the same voltage. In addition, current oscillation is observed on the C-V curves and consistent with the formation and detachment of an anodic film on Nb surface [10]. The current oscillation is also temperature-dependent as its magnitude and frequency decrease with decreasing temperature.

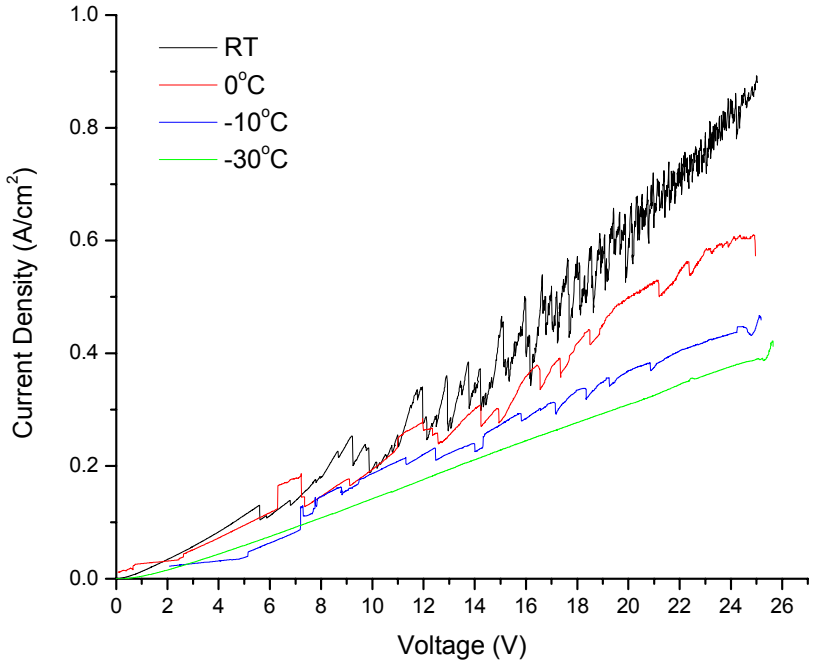

Figure 3.4: Nb C-V curves measured in the 0.1 M sulfuric acid-methanol electrolyte at various temperatures.

EP process was performed by holding the potential at 22 V for 30 min, 1 h, and 2 h at room temperature, 0°C, -10°C, and -30°C. Figure 3.5 shows the C-t curves tracked during all the EP processes. The current and the oscillation are both temperature-dependent. The average current (i_a) and its standard deviation are calculated from the C-t curves and shown in figure 3.5 (d). The i_a measured during EP is influenced by both temperature and EP duration. The standard deviation is also temperature-dependent and thought to be

corresponding to the current oscillation. The magnitude of the standard deviation also shows a dependence on EP duration. The mechanism of this observation is still unknown.

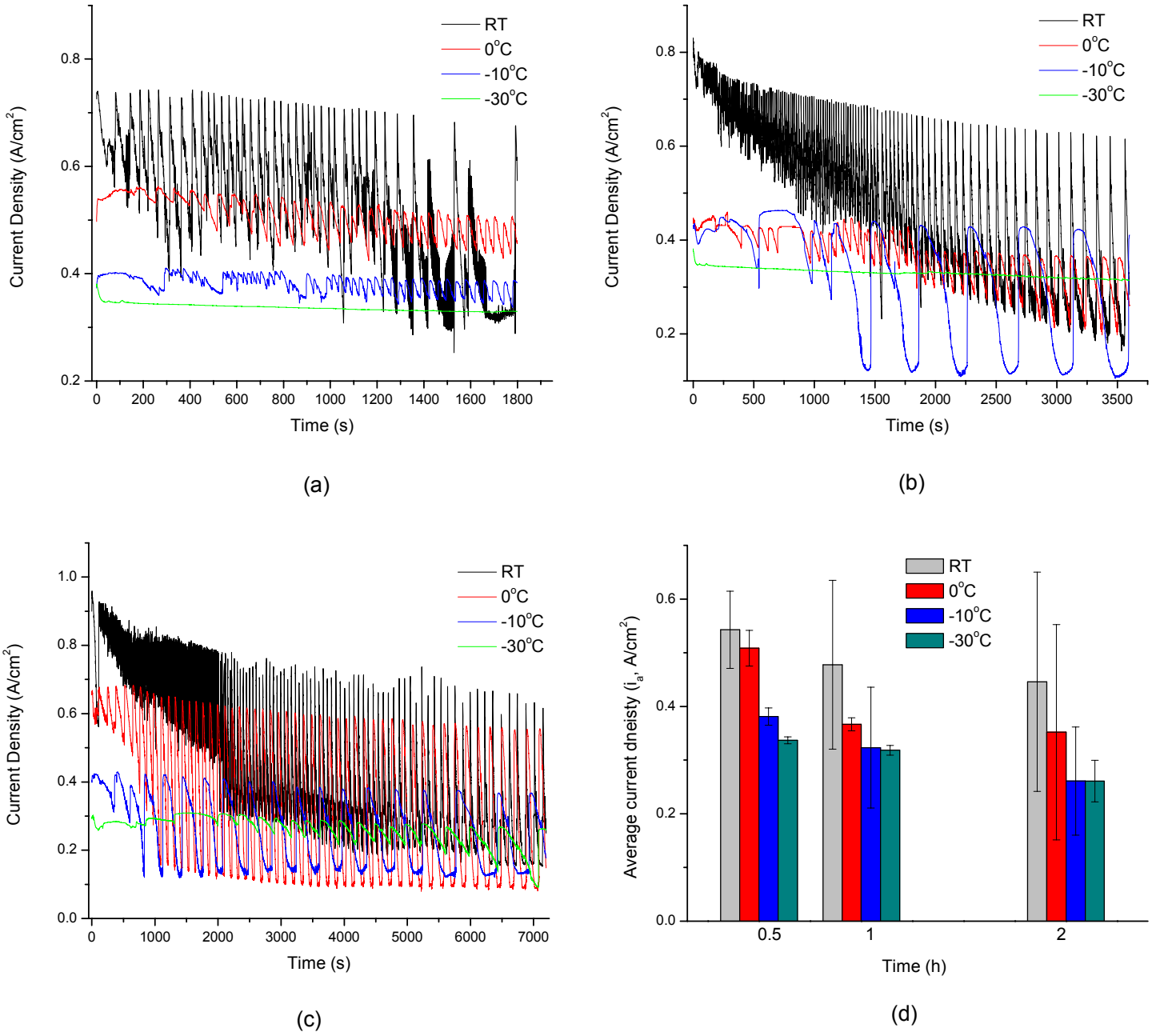

Figure 3.5: Nb C-t curves measured in the 0.1 M electrolyte during EP at 22 V for (a) 30 min, (b) 1 h and (c) 2 h at various temperatures; and (d) the i_a vs. electrolyte concentration and temperature.

Weight loss of each electropolished Nb working electrode was recorded to calculate the corrosion rate (r , μm/min) by the equation:

$$r = \frac{\Delta m}{A\rho t} \tag{3.1}$$

where Δm is the weight loss (g), A is the working electrode area (cm^2), ρ is the density of Nb (8.57 g/cm^3), and t is the EP duration (min). Figure 3.6 shows the corrosion rate calculated for each EP process by weight loss measurements. The corrosion rate is in the range of 3.5 to 7.5 μm/min. The value is comparable to that obtained from HF-based BCP (2 to 4 μm/min, up to 10 μm/min) [11], but much faster than that from HF-based EP (0.4 μm/min) [2]. The pattern of corrosion rate looks similar to that of i_a, because the mass dissolution is proportional to the charged specie transfer.

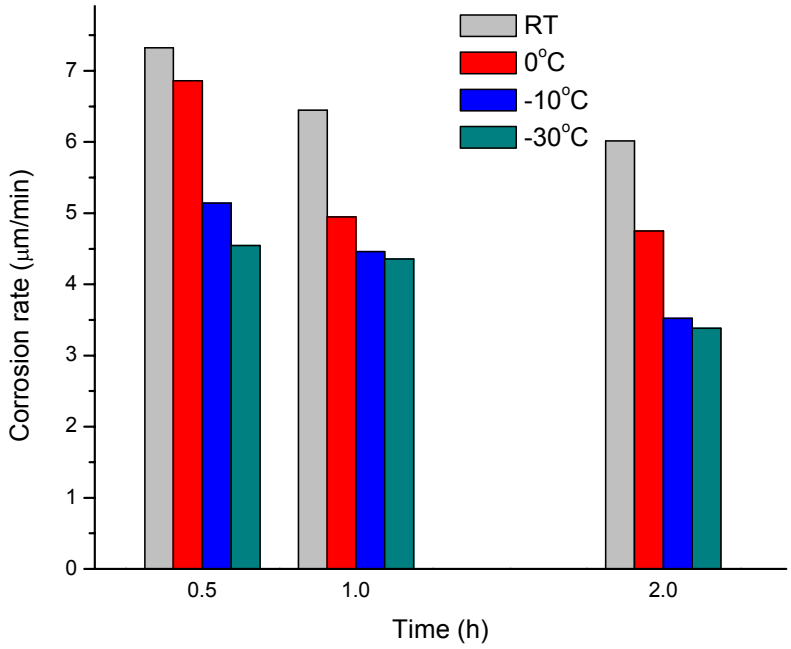

Figure 3.6: The corrosion rate calculated from the weight loss measurements following EP at 22 V in the 0.1 M electrolyte.

Surface characterization

Figure 3.7 shows SEM images of Nb working electrodes electropolished in the 0.1 M sulfuric acid-methanol electrolyte at 22 V for 30 min, 1 h, and 2 h at room temperature by using RBSD. All the images show a height contrast corresponding to the existence of grains. The average size of grains is about 50 μm. A longer EP contributes little to the grain boundary elimination as shown in the SEM images. On the other hand, pits are observed on the surface polished for 30 min. The appearance of pits is corresponding to the insufficient EP resulting non-uniform material removal in the low concentration of 0.1 M. On surface electropolished over 1 h, pit is no longer observed. A longer EP is proposed by Tian et al to remove the difference caused by different prior treatments [2] and also removes the pits caused by a shorter EP in this case. The results suggest that the longer EP in the 0.1 M electrolyte realizes uniform material removal on faucets but does not enhance the grain boundary elimination.

Figure 3.8 shows the SEM images of Nb surfaces electropolished in the 0.1 M sulfuric acid-methanol electrolyte at 22 V for 30 min at 0^{o}C, -10^{o}C, and -30^{o}C by using RBSD. Same pits are also observed on the surfaces polished at low temperatures. This is related to the smaller corrosion rate at low temperature than at room temperature as shown in figure 3.6. Low temperature results in an identical surface topography to room temperature. On the other hand, no clear orientation contrast is observed on all the surfaces electropolished in the 0.1 M electrolytes under all conditions of temperatures and durations. This indicates that the height contrast on the surfaces electropolished in the 0.1 M sulfuric acid-methanol electrolyte masks the surface orientation contrast.

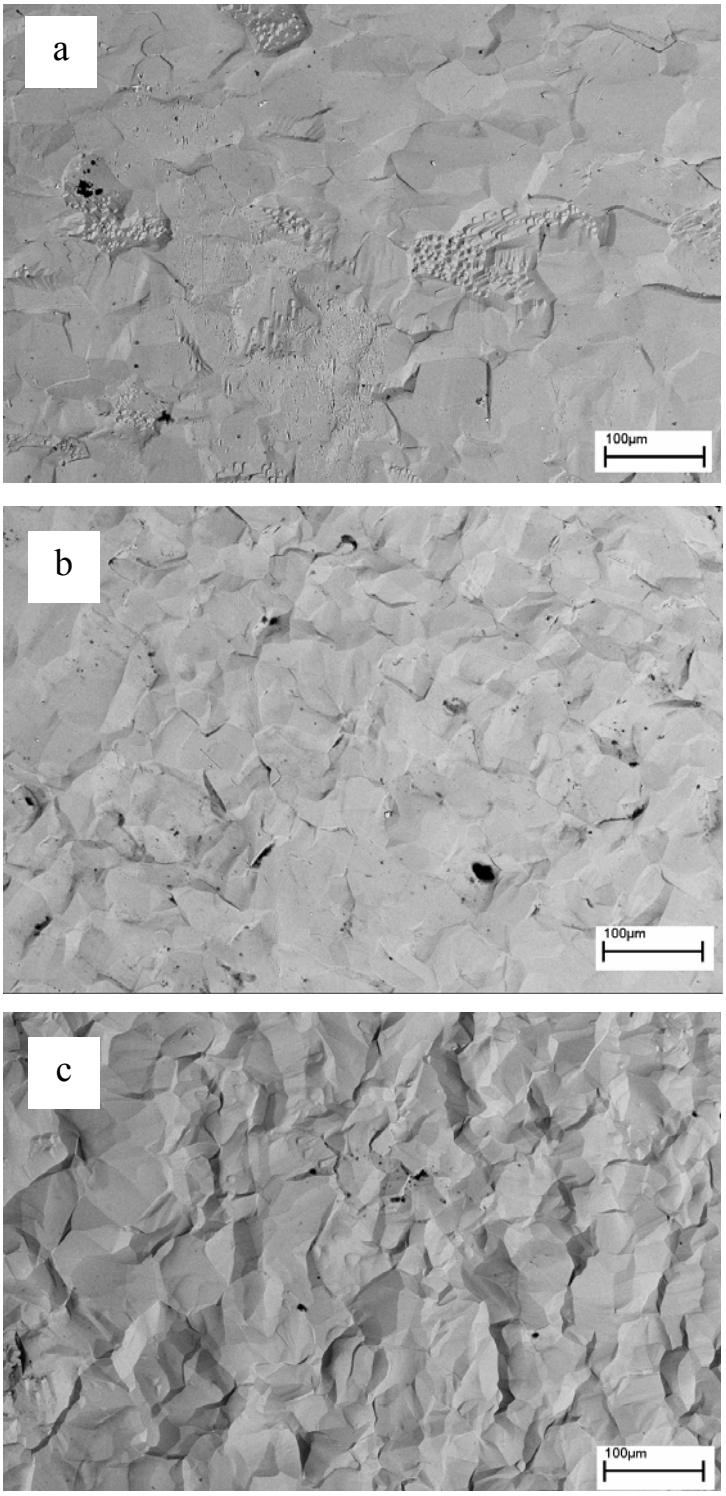

Figure 3.7: SEM images by using RBSD of Nb surfaces electropolished in the 0.1 M electrolyte at 22 V for (a) 30 min, (b) 1 h, and (c) 2 h at room temperature.

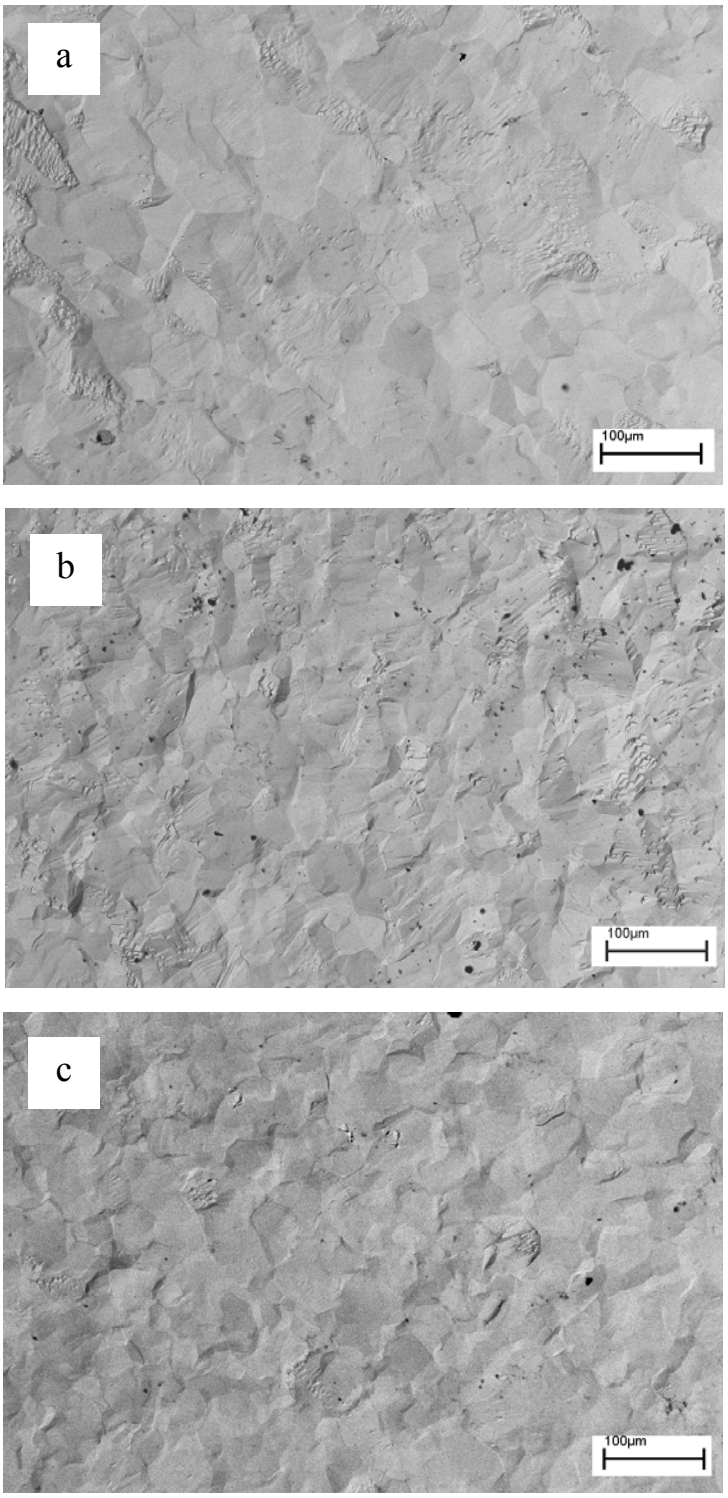

Figure 3.8: SEM images by using RBSD of Nb surfaces electropolished in the 0.1 M electrolyte at 22 V for 30 min at (a) 0°C, (b) -10°C, and (c) -30°C.

Figure 3.9 shows the average roughness (R_a) with standard deviation measured on the Nb surfaces electropolished in the 0.1 M electrolyte under various conditions of concentrations and temperatures. The scan length was 1 mm with a lateral resolution of 1 μm. The R_a value distributes in the range of a few hundred nanometers to a few microns. The majority of the R_a values are comparable to those obtained by HF-based BCP (2 to 5 μm/mm) and EP (1.2 μm/mm) at the same measurement dimension [2]. Some R_a measured at lower temperature—for example about 500 nm/mm resulted from 30 min EP at -10°C and -30°C—are smaller than those obtained by HF-based surface finish. The R_a value decreases with decreasing temperature and decreasing EP duration. It is likely that lower temperature EP flattens macroscopic surface profile while longer EP creates more surface waviness at macroscopic scale.

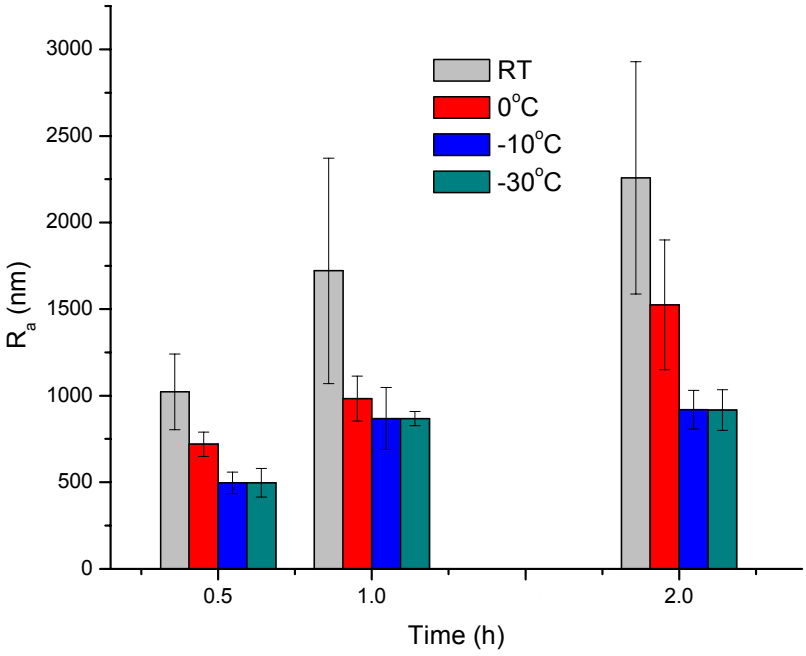

Figure 3.9: R_a of Nb surfaces electropolished in the 0.1 M sulfuric acid-methanol electrolyte under various conditions.

For more detail understanding of the surface finish at microscopic scale, the relationship between R_{rms} and length scale was investigated by the model developed by Chauvy [12]. Figure 3.10 shows the R_{rms} as a function of length scale in various conditions. Figure 3.10 (a) shows that the R_{rms} value of surfaces electropolished at room temperature increases with increasing duration along the whole length scale. This indicates that longer EP results in a rougher surface at both macroscopic and microscopic scales. Figure 3.10 (b) shows that the R_{rms} of surfaces electropolished at various temperatures overlaps each other at the scale of single grain (about 50 μm) and then progresses separately until reaching the maximum. The R_{rms} of the surface electropolished at lower temperature increases more slowly and reaches a smaller maximum. This phenomenon indicates that the EP process at low temperature contributes little to the grain boundary elimination but helps to suppress surface waviness at macroscopic scale, which is identical to the discussion about R_a.

As a complementary study of grain boundary elimination, figure 3.11 shows the profile study of surfaces electropolished under various conditions. For an easier observation of grain boundaries, the surface curvatures were flattened by a mathematical method and thus the surface waviness of macroscopic scale is no longer observed. Figure 3.11 (a) shows that the grain height of surfaces electropolished at room temperature decreases with decreasing duration. On the other hand, there is no obvious variation in height observed on surfaces electropolished at various temperatures (figure 3.11 (b)). The profile study proves the assumption obtained from the R_{rms} study that: for EP process in the 0.1 M sulfuric acid-methanol electrolyte, 1) longer EP causes a superior grain

boundary etching; 2) temperature contributes little to the suppression of grain boundary at microscopic scale.

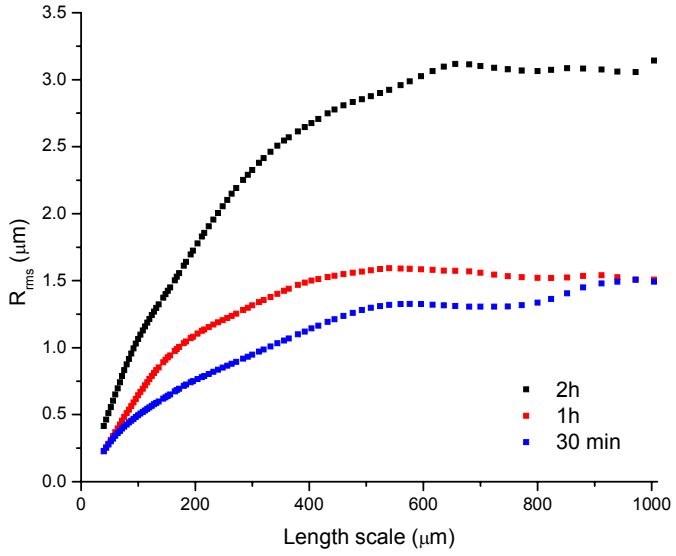

(a)

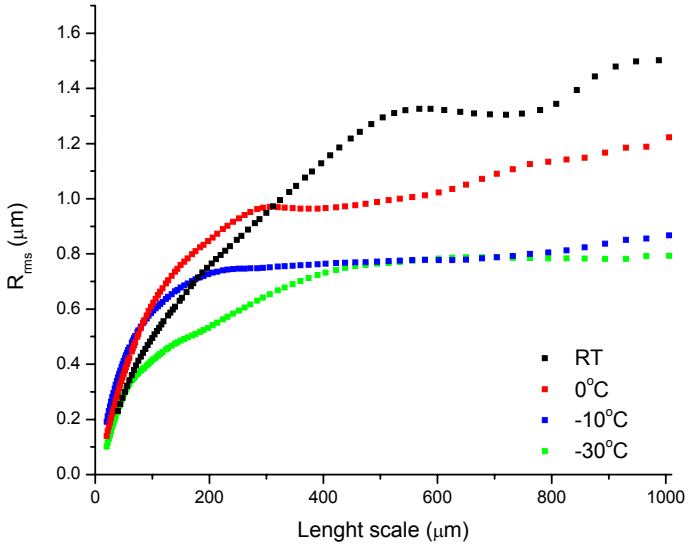

(b)

Figure 3.10: R_{rms} as a function of length scale of surfaces electropolished for (a) various durations at room temperature and (b) 30 min at various temperatures.

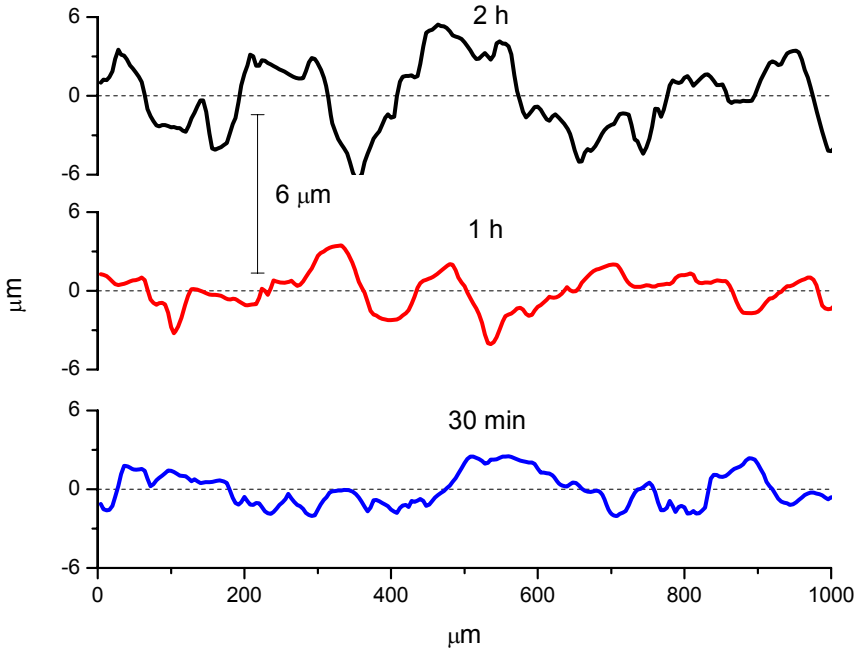

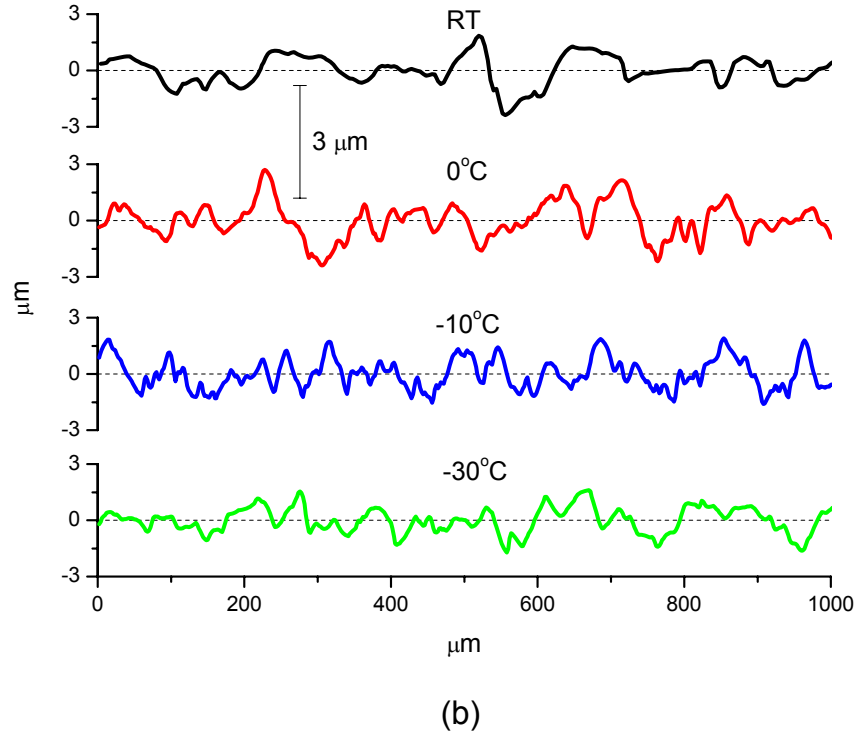

Figure 3.11: Profiles of surfaces electropolished for (a) various durations at room temperature and (b) 30 min at various temperatures.

3.3.2 EP in higher concentrations at -30°C

Nb surfaces were electropolished in the 1 M and 2 M sulfuric acid-methanol electrolytes at -30°C. The same electrochemical experiments and surface characterization were conducted.

Electrochemical experiments

Figure 3.12 (a) shows the C-V curves measured in the 0.1 M, 1 M, and 2 M sulfuric acid-methanol electrolytes at -30°C. The voltage was scanned from 26 to 0 V at a rate of -10 mV/s. C-V data measured in the 2 M electrolyte shows a well-pronounced limiting current plateau. A current plateau indicates a mass transport controlled current [1, 8, 13]. The current measured in the 1 M electrolyte is larger than that measured in both the 0.1 M and 2 M electrolytes. However, there is only a short current plateau observed at the beginning of the voltage scan in the 1 M electrolyte. The majority of the C-V curve shows a linear relationship between current and voltage. The current minimum at the beginning of the voltage scan is related to the formation and detachment of an anodic film [8]. In addition, the current is concentration-independent. The current on the plateau measured in the 2 M electrolyte is even lower than that measured in the 0.1 M electrolyte.

The C-t curves (figure 3.12 (b)) were measured in the 1 M and 2 M electrolytes during the potential hold experiments at 22 V for 30 min. The C-t curves show the same concentration-independent current. A rapid current drop and reversion occurs at the beginning of EP in the 1 M electrolyte but not in the 0.1 M or 2 M electrolytes. This current behavior is consistent with the anodic film deposition and dissolution [1]. The

corrosion rate of EP in the 1 M and 2 M electrolytes were measured to be 14.2 μm/min and 1.8 μm/min, respectively.

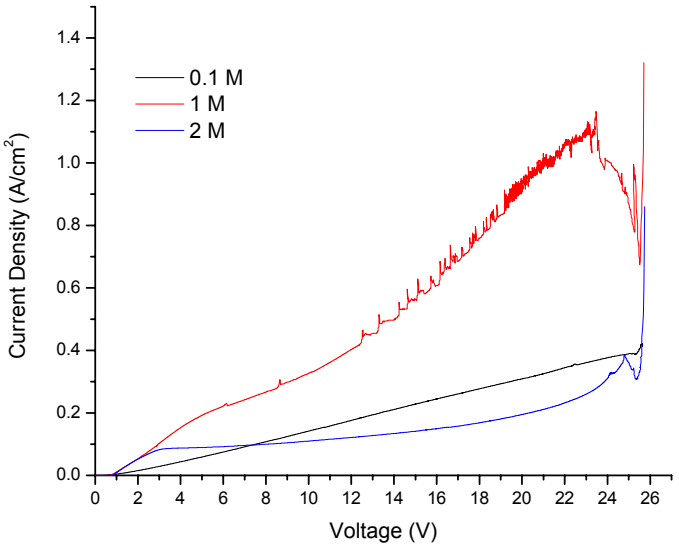

(a)

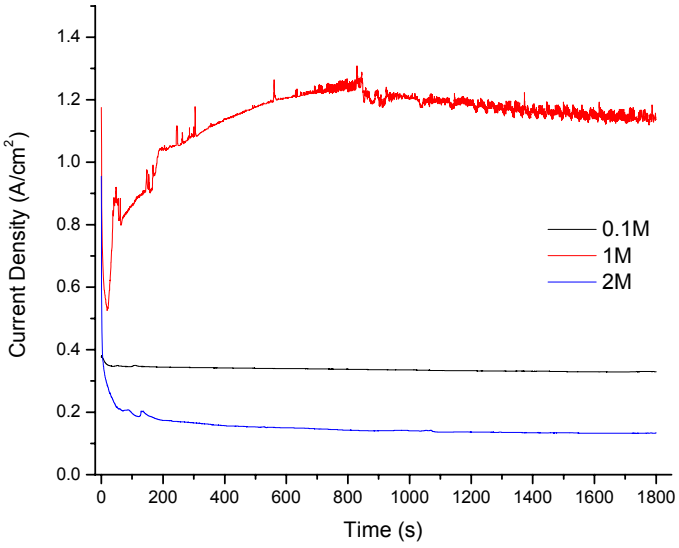

(b)

Figure 3.12: Nb (a) C-V and (b) C-t curves (22 V, 30 min) measured in 0.1 M, 1 M, and 2 M sulfuric acid-methanol electrolytes at -30^{o}C.

Surface characterization

Figure 3.13 shows the SEM images of the Nb surfaces electropolished in the 1 M and 2 M electrolytes at -30^{o}C. The height contrast corresponding to the grain is no longer observed while the orientation contrast dominates on both images. The orientation contrast indicates that EP in the 1 M and 2 M electrolytes result in less preferential dissolution at grain boundaries or due to the crystal orientation than that in the 0.1 M electrolyte. The surface polished in the 1 M and 2 M electrolytes at -30^{o}C is flat enough to present the surface orientation contrast other than the height contrast. The image contrast indicates that EP in the 1 M electrolyte results in a stronger surface waviness than that in the 2 M electrolyte. The dark area denotes the recess on Nb surface. The R_a measured on the surfaces electropolished in the 1 M and 2 M electrolytes are approximately 80 nm/mm and 40 nm/mm, respectively, which are much smaller than that measured on the surface electropolished in the 0.1 M electrolyte (several hundred nanometers to several microns).

The investigations of R_{rms} and surface profile as a function of length scale (figure 3.14) show that surfaces electropolished in the 1 M and 2 M electrolytes are much smoother than that electropolished in the 0.1 M electrolyte at both macroscopic and microscopic scales. The smaller roughness at the microscopic scale denotes a stronger grain boundary elimination. On the other hand, figure 3.14 (a) shows that R_{rms} of surface electropolished in the 2 M electrolyte is smaller than that in the 1 M electrolyte along the whole length scale, which indicates that EP in the 2 M electrolyte provides an even better surface finish than that in the 1 M electrolyte at both macroscopic and microscopic scales. The surface

profile curves as shown in figure 3.14 (b) present high noises, however it is enough to demonstrate that the surface profile of the surface electropolished in the 2 M electrolyte distributes in a smaller range than that electropolished in the 1 M electrolyte.

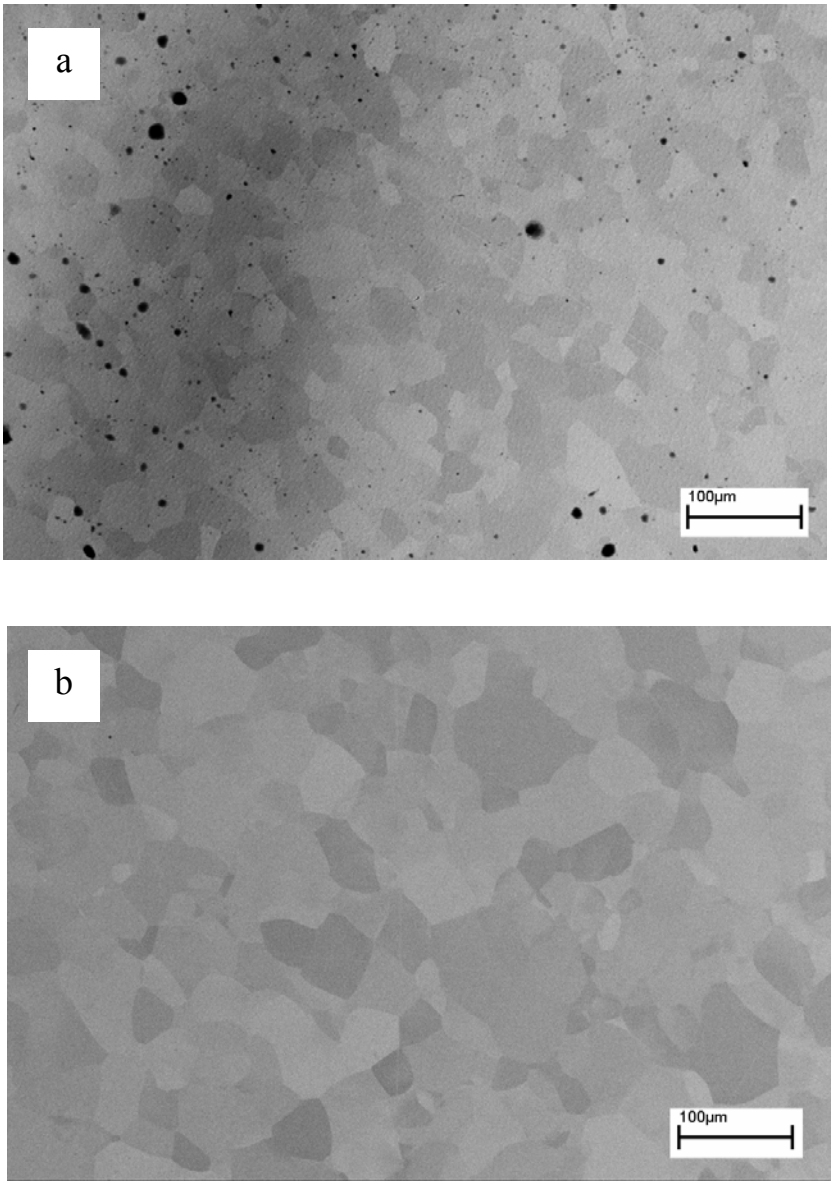

Figure 3.13: SEM images by using RBSD of Nb surfaces electropolished in the (a) 1 M and (b) 2 M sulfuric acid-methanol electrolytes at 22 V for 30 min at -30^{o}C.

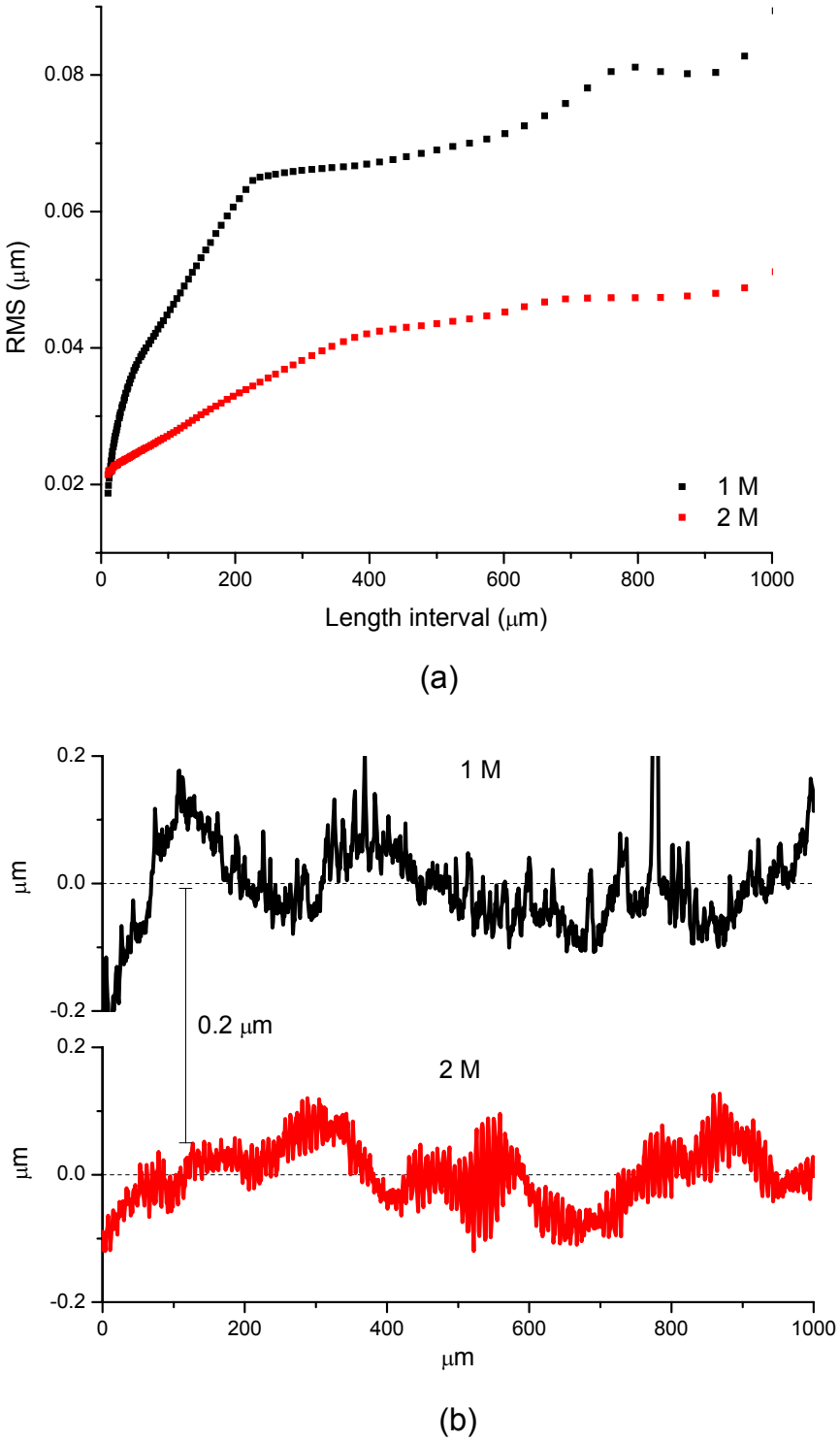

Figure 3.14: (a) R_{rms} as a function of length scale and (b) surface profiles of Nb surfaces electropolished in the 1 M and 2 M electrolytes at 22 V for 30 min at -30°C.

3.4 Summaries

EP processes of Nb were performed in sulfuric acid-methanol electrolytes in an electrochemical cell of two-electrode setup. During EP in the 0.1 M electrolyte, the current shows temperature dependence. The surface finish shows that longer EP results in a roughing surface at both macroscopic and microscopic scales. Low temperature EP contributes little to the grain boundary elimination but helps to flatten macroscopic surface profile. Both the corrosion rate and the surface roughness obtained by EP in the 0.1 M electrolyte are comparable to and even better than those obtained by HF-based BCP and EP. Compared to EP in the 0.1 M electrolyte, EP processes in the 1 M and 2 M sulfuric acid-methanol electrolytes at -30^{o}C obtain a smoother surface profile at macroscopic scale and a stronger grain boundary elimination at microscopic scale. The surface electropolished in the 2 M electrolyte shows the best surface finish, which is independent on current. Further, the higher water content—0.49wt% for the 2 M electrolyte and 0.21wt% for the 1 M electrolyte—does not lead to the formation of the protective oxides preventing further surface finish.

References

1. O. Piotrowski, C. Madore, and D. Landolt, Electrochim. Acta **44**, 3389 (1999).
2. H. Tian, Surface study of niobium for superconducting radio frequency (SRF) accelerators, PhD thesis, College of William and Mary (2008).
3. R. Peng, C. Crawford, H. Padamsee, A Seaman, Proceeding of 12th international workshop of RF superconductivity, Ithaca, NY USA (2005).
4. K. Satio, Y. Kojina, T. Furuya, S. Mitsunobu, S. Noguchi, K. Hosoyama, T. Nalazato, T. Tajima, K. Asano, K. Inoue, Y. Lino, H. Nomura, and K. Takeuchi, Proceeding of 4th of RF superconductivity, KEK, Tsukuba, Japan, p635 (1989).
5. F. Juliao, J. Chagas, H. Cesar, N. Dias, F. Decker, and U. Gomes, Electrochim. Acta **36**, 1297 (1991).
6. Arsova, A. Prusi, T. Grcev, and L. Arsov, J. Serb. Chem, Soc. **71**, 177 (2006).
7. H. Tian, G. Ribeil, M. Kelley, and C. Reece, Proceeding of 13th international workshop of RF superconductivity, Beijing, China (2007).
8. O. Piotrowski, C. Madore, and D. Landolt, J. Electrochem. Soc. **145**, 2362 (1998).
9. D. Landolt, Electrochim. Acta. **32**, 1 (1987).
10. K. Satio, Proceeding of the 2003 particle accelerator conference, Portland, OR USA, p462 (2002).
11. H. Tian, C. Reece, M. Kelley, S. Wang, L. Plucinski, and K. Smith, Appl. Surf. Sci. **253**, 1236 (2006).
12. F. Chauvy, C. Madore, and D. Landolt, Surf. Coat. Technol. **110**, 48 (1998).
13. O. Piotrowski, C. Madore, and D. Landolt, Plat. Surf. Finish. **85**, 115 (1998).

Chapter 4

Electropolishing of niobium: Three-electrode setup

4.1 Introduction

In the present chapter, EP of Nb in a three-electrode electrochemical cell is presented. The electrolytes are sulfuric acid-methanol solutions. The influence of electrolyte concentration, temperature, and EP duration is investigated. The limiting current plateau is shown to depend upon concentration and temperature. Both macrosmoothing and microsmoothing are achieved according to the surface characterization. Also present is the improvement of surface finish after sufficient long potential hold to remove material over 100 μm.

4.2 Experimental procedures

Nb working electrodes

The polycrystalline Nb plates were embedded in epoxy cylinder with a diameter of 10 mm. The area of working electrode was about 0.4 cm^2. The Nb plates were cut from the

high-RRR-grade fine grain Nb sheet stock used to make standard SRF cavities. The stock has a purity of 99.9999% according to the manufacture (Wah Chang, USA). Prior to the electrochemical experiments, each Nb working electrode was mechanically polished by 600 grit emery papers, rinsed in methanol, and then conserved in the dry keeper (SANPIA, USA).

Electrolytes

The electrolytes were prepared by sulfuric acid (Certified ACS plus, 98%, Fisher Chemical) and methanol (HPLC grade, 99.9%, Fisher Chemical). The concentrations of sulfuric acid in the methanol solutions were 0.5 M, 1 M, 2 M, and 3 M. The water content of each concentration was calculated from the weight ratio and is shown in table 4.1. The detail of calculation is introduced in Appendix A. The maximum water content is calculated to be 0.66 wt% for the 3 M electrolyte. This is lager than the practical measurement (0.2%) by Karl-fisher methods for the 3 M electrolyte prepared by the identical reagents [1-3]. Since the calculation was performed by assuming water content the only impurity in each reagent, the practical water content is expected to be smaller than the calculated value.

Table 4.1: Water content in sulfuric acid-methanol electrolytes calculated from the weight ratio.

Concentration (M)	Water content (wt%)
0.5	0.21
1	0.31
2	0.49
3	0.66

Electrochemical experiments

The electrochemical experiments were performed in an electrochemical cell with a three-electrode setup. The counter electrode was a platinum foil and the reference electrode was mercury/mercurous sulfate electrode (MSE). All the potential given in the present chapter refer to the MSE reference electrode. The working-to-counter separation was about 3 cm. A potentiostat (Model 263A, EG&G, Princeton Applied Research) was used to measure the anodic polarization (C-V) curves. The voltage was swept from 9 V to 0 V at a rate of -10 mV/sec. The negative scanning direction was for the reproducible limiting current [1]. The EP processes were performed by holding potential at 9 V and the transient current (C-t) curves were measured simultaneously. During low temperature experiments, the cell was placed in a reservoir and cooled by ethanol. The temperatures were controlled by a chiller. A thermometer was used to monitor the electrolyte temperature. All the electropolished working electrodes were conserved in the dry keeper again until no more weight loss was measured. The finally recorded weight loss was used to estimate the corrosion rate.

Surface characterization

The topography of electropolished Nb working electrodes was captured by scanning electron microscopy (SEM, Leo (Zeiss) 1550). A Robinson backscatter detector (RBSD) was used to acquire the surface orientation contrast. A profilometry (Alfa-step 500, KLA-TENCOR) was also performed to study the surface roughness. The scan length was 1 mm. The roughness of each surface was measured at five different places at least. The average roughness with standard deviation was calculated. As a characterization of

microsmoothing, relationship between the root mean square roughness (R_{rms}) and the length scale was calculated. Detail of these characterization techniques is introduced in chapter 2.

4.3 Results and discussion

4.3.1 Electrochemical experiments

C-V curves

Figure 4.1 shows the C-V curves measured in sulfuric acid-methanol electrolytes of 0.5 M, 1 M, 2 M, and 3 M at room temperature, 0°C, -10°C, and -30°C. The C-V curves show well-pronounced limiting current plateaus for multiple conditions and behave similar to those measured by Piotrowski on Ta and Ti in sulfuric acid-methanol electrolytes [1-3]. For example, at room temperature (figure 4.1 (a)), there is only a very short plateau at the beginning of the voltage scan in the 0.5 M electrolyte. The majority of the curve shows a linear relationship between current and voltage. A linear current-voltage behavior is also observed for the EP of Ta in the 0.5 M electrolyte. Linear C-V curve is indicative of an ohmic resistance limited current. No polishing but rather etching and/or pitting is observed in this voltage range [1]. The Nb surface in this work appeared etched after the voltammetry. The current minimum appearing at the beginning of the voltage scan is consistent with the formation and detachment of an anodic film [1]. The C-V curve measured in the 3 M electrolyte on the other hand displays a well-pronounced limiting current plateau extending from approximately 1 to 9 V. A current plateau indicates a

mass transport controlled current [1, 4]. The surface after dissolution under conditions within the plateau appeared polished and bright to the unaided eyes.

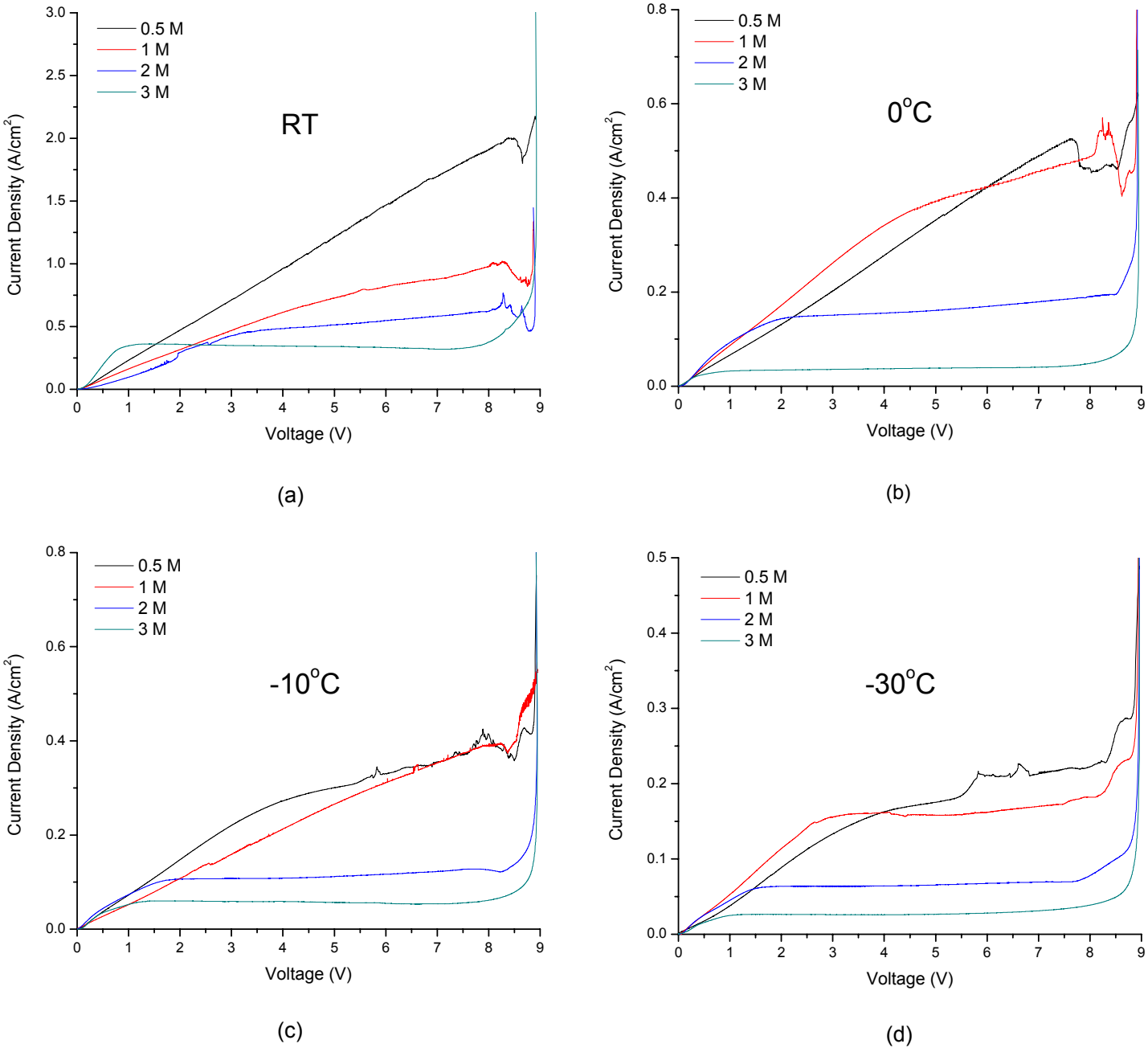

Figure 4.1: Nb C-V data measured in 0.5 M, 1 M, 2 M, and 3 M sulfuric acid-methanol electrolytes at (a) room temperature, (b) 0°C, (c) -10°C, and (d) -30°C at a scan rate of -10 mV/s.

The value of the current plateau decreases as the electrolyte concentration increases—the plateau measured in the 0.5 M electrolyte is about 2 A/cm^2, which is almost an order of magnitude larger than that in the 3 M electrolyte (about 0.3 A/cm^2). The decreasing current plateau is consistent with a decreasing solubility of metal ions and an increasing stability of an anodic film [3]. On the other hand, as the value of the plateau decreases, the voltage range of the plateau expands—the plateau range measured in the 0.5 M electrolyte is smaller than 1 V while that in the 3 M electrolyte extends from 1 to 9 V. The limiting current in this region is controlled by a surface anodic film which we show in chapter 5 is of a compact film nature.

The current plateau is also influenced by temperature. Figures 4.1 (b) to (d) show C-V curves measured at 0^{o}C, -10^{o}C, and -30^{o}C. The value of the plateau decreases as the temperature is decreased. With the decreasing temperature, we expect a decreased Nb ion solubility, an increased anodic film stability, and a decreased dissolution rate in the electrolyte. The magnitude of decrease depends upon electrolyte concentration—the current measured in the 0.5 M electrolyte decreases from 2 to 0.24 A/cm^2, while the current measured in the 3 M electrolyte decreases little. The plateau also expands with decreasing temperature. At -30^{o}C, all electrolytes display well-pronounced current plateaus consistent with increased mass transport limitations at the low temperature.

C-t curves

Figure 4.2 shows the C-t curves measured during Nb as a function of temperature and electrolyte concentration. An EP voltage of 9 V was used for a duration of 30 min. The

current minimum at the beginning of the potential hold is consistent with the formation and dissolution of an anodic surface film [1]. The current value decreases as the concentration increases and also as the temperature decreases. The magnitude of the current decrease depends on the electrolyte concentration. These behaviors are similar to those observed for the C-V data. There appears to be a transition of the limiting current from a larger value measured in the lower concentrations of 0.5 M and 1 M to a smaller value measured in the higher concentrations of 2 M and 3 M. These differences are also reflected in the final surface finish.

Average current

Figure 4.3 shows the average current calculated from the current displayed in figure 4.2. The average current can be used to predict the dissolution rate of Nb assuming the current is solely due to the Nb dissolution. This dissolution rate (*r'*, μm/min) is defined as:

$$r' = \frac{\frac{Q}{96500 \times n} \times M}{A \times \rho \times t} = \frac{i \times M}{96500 \times n \times \rho} \tag{4.1}$$

where Q is the total charge passed (C), M is the atomic weight of Nb (93 g/mol), n is the oxidation state of Nb ions (assumed to be five), A is the electrode surface area (cm^2), t is the EP duration (min), ρ is the density of Nb (8.57 g/cm^3), and i is the average current density (A/cm^2). One can also find from figure 4.3 that the dissolution rate decreases with decreasing temperature for the majority of concentrations. However, temperature does not influence the dissolution rate in the 3 M electrolyte. Concentration also influences the dissolution rate. Higher concentrations such as 2 M and 3 M result in lower dissolution rates.

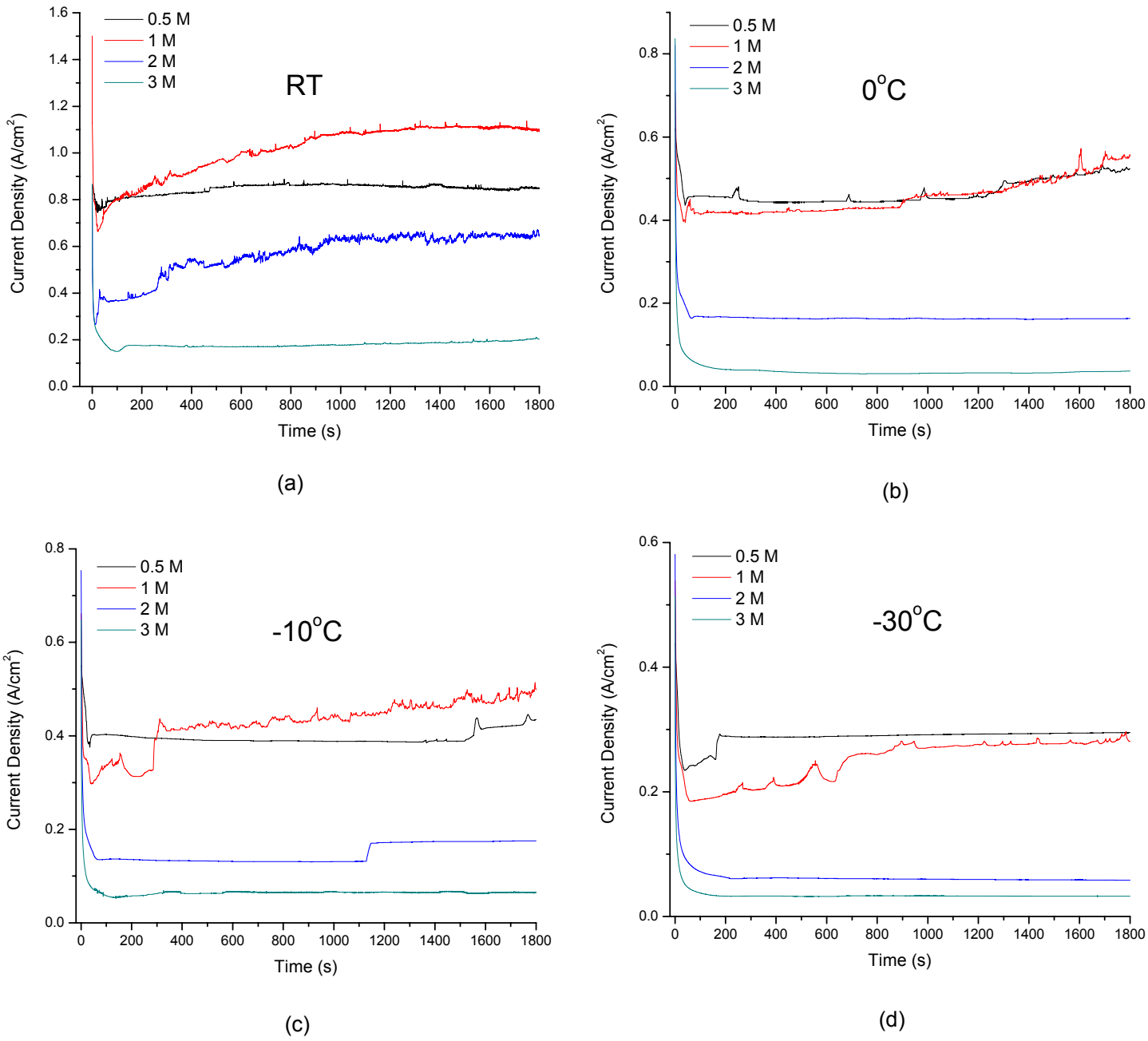

Figure 4.2: Nb C-t curves measured during EP at 9 V for 30 min in 0.5 M, 1 M, 2 M, and 3 M sulfuric acid-methanol electrolytes at (a) room temperature, (b) 0°C, (c) -10°C, and (d) -30°C.

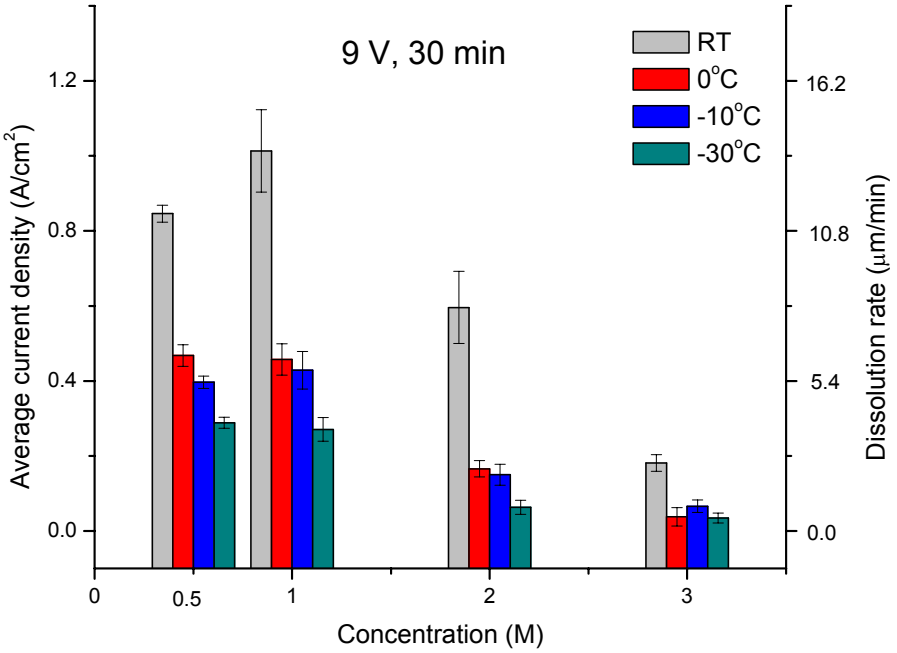

Figure 4.3: Average current versus electrolyte concentration and temperature. Dissolution rate calculated from the average current assuming 5 e^- transfer is shown on the right vertical axis.

Corrosion rate and thickness removal

Figure 4.4 shows the corrosion rate and the thickness removal calculated from weight loss measurements for EP at 9 V for 30 min. The corrosion rate is calculated by the equation 3.1. The thickness removal is calculated assuming a consistent corrosion rate for the 30 min EP., The methanol-based EP under multiple conditions results in comparable corrosion rates (> 0.4 μm/min) to the HF-based BCP and EP. The corrosion rates obtained in the 0.5 M and 1 M electrolytes are comparable to the HF-based BCP rates—up to 10 μm/min [5, 6]. Further, the corrosion rates shown in figure 4.4 (a) are approximately equivalent to the dissolution rates shown in figure 4.3. This confirms the assumption that the recorded EP current is mainly due to Nb dissolution.

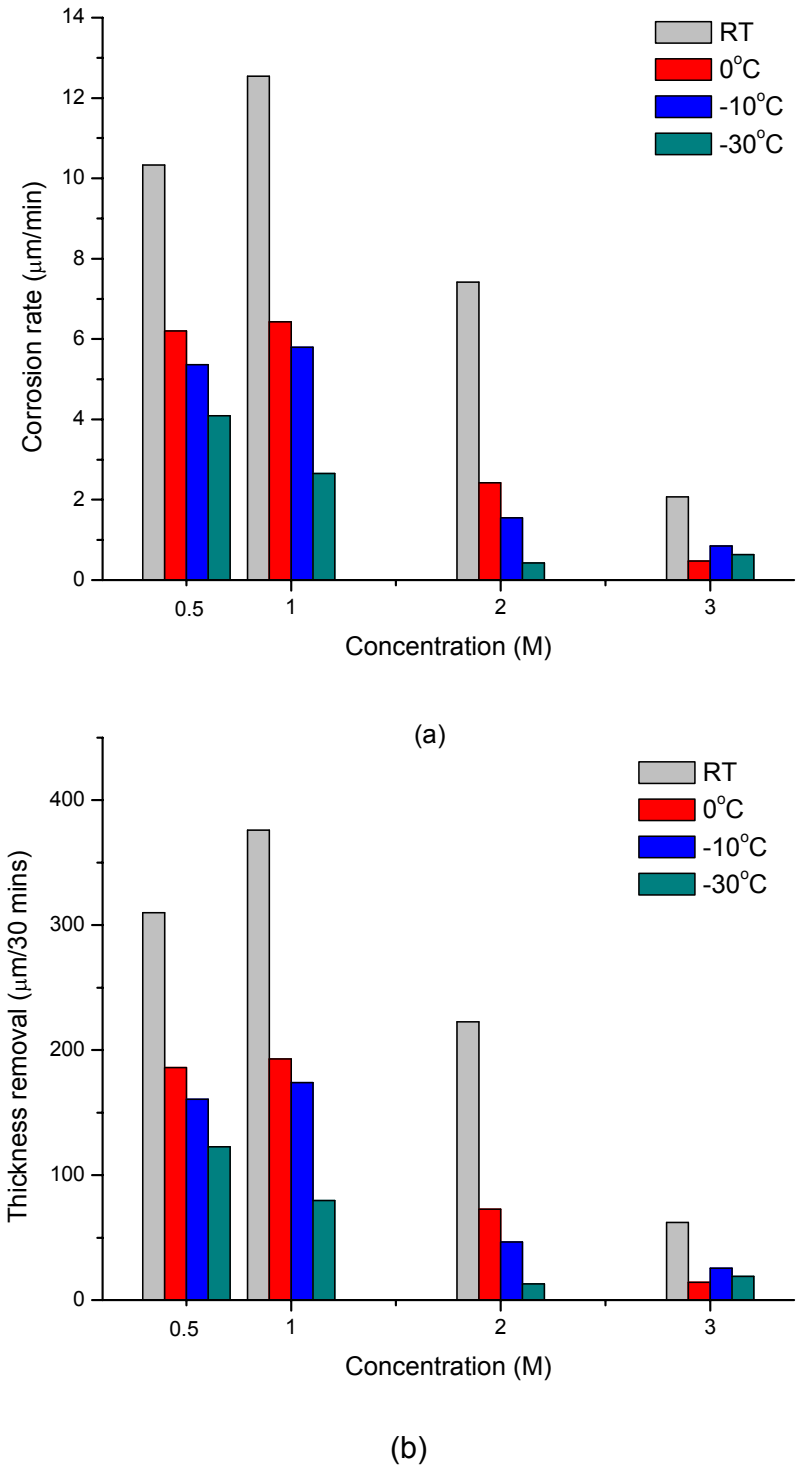

Figure 4.4: (a) Corrosion rate and (b) thickness removal calculated from weight loss measurements following EP at 9 V for 30 min.

Figure 4.4 (b) represents the thickness removal. The EP process performed in the 0.5 M and 1 M electrolytes results in a total material removal of > 100 μm under most conditions. However, the EP process in the 2 M and 3 M electrolytes results in a material removal of < 100 μm.

4.3.2 SEM images by using RBSD

Figures 4.5 and 4.6 show SEM images by using RBSD of Nb surfaces electropolished in the 0.5 M electrolyte at 9 V for 30 min. The two magnifications are 600 x and 1500 x, respectively. Surface polished at -30^{o}C shows a surface orientation contrast image while surfaces polished at the other temperatures show a height contrast. The average size of grains is about 50 μm. The sharp grain boundaries may be related to etching or macrosmoothing. The orientation contrast resulted only from -30^{o}C is confirmation of microsmoothing, i.e. no preferential dissolution is observed at grain boundaries or due to the crystal orientation. Further, one may observe from the higher resolution images that the height variation across grains decreases with decreasing temperature. Note that the small black spots are contaminations that do not channel the backscattered electrons.

Figures 4.7 and 4.8 show SEM images for Nb surfaces electropolished in the 1 M electrolyte at 9 V for 30 min by using RBSD. Height variations across grains are evident at room temperature while orientation contrast dominates on the surfaces polished at the other three temperatures (again indicating the smoothness achieved in these surfaces). Both the 0.5 M and the 1 M electrolytes result in microsmoothing at -30^{o}C indicating mass transport control.

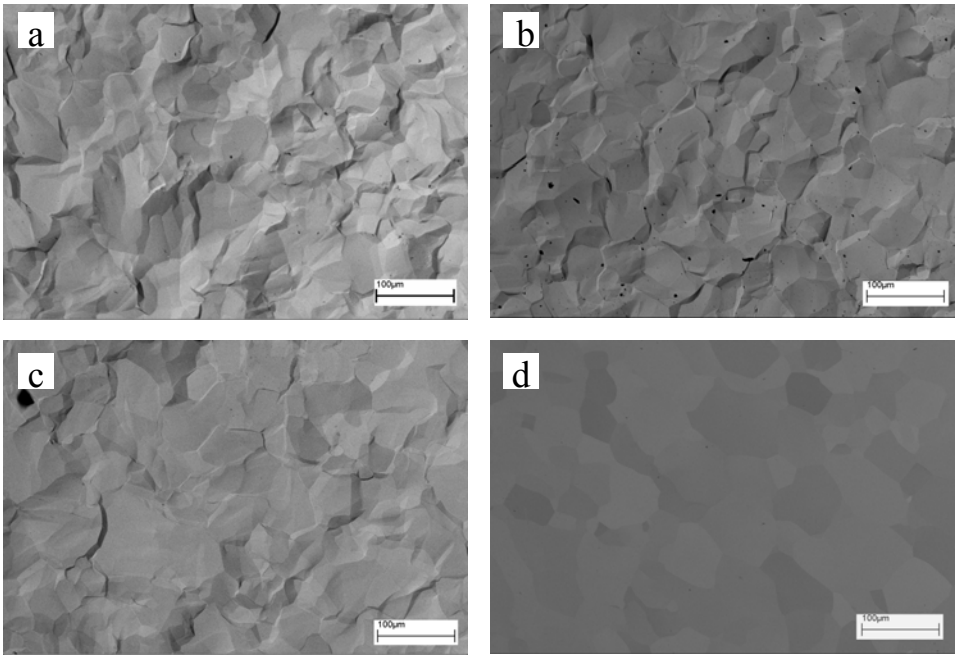

Figure 4.5: SEM images (600 x) by using RBSD of Nb surfaces electropolished in the 0.5 M electrolyte at 9 V for 30 min at (a) room temperature, (b) 0^{o}C, (c) -10^{o}C, and (d) -30^{o}C.

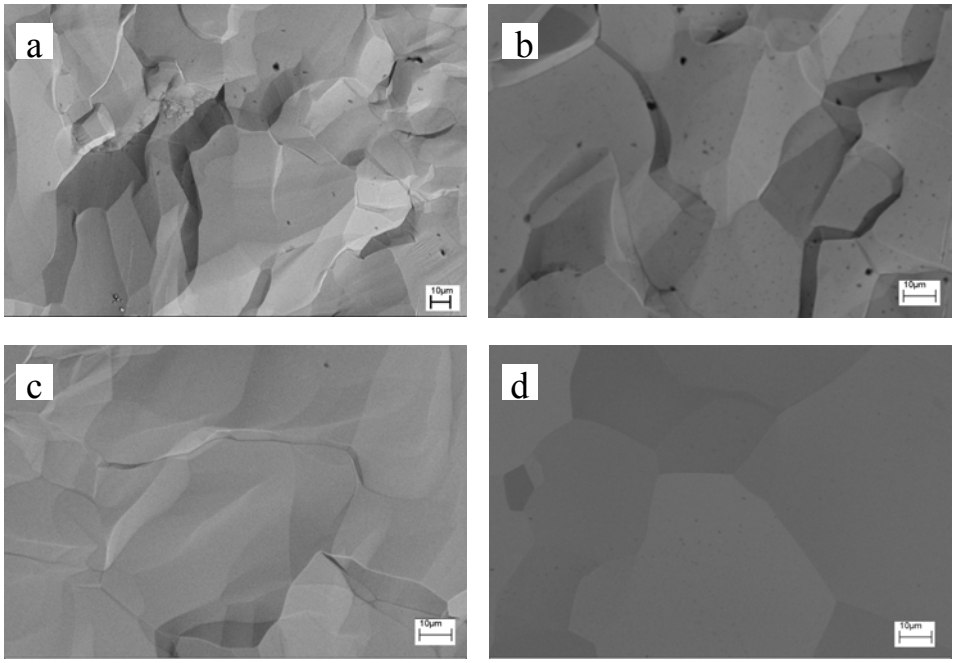

Figure 4.6: SEM images (1500 x) by using RBSD of Nb surfaces electropolished in the 0.5 M electrolyte at 9 V for 30 min at (a) room temperature, (b) 0^{o}C, (c) -10^{o}C, and (d) -30^{o}C.

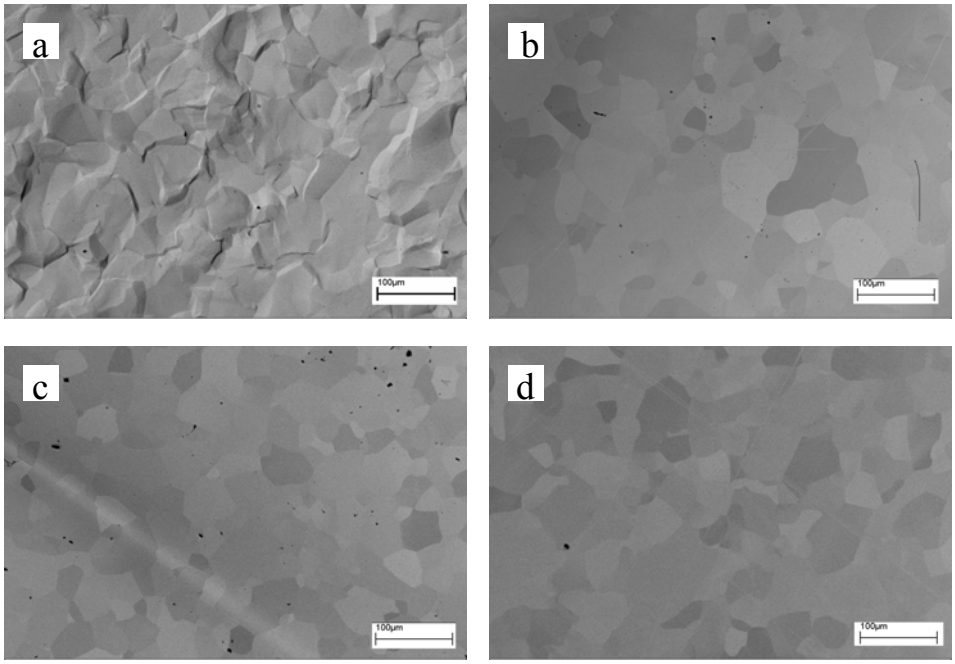

Figure 4.7: SEM images (600 x) by using RBSD of Nb surfaces electropolished in the 1 M electrolyte at 9 V for 30 min at (a) room temperature, (b) 0^{o}C, (c) -10^{o}C, and (d) -30^{o}C.

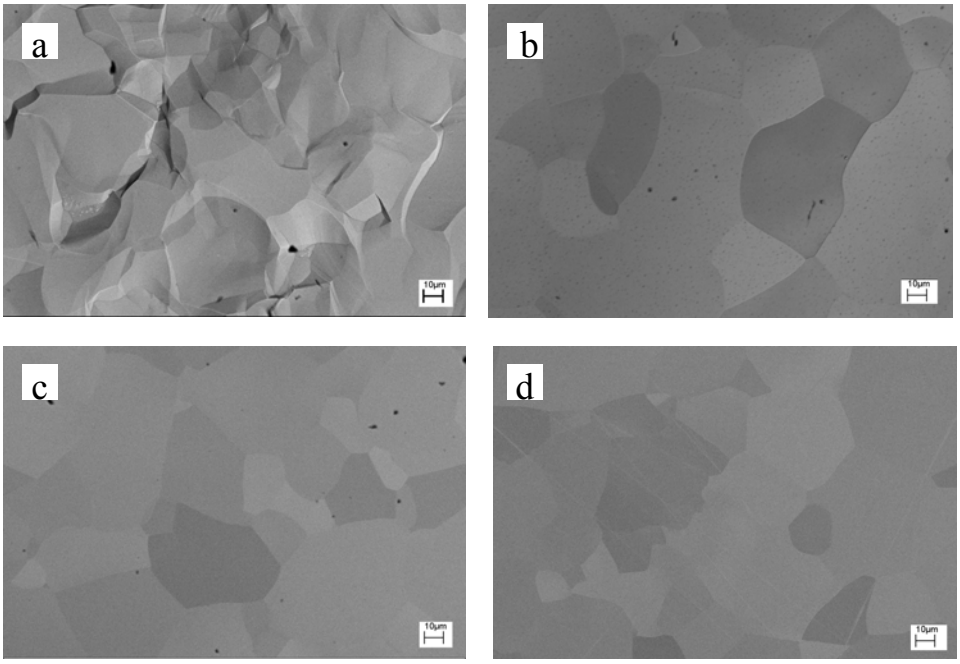

Figure 4.8: SEM images (1500 x) by using RBSD of Nb surfaces electropolished in the 1 M electrolyte at 9 V for 30 min at (a) room temperature, (b) 0^{o}C, (c) -10^{o}C, and (d) -30^{o}C.

Figures 4.9 and 4.10 show SEM images captured on Nb surfaces electropolished in the 2 M electrolyte at 9 V for 30 min by using RBSD. Orientation mapping appear on surfaces polished at all four temperatures. Array of tiny pits observed on the surface polished at room temperature (figure 4.10 (a)) is identical to those observed on the copper surface polished by Sautebin et al, who related the tiny pits to uniform atoms removal [4, 7, 8]. Corresponding to the limiting current plateau at every temperature, microsmoothing is believed to be achieved in the 2 M electrolyte under mass transport control. Figures 4.11 and 4.12 show identical surfaces polished in the 3 M electrolyte to those polished in the 2 M electrolyte. It is likely that EP at a lower temperature or in a higher concentration result in a better surface finish. However, EP processes at these conditions also result in a slower corrosion rate and an insufficient thickness removal—mechanically introduced scratches appear on the surfaces polished at -30^{o}C.

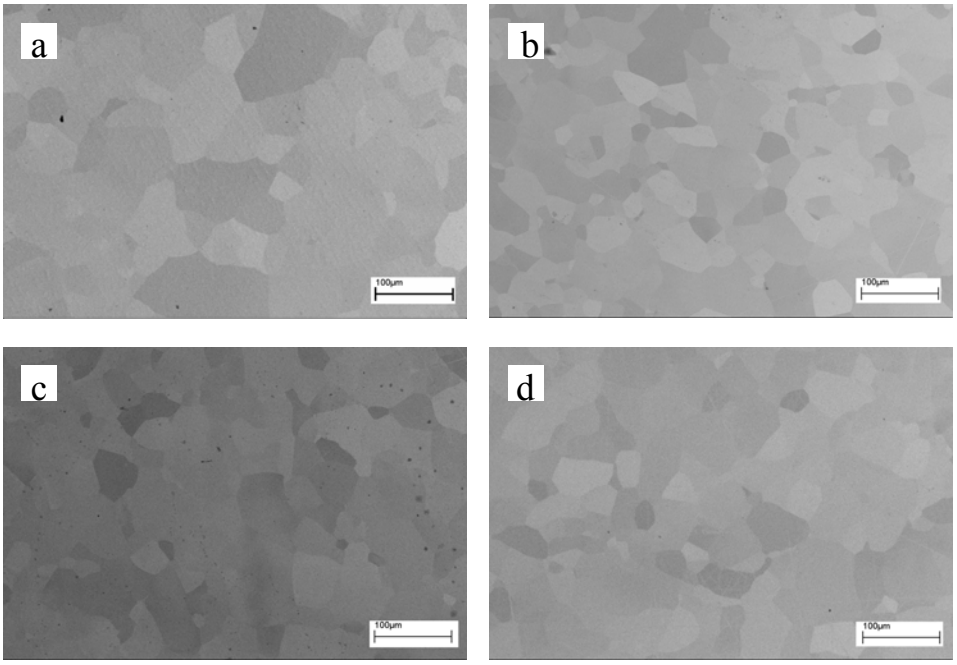

Figure 4.9: SEM images (600 x) by using RBSD of Nb surfaces electropolished in the 2 M electrolyte at 9 V for 30 min at (a) room temperature, (b) 0^{o}C, (c) -10^{o}C, and (d) -30^{o}C.

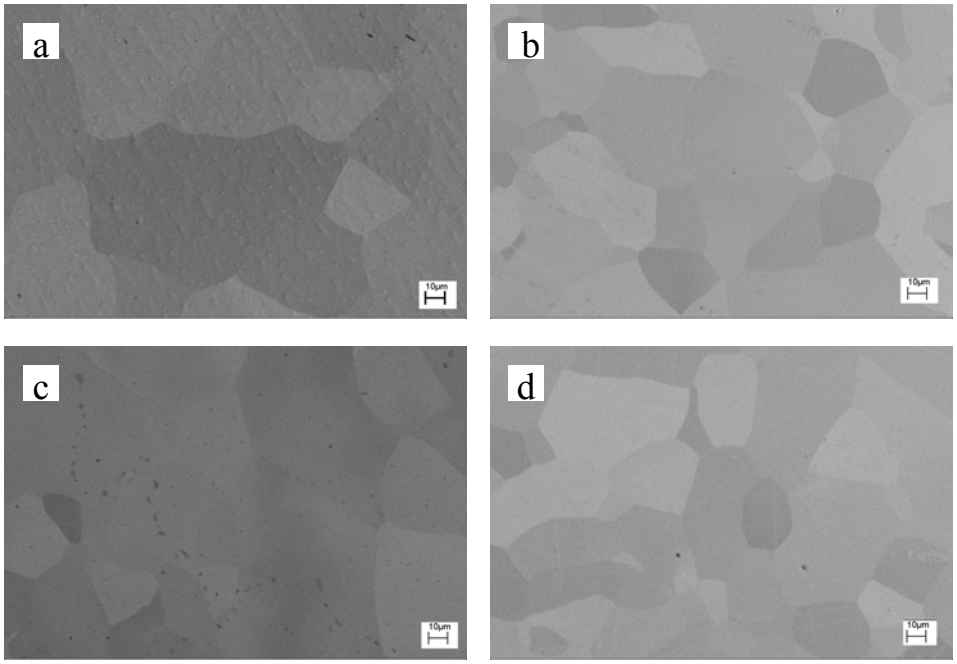

Figure 4.10: SEM images (1500 x) by using RBSD of Nb surfaces electropolished in the 2 M electrolyte at 9 V for 30 min at (a) room temperature, (b) 0^{o}C, (c) -10^{o}C, and (d) -30^{o}C.

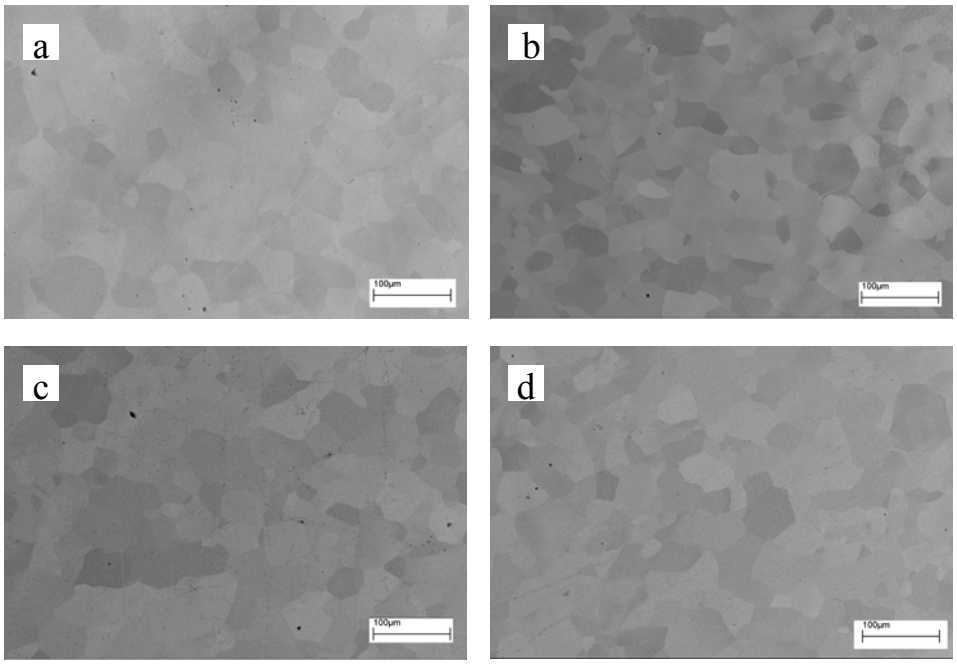

Figure 4.11: SEM images (600 x) by using RBSD of Nb surfaces electropolished in the 3 M electrolyte at 9 V for 30 min at (a) room temperature, (b) 0^{o}C, (c) -10^{o}C, and (d) -30^{o}C.

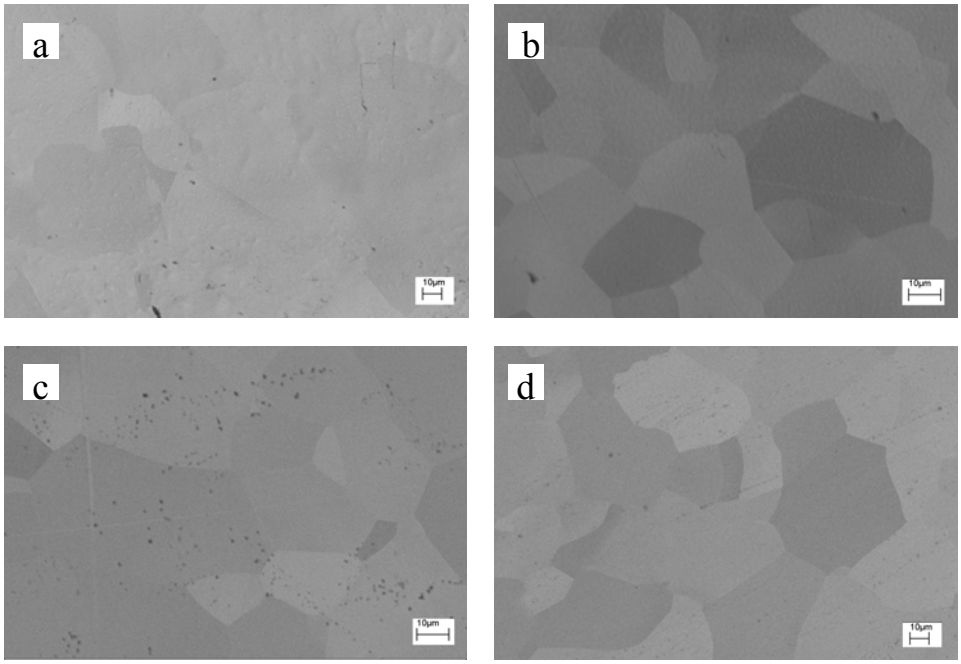

Figure 4.12: SEM images (1500 x) by using RBSD of Nb surfaces electropolished in the 3 M electrolyte at 9 V for 30 min at (a) room temperature, (b) 0°C, (c) -10°C, and (d) -30°C.

4.3.3 Profilometry

As a quantitative characterization of the surface finish, table 4.2 summarizes the average roughness (R_a) and standard deviation measured on the Nb surfaces electropolished under the indicated conditions. The scan length was 1 mm with a lateral resolution of 1 μm. The 1 M EP at room temperature, the 0.5 M EP at room temperature, and the 0.5 M EP at 0°C resulted in a roughness on the scale of a few microns. This result is comparable to that obtained by HF-based EP and is related to the differences in dissolution rate across grains. Significant EP improvement is found under the conditions shaded gray in table 4.2. The R_a values of these surfaces were of order of a few hundred nanometers and decreased with decreasing temperature. The surfaces were sufficiently flat that crystallographic

orientation contrast is observed in the SEM images with no height contrast observable. The C-V data for theses conditions show well-pronounced current plateaus. The R_a value over the 1 mm length scale represents the degree of macrosmoothing. To fully characterize the surface polishing, the roughness values over smaller length scale are needed.

Table 4.2: Average surface roughness (R_a, nm) of Nb working electrodes electropolished at 9 V for 30 min under conditions of various concentrations and temperatures.

	0.5 M	**1 M**	**2 M**	**3 M**
RT	2772±566	2832±1182	249±63	703±46
0°C	1517±769	240±78	134±27	478±36
-10°C	548±182	229±92	204±115	102±18
-30°C	298±38	278±118	132±34	140±27

4.3.4 Advanced surface characterization

Figure 4.13 shows the investigation on surface profile and R_{rms} of surfaces finished in the 0.5 M sulfuric acid-methanol electrolyte at 9 V for 30 min. Figure 4.13 (a) shows decreasing grain height with decreasing temperature. The R_{rms} shown in figures 4.13 (b) also shows decreasing roughness values along the whole length scale as temperature decreased. On the microscopic scale (figure 4.13 (c))—for example the scale smaller than 200 μm—the R_{rms} of surface polished at -30°C is only about 20 nm and remains constant.

Since the 200 μm scale already covers several grains (the average size of grain is 50 μm), the constant R_{rms} demonstrates that the polishing is completely uniform across the surface.

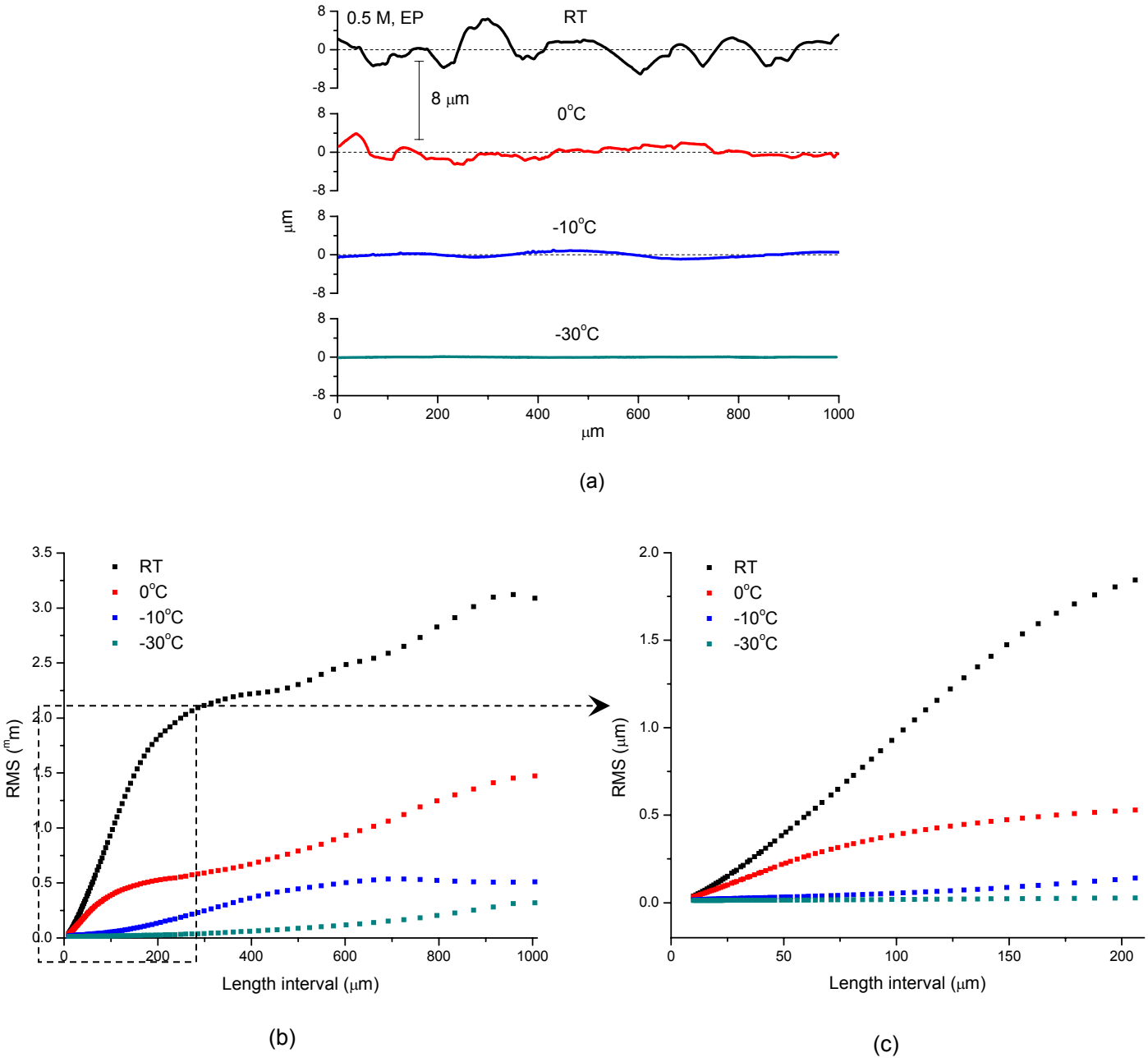

Figure 4.13: (a) Surface profile, (b) R_{rms} as a function of length scale (1 mm), and (c) R_{rms} as a function of length scale (0.2 mm) of Nb surfaces electropolished in the 0.5 M electrolyte at 9 V for 30 min.

Figure 4.14 shows the surface profile and the R_{rms} of surfaces electropolished in the 1 M sulfuric acid-methanol electrolyte at 9 V for 30 min. In contrast to surfaces polished in the 0.5 M electrolyte, the surface profile of 1 M EP shows good results at 0°C, -10°C, and -30°C. The surfaces polished at these three temperatures have a smaller R_{rms} value than that polished at room temperature. The R_{rms} values are similar for the 0°C, -10°C, and -30°C samples along the whole length scale (figure 4.14 (b)) and no grain boundary etching is observed (figure 4.14 (c)).

Figure 4.15 shows the temperature-independent surface finish for EP in the 2 M sulfuric acid-methanol electrolyte at 9 V for 30 min. Although the surface profile shows waviness with a wavelength of 100 to 300 μm, no sharp grain boundaries are present on the surface profile. The waviness only evolves in a small range of ±400 nm. The R_{rms} is temperature-independent along the whole length scale. The microscopic roughness characterization (figure 4.15 (c)) shows roughness smaller than 60 nm at 200 μm scale. According to the R_a of 100 to 200 nm/mm, EP in the 2 M electrolyte results in not only a smoother surface at macroscopic scale but also a more homogeneous polishing across grains.

The studies of the surface profile and R_{rms} of surfaces polished in the 3 M sulfuric acid-methanol electrolyte at 9 V for 30 min (figure 4.16) also show good agreement between microscopic and macroscopic characterization. The surface quality does not improve further at -30°C and is even worse than that obtained at -10°C. This fluctuation of surface finish may be related to the insufficient thickness removal of mechanical damage. If this

is true, then longer EP causing a sufficient thickness removal is expected to result in a better surface finish.

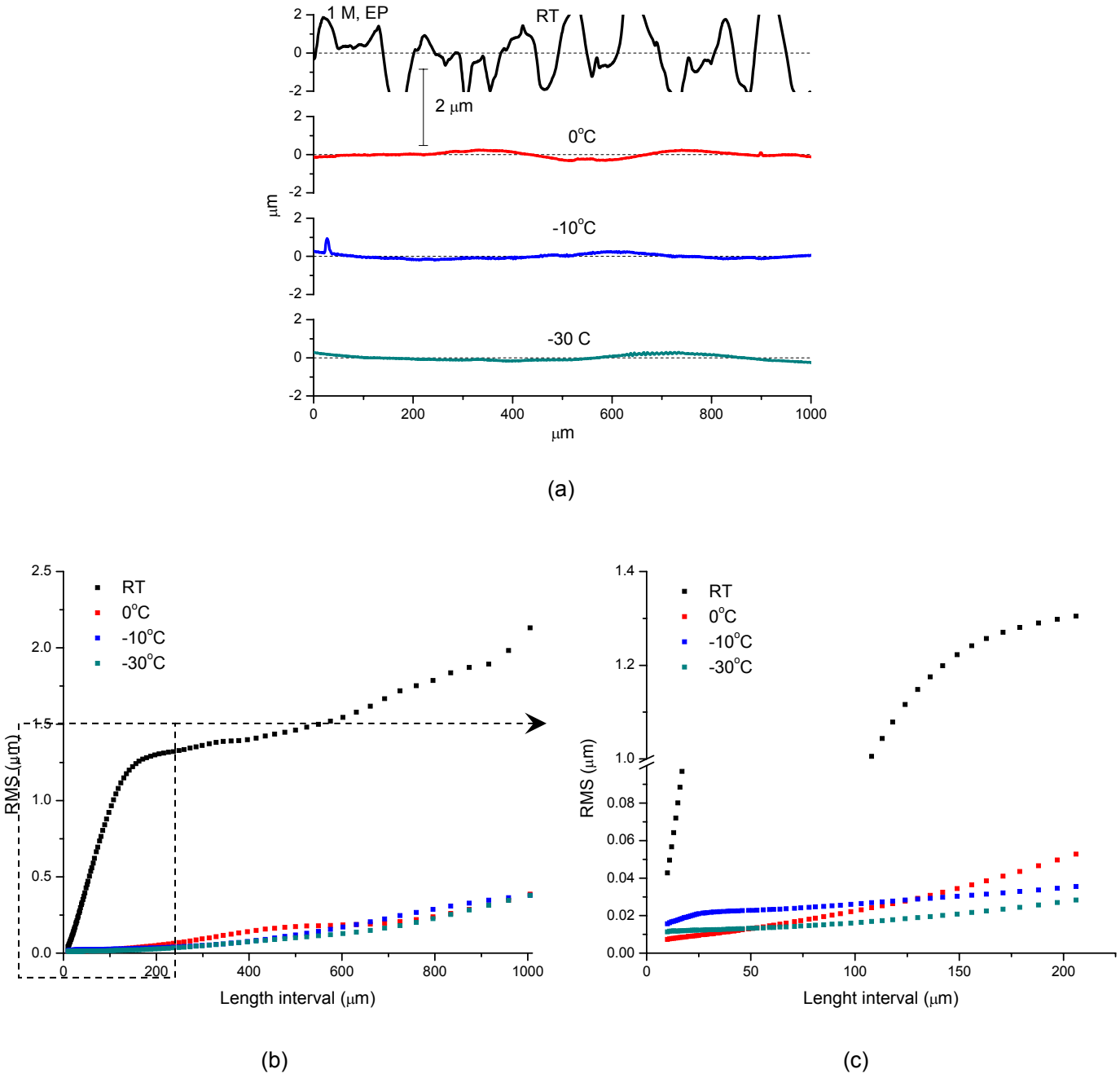

Figure 4.14: (a) Surface profile, (b) R_{rms} as a function of length scale (1 mm), and (c) R_{rms} as a function of length scale (0.2 mm) of Nb surfaces electropolished in the 1 M electrolyte at 9 V for 30 min.

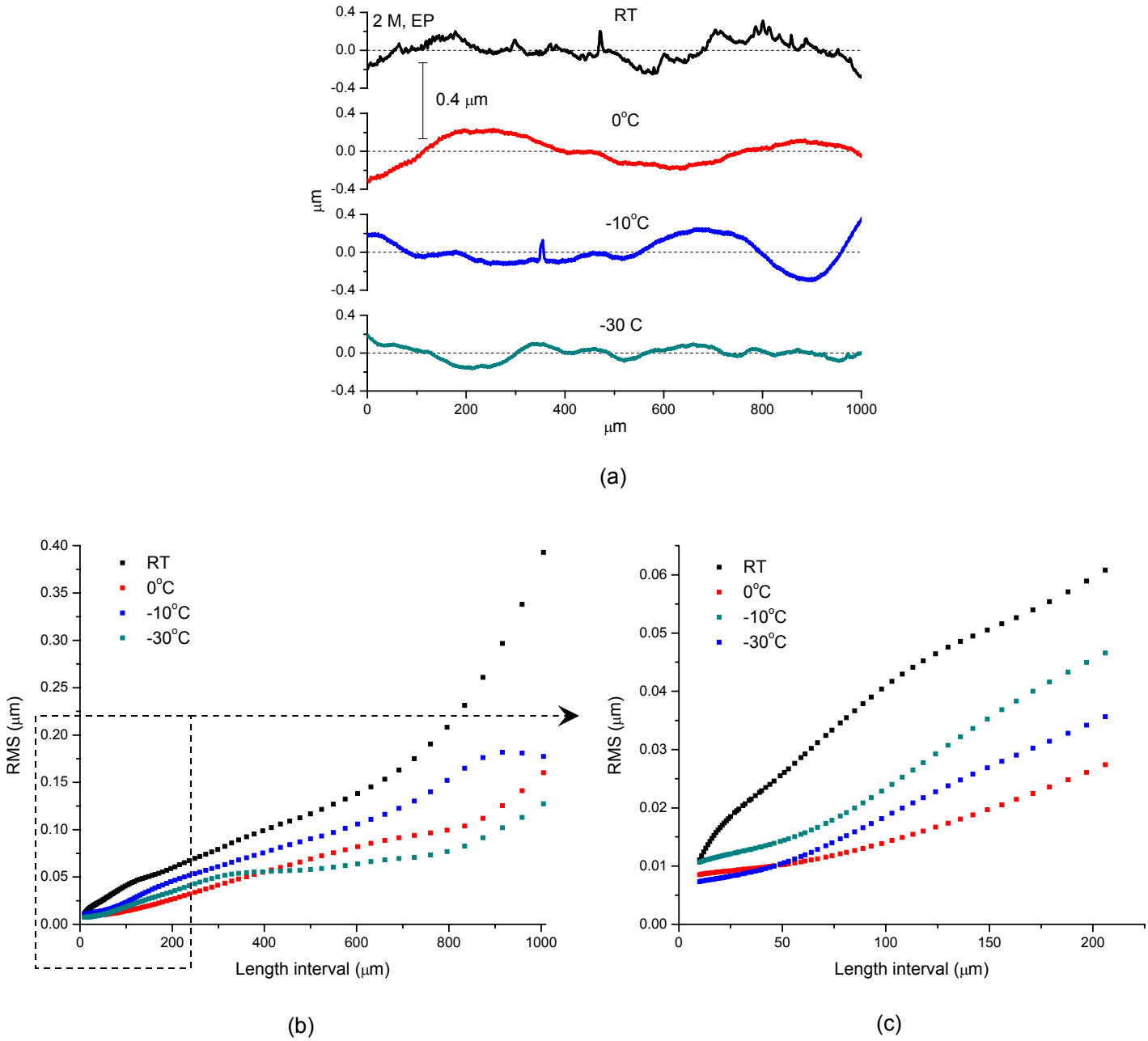

Figure 4.15: (a) Surface profile, (b) R_{rms} as a function of length scales (1 mm), and (c) R_{rms} as a function of length scale (0.2 mm) of Nb surfaces electropolished in the 2 M electrolyte at 9 V for 30 min.

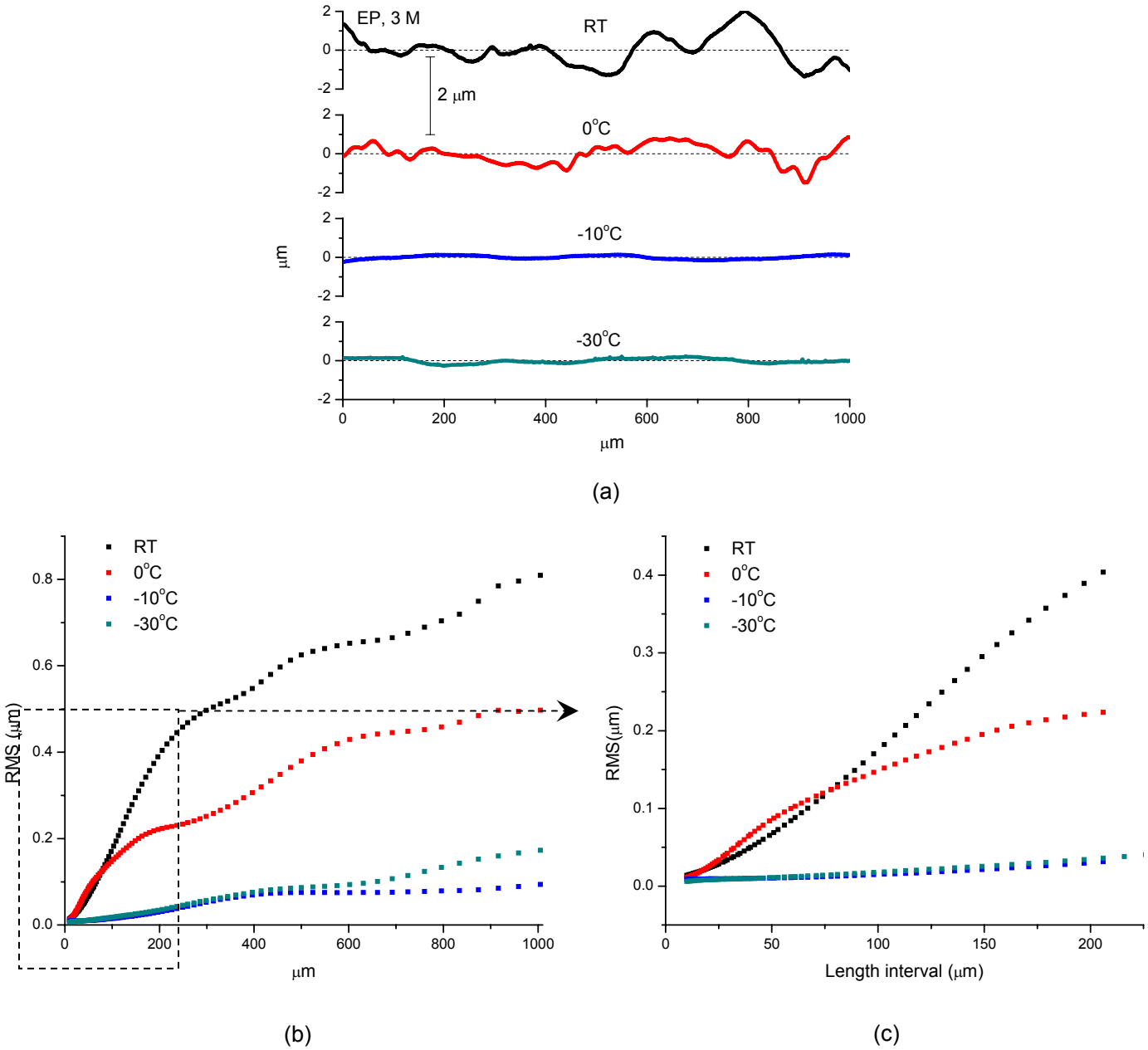

Figure 4.16: ((a) Surface profile, (b) R_{rms} as a function of length scale (1 mm), and (c) R_{rms} as a function of length scale (0.2 mm) of Nb surfaces electropolished in the 3 M electrolyte at 9 V for 30 min.

4.3.5 Influence of EP parameters on microsmoothing

As discussed previously, microsmoothing was achieved under various concentrations and temperatures. Temperature strongly influences the elimination of grain boundary etching in the 0.5 M electrolyte. However, microsmoothing is achieved at all temperatures in the 2 M electrolyte. Figure 4.17 shows the results of microsmoothing in various concentrations. At room temperature (figures 4.17 (a)), the electrolyte concentration strongly influences the R_{rms}. The surface quality improves dramatically with increasing concentration. At -30^{o}C (figures 4.17 (b)), the R_{rms} corresponding to each concentration overlaps each other and behaves concentration-independent. The impact of concentration decreases with decreasing temperature. The temperature appears to be the more critical parameter for microsmoothing.

Current is also not a critical parameter influencing microsmoothing. For example, the current measured during EP in the 0.5 M electrolyte is larger than that in the 2 M electrolyte at room temperature (figure 4.2 (a)), nevertheless the surface polished in the 2 M electrolyte shows better microsmoothing. Moreover the surfaces polished at -30^{o}C are similar in the 0.5 M and 2 M electrolytes, but the current in the 0.5 M electrolyte is much higher (figure 4.2 (d)).

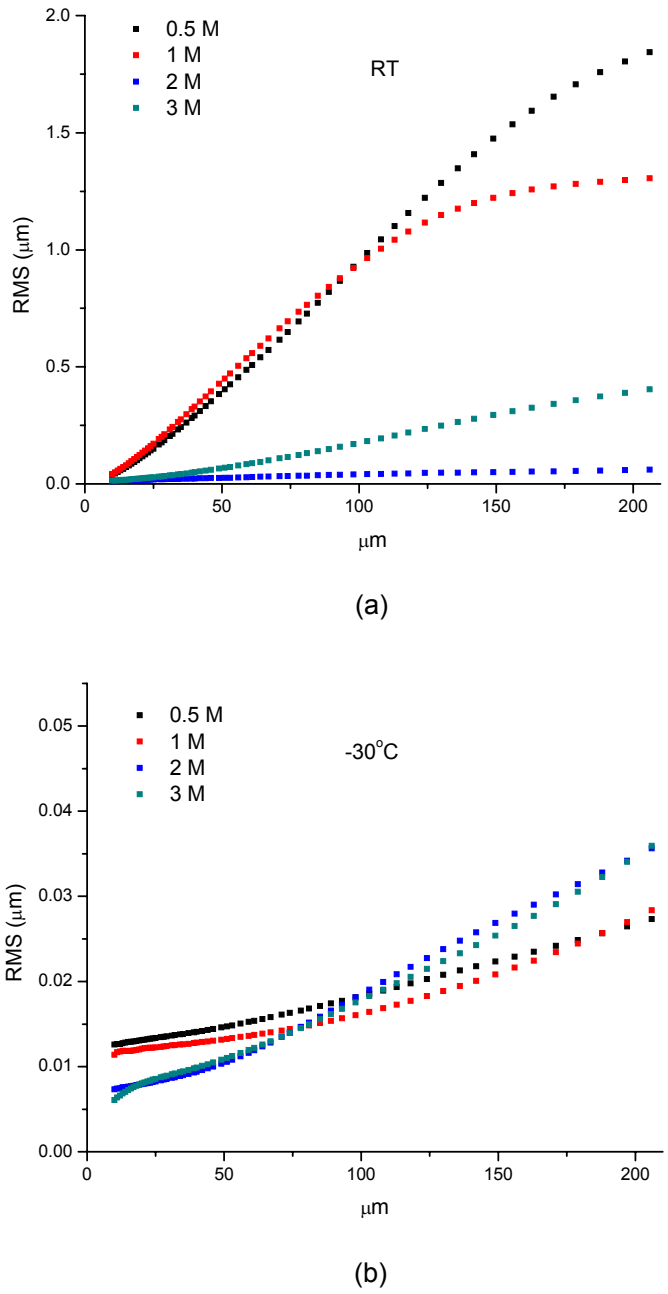

Figure 4.17: R_{rms} as a function of length scale (0.2 mm) of Nb surfaces electropolished at 9 V for 30 min at (a) room temperature and (b) -30°C.

4.3.6 Deep electropolishing – long time potential hold

In order to study the surface finish after sufficient thickness removal, longer EP was performed by holding the potential at 9 V for 3 h and 7 h in the 3 M sulfuric acid-methanol electrolyte at -30^{o}C. The corresponding thickness removal was 113 μm and 252 μm as listed in table 4.3. These EP processes show the identical current and corrosion rate to the EP of 30 min. The identical current indicates stable mass transport. The uniform corrosion rate indicates a linear relationship between thickness removal and EP duration.

Table 4.3: Parameters of EP in the 3 M sulfuric acid-methanol electrolyte at 9 V for 30 min, 3 h, and 7 h at -30^{o}C.

Duration (hr)	Current (A/cm^2)	Corrosion rate (μm/min)	Thickness removal (μm)	Roughness (Ra, nm)
0.5	0.034±0.0128	0.63	19	140±27
3	0.030±0.0051	0.64	113	83±18
7	0.031±0.0041	0.60	252	77±5

Figures 4.18 and 4.19 show the SEM images captured on surfaces polished for various durations. Scratches are removed on the surface polished over 3 h. Macroscopic surface roughness measurements (table 4.3) show this improvement as smaller R_a value for longer EP. As the microscopic roughness characterization, figure 4.20 shows further suppression of grain boundary etching (figure 4.20 (a)) and a decreasing R_{rms} along the whole length scale as the duration is increased (figure 4.20 (b)). This indicates that sufficient thickness removal—over 100 μm—is necessary to remove the mechanically damaged surface layer and enhances the microsmoothing result. On the other hand, the

R_{rms} increases for the surface polished for 7 h at scales smaller than 100 μm (figures 4.20 (c)). This increase is not fully understood.

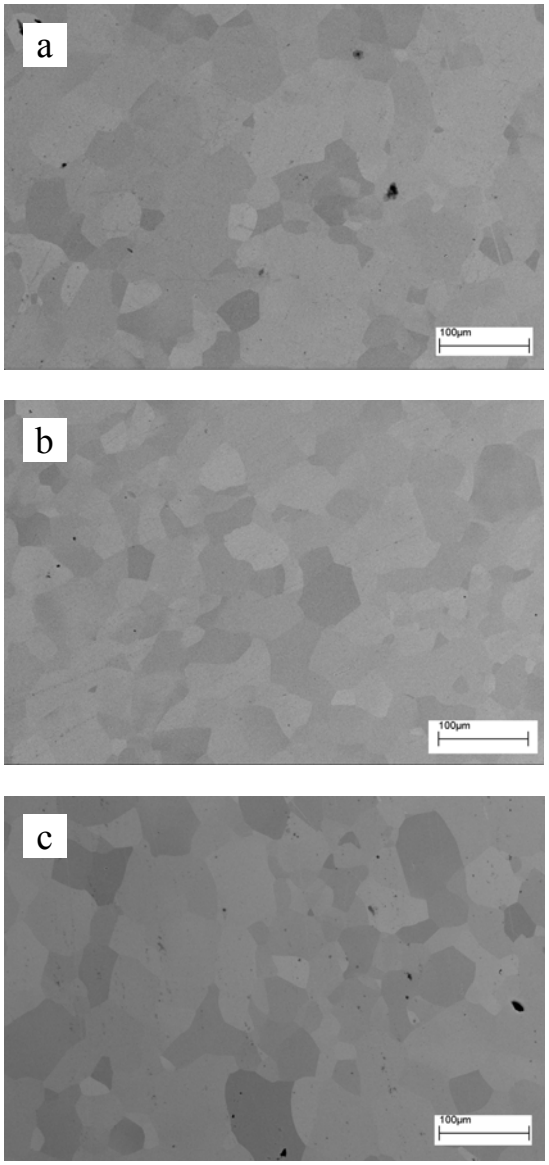

Figure 4.18: SEM images (600 x) by using RBSD of Nb surfaces electropolished in the 3 M electrolyte at 9 V for (a) 30 min, (b) 3 h, and (c) 7 h at -30^{o}C.

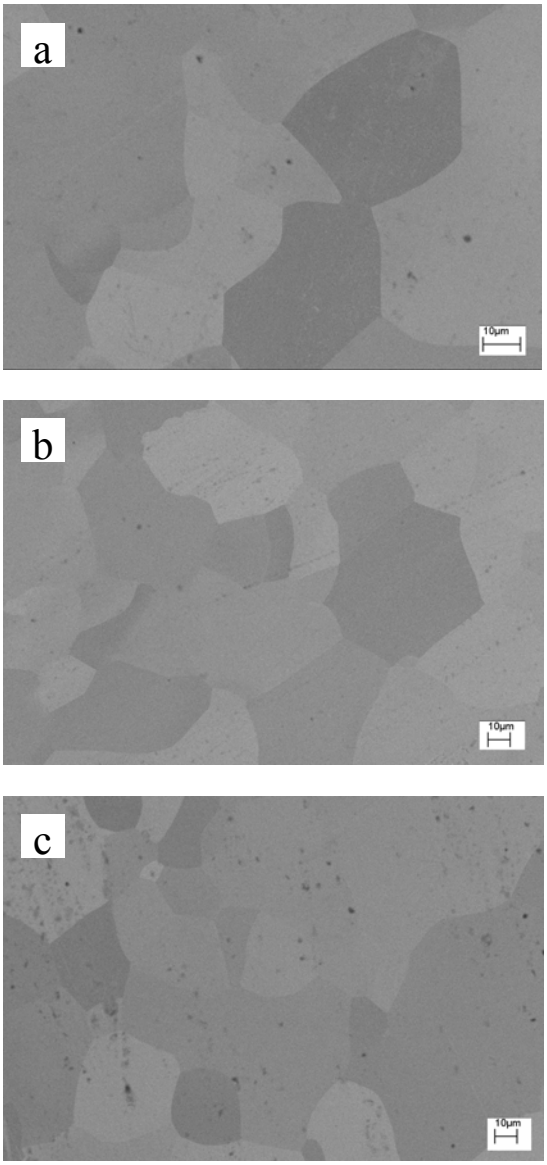

Figure 4.19: SEM images (1500 x) by using RBSD of Nb surfaces electropolished in the 3 M electrolyte at 9 V for (a) 30 min, (b) 3 h, and (c) 7 h at -30^{o}C.

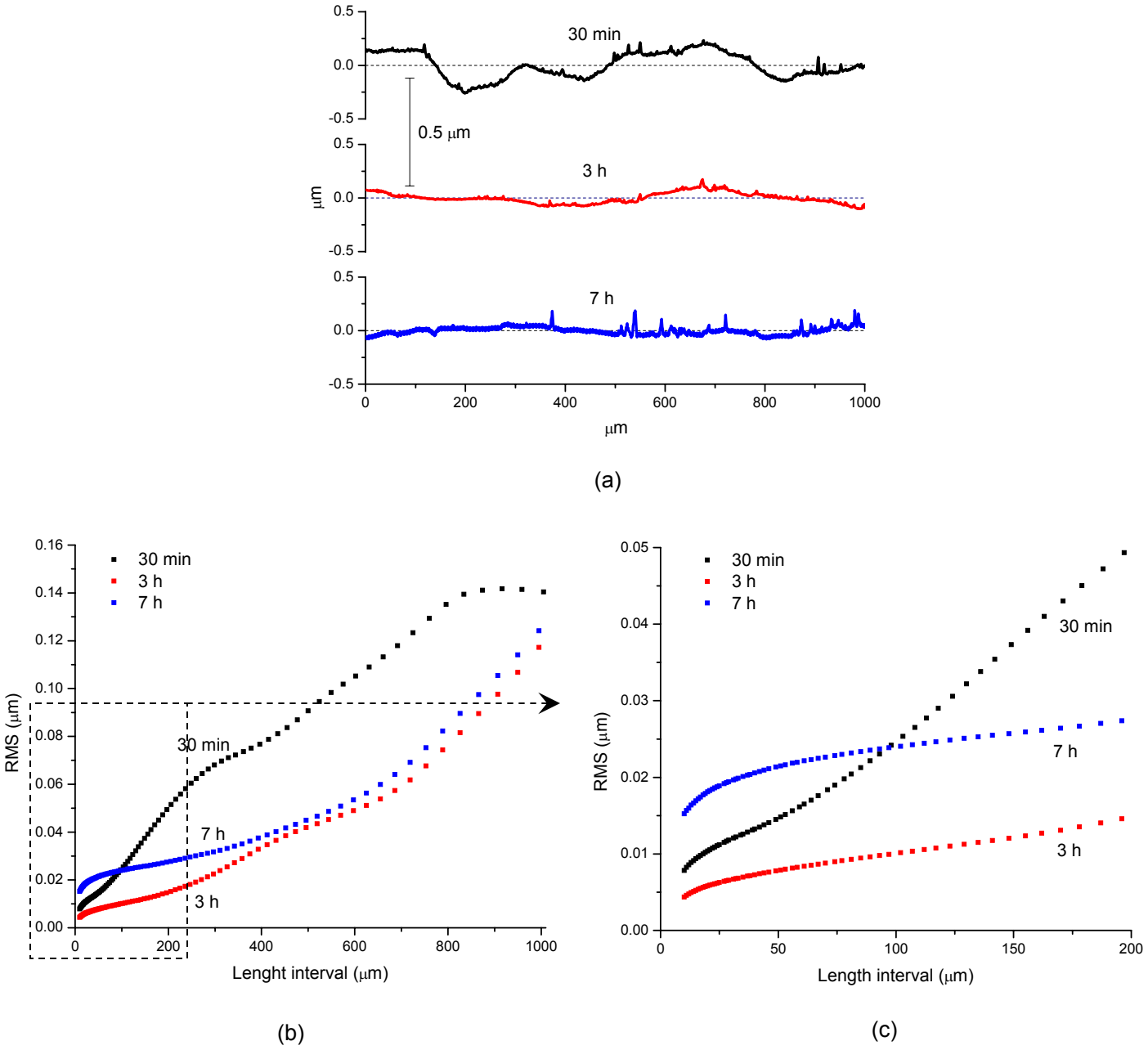

Figure 4.20: (a) Surface profile, (b) R_{rms} as a function of length scale (1 mm), and (c) R_{rms} as a function of length scale (0.2 mm) of Nb surfaces electropolished in the 3 M electrolyte at 9 V for 30 min, 3 h, and 7 h at -30°C.

4.4 Two-electrode setup versus three-electrode setup

In practical Nb SRF cavity fabrication, the two-electrode setup is typically used, while in experimental metal EP the three-electrode setup is predominately used [1-3, 9, 10]. The advantage of the three-electrode electrochemical cell is: the reference electrode monitors the anodic polarization, which thermodynamically corresponds to various levels of surface finish, such as pitting, smoothing, or even passivation. However, the small voltage range of the potentiostat typically used—for example, in this dissertation project potentiostat 263A has been used supporting a voltage range of ±9 V—may limit the high voltage applications. This limitation can be eliminated by the two-electrode setup used in this dissertation project. Through the use of a pre-amplifying circuit, the voltage between the working and counter electrodes can reach any desired value. In the two-electrode setup the reference electrode is removed and the surface polarization is no longer monitored.

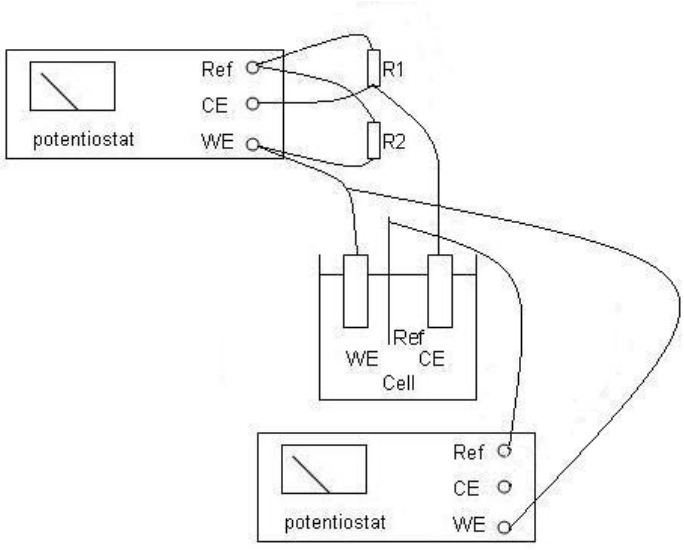

Figure 4.21: Schematic diagram of anodic polarization measurement in the two-electrode setup.

Figure 4.21 shows a schematic diagram of a setup used to measure the surface potential in a two-electrode setup. The primary potentiostat connects to a pre-amplifying circuit to output the magnified voltage across the cell. The secondary potentiostat connects to the working and reference (MSE) electrodes to measure the anodic polarization. During EP by holding the voltage at 22 V, the anodic polarization is measured to be approximately 11 V vs. MSE. This value is close to the potential of 9 V held during EP in the three-electrode setup. During the EP at -30^{o}C (figure 4.22), it is likely that the currents measured during EP in the 2 M electrolyte are comparable. However, this may not be the case for the current measured in the 1 M electrolyte in the two-electrode setup, which may be much larger than that measured in the three-electrode setup. On the other hand, the surface polished in the two-electrode setup is much smoother than that polished in the three-electrode setup, illustrated in table 4.4. The mechanism for this observation is currently still unknown.

Table 4.4: Roughness measurements of surfaces electropolished in both two-electrode and three-electrode setups in the 1 M and 2 M sulfuric acid-methanol electrolytes. The potential hold for two-electrode setup is 22 V and is measured to be 11 V vs. MSE. The potential hold for three-electrode setup is 9 V vs. MSE. The duration is 30 min and the temperature is -30^{o}C.

Concentration	Two-electrode setup	Three-electrode setup
1 M	80±23 nm/mm	278±118 nm/mm
2 M	40±18 nm/mm	132±34 nm/mm

Although it is still difficult to distinguish the two-electrode setup from the three-electrode setup only by surface finish, the results indicate that EP is feasible in both types of setup. Furthermore, the surface finish achieved by methanol-based EP is comparable to or better than that by HF-based EP. People may refer to the two-electrode setup for practical fabrication of Nb cavities and refer to the three-electrode setup for experimental understanding of HF-free EP.

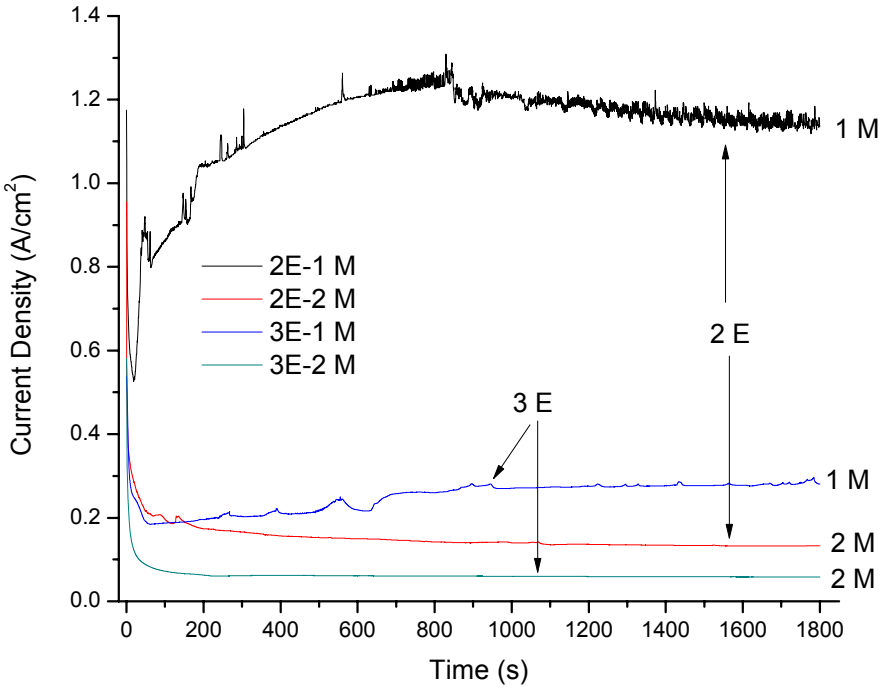

Figure 4.22: Current measured during EP in both two-electrode and three-electrode setups. The potential hold for two-electrode setup is 22 V, and measured to be 11 V vs. MSE; the potential hold for three-electrode setup is 9 V vs. MSE. The duration is 30 min and the temperature is -30^{o}C.

4.5 Summaries

The EP of Nb in sulfuric acid-methanol electrolytes was performed in an electrochemical cell with a three-electrode setup in sulfuric acid-methanol electrolytes. The electrochemical experiments indicate the dependence of the limiting current plateau on both concentration and temperature. Macrosmoothing and microsmoothing were obtained under multiple EP conditions. Temperature is determined to be a more critical parameter than concentration and current to achieve microsmoothing. Sufficient thickness removal is necessary to eliminate the surface mechanical damage resulting in an improvement on surface finish.

References

1. O. Piotrowski, C. Madore, and D. Landolt, Electrochim. Acta **44**, 3389 (1999).
2. O. Piotrowski, C. Madore, and D. Landolt, Plat. Surf. Finish. **85**, 115 (1998).
3. O. Piotrowski, C. Madore, and D. Landolt, J. Electrochem. Soc. **145**, 2362 (1998).
4. D. Landolt, Electrochim. Acta **32**, 1 (1987).
5. H. Tian, Surface study of niobium for superconducting radio frequency (SRF) accelerators, PhD dissertation, College of William and Mary, (2008).
6. H. Tian, C. Reece, M. Kelley, S. Wang, L. Plucinski, and K. Smith, Appl. Surf. Sci. **253**, 1236 (2006).
7. R. Sautebin, H. Froidevaux, and D. Landolt, J. Electrochem. Soc. **127**, 1096 (1980).
8. R. Sautebin, and D. Landolt, J. Electrochem. Soc. **129**, 947 (1982).
9. H. Diepers, O. Schmidt, H. Martens, and F. Sun, Phys. Lett. **37(A)**, 139 (1971).
10. K. Satio, Y. Kojina, T. Furuya, S. Mitsunobu, S. Noguchi, K. Hosoyama, T. Nalazato, T. Tajima, K. Asano, K. Inoue, Y. Lino, H. Nomura, and K. Takeuchi, Proceeding of 4th of RF superconductivity, KEK, Tsukuba, Japan, p635 (1989).

Chapter 5

Electrochemical impedance spectroscopy: Toward an understanding of electropolishing in sulfuric acid-methanol electrolyte

5.1 Introduction

In practical electropolishing (EP) applications, one usually wants achieve both macrosmoothing and microsmoothing. The macrosmoothing can be achieved under ohmic and transport control while only the later leads to microsmoothing [1-6]. The three possible transport mechanisms proposed by Landolt are [1]: the salt film precipitation, the rate limited acceptor diffusion, and the rate limited water diffusion. One can refer to chapter 2 for a detailed description of these three mass transport mechanisms.

If one takes the water as a special acceptor, then there will be two different mechanisms: salt film and acceptor. Matlosz et al found the adsorbate-acceptor model for the EP of iron-chromium—for example Fe-13Cr—in a solution of sulfuric and phosphoric acids. They propose the acceptor to be water or a water-related species necessary for solvation

of the dissolving cations [7]. A salt film mechanism has been identified for the microsmoothing of copper in nitrate and sulfate electrolytes, of iron and nickel in nitrate and chlorate electrolytes, and of tantalum and titanium in sulfuric acid-methanol electrolytes [2-6, 8-10].

5.1.1 Electrochemical impedance spectroscopy

The Electrochemical impedance spectroscopy (EIS) technique has the potential to distinguish between mass transport mechanisms during EP [8]. Assuming that the high frequency part of the impedance diagram can be described as a semicircle—Nyquist diagram, it is possible to distinguish between the salt film and acceptor mechanisms. Landolt et al investigated the mechanisms of EP by EIS for several systems. They identified the presence of a compact film for tantalum and titanium in an electrolyte of sulfuric acid-methanol. The presence of both an outer porous layer and an inner compact layer was found for EP of iron-chromium alloys—Fe-25Cr and Fe-15Cr—in concentrated chloride media while an acceptor mechanism for EP of Fe-13Cr in sulfuric and phosphoric acids system [7-11].

When one applies a potential across an electrochemical cell, a resultant current will flow with a value determined by the mechanisms of the reaction taking place and the potential difference established in the electrolyte due to the movement of charged species. The application of a sinusoid potential:

$$V = V_0 \sin(\omega t) \tag{5.1}$$

results in a sinusoidal current:

$$I = I_0 \sin(\omega t + \phi). \tag{5.2}$$

The ratio between the potential and current is known as impedance (Z), which is analogous to the resistance-current-potential relationship of dc circuit:

$$Z = \frac{V}{I}, \tag{5.3}$$

where Z has a magnitude of (V/I) and a phase of ϕ, and is thus a vector of quantity:

$$Z = Z' + jZ'', \tag{5.4}$$

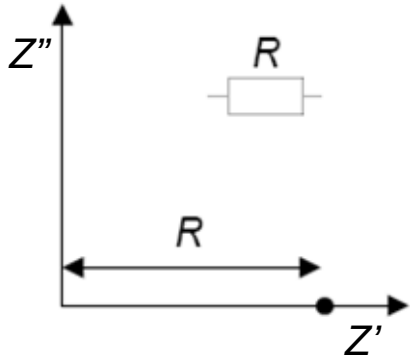

(a)

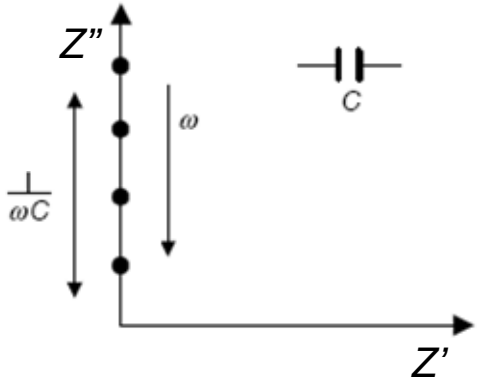

(b)

Figure 5.1: Schematic diagram of impedance spectrum for (a) pure resistance and (b) pure capacitance.

Now, if the potential is applied through a pure resistance R, then the magnitude of Z is R and $\phi = 0$ for all frequencies—point on the x-axis shown on the plot of the real (Z') and imaginary (Z'') components in figure 5.1 (a). If the potential is applied through a pure capacitance, the impedance is dependent on the frequency according to $Z = j/\omega C$ and $\phi = 90^{o}$ (figure 5.1 (b)). The results of combining these two basic circuit components, in series and in parallel, can be easily deduced by a complex impedance spectrum—Nyquist diagram—as shown in figure 5.2 [12]. Interpretation of the Nyquist data is used to determine the mechanism of mass transport [13].

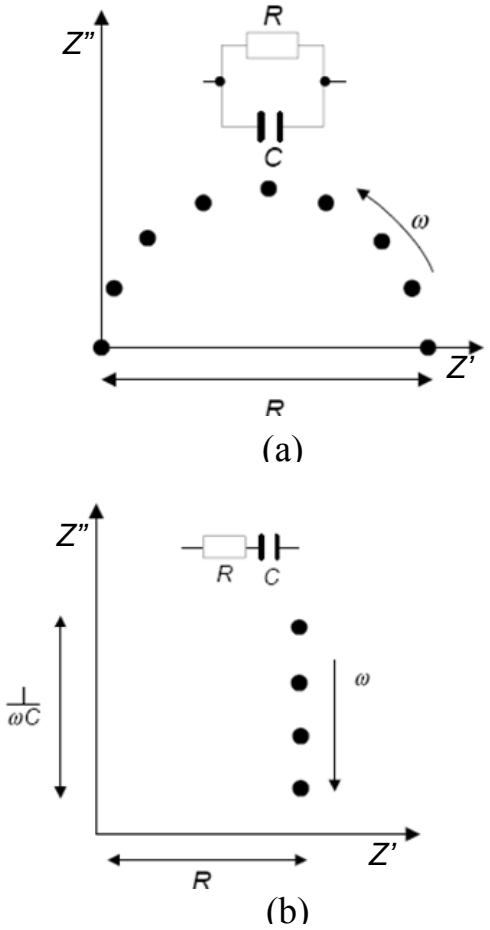

Figure 5.2: Schematic diagram of impedance spectrum for (a) resistance and capacitance parallel and (b) resistance and capacitance series.

5.1.2 The duplex salt film model

Figure 5.3 is a schematic diagram of a duplex salt film. The presence of a salt film is thought to contribute to microsmoothing [13-17]. The salt film is thought to have a duplex structure in the general case which consists of an outer porous layer and an inner compact layer. Dissolved ions transport through the porous layer by migration in the liquid phase under an electric field. The thickness of porous layer remains constant–up to a few microns—due to equal rates of precipitation at the inner surface and dissolution at the outer surface. In the inner compact layer, only metal ions are mobile and transport through the compact layer is by high-field solid state conduction. The compact film typically has a thickness of order of 10 nm [14]. The salt film need not to be duplex but may consist of either a porous film or a compact film [13].

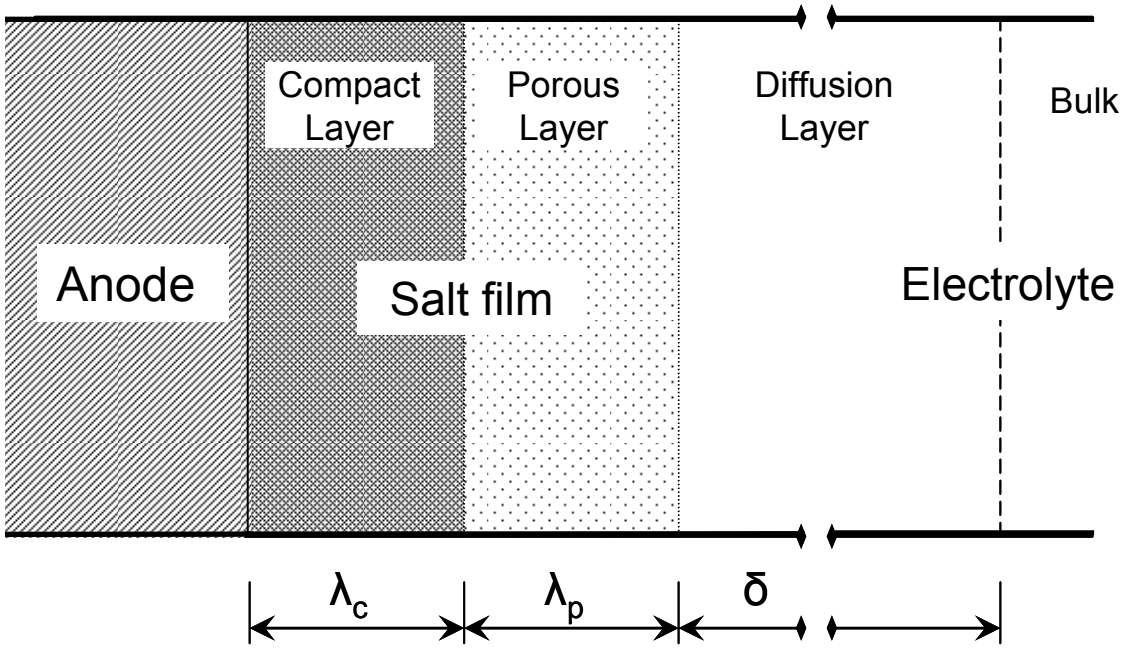

Figure 5.3: Schematic diagram of a duplex salt film.

In the EIS diagram, only the higher frequency data is used to determine the mechanism. Figure 5.4 shows the equivalent circuit and corresponding Nyquist plot for the high frequency part of the impedance diagram. R_s is the starting point of the semicircle and represents the electrolyte resistance between the metal surface and the reference excluding any compact film. If a porous film is present, then R_s is sum of the electrolyte resistance and the ohmic resistance of the porous film. The polarization resistance, R_p, is given by the diameter of the semicircle and characterizes the compact film if present. The effective double layer capacitance C_{dl} is determined from the frequency value (ω) at the top of semicircle and R_p by $C_{dl} = 1/(\omega R_p)$ [8, 14].

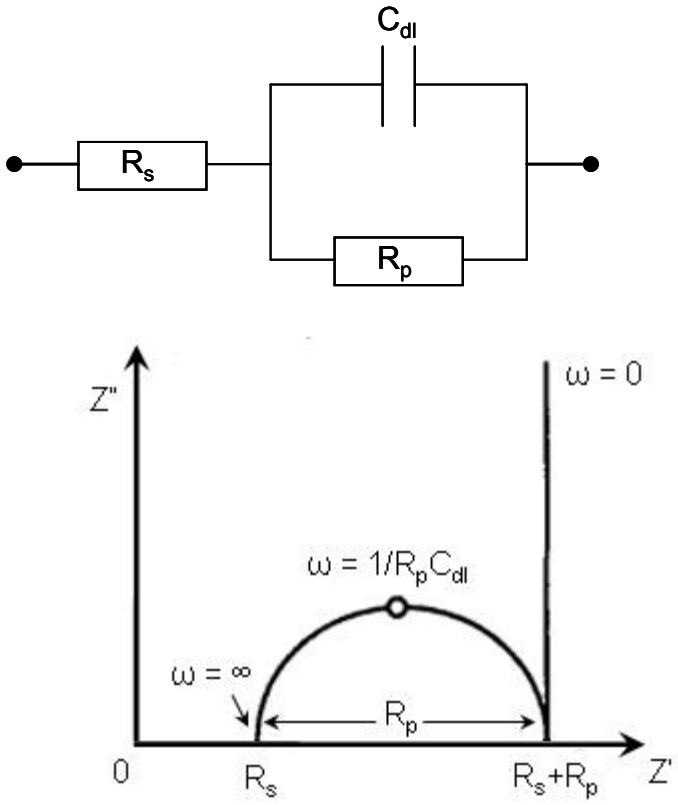

Figure 5.4: Equivalent circuit (upper) and corresponding Nyquist plot (lower) for the interpretation of the high frequency part of the impedance diagram.

In the present chapter, EIS diagrams were measured in the 0.5 M, 1 M, 2 M, and 3 M sulfuric acid-methanol electrolytes at both room temperature and -30^{o}C. The mechanism leading to microsmoothing is determined. Also present is a mechanism transfer with decreasing temperature. The mass transport limiting specie is also discussed.

5.2 Experimental procedures

Nb working electrode and sulfuric acid-methanol electrolytes

The Nb working electrodes were fabricated by the same method mentioned in the prior two chapters. The Nb plates—0.2 cm^2 areas—were cut from the high-RRR-grade fine grain Nb sheet stock and embedded into the epoxy. The Nb stock has a purity of 99.9999% and is used for standard SRF cavity construction. Prior to each impedance measurement the Nb working electrode was mechanically polished by 600 grit emery paper, rinsed in methanol, and then conserved in a dry-keeper (SANPIA, USA). The electrolyte was prepared by sulfuric acid (Certified ACS plus, 98%, Fisher Chemical) and methanol (HPLC grade, 99.9%, Fisher Chemical). The sulfuric acid concentrations in the methanol solution were 0.5 M, 1 M, 2 M, and 3 M. The maximum water content in these solutions was estimated and given in table 4.1 and did not support a protective oxide film which would prevent further metal dissolution (chapters 3 and 4).

EIS

Impedance measurements were performed in the limiting current region at constant potential using a frequency response analyzer (Solartron 1260) connected to a

potentiostat (Model 263A, EG&G, Princeton Applied Research) and controlled by a computer interface. A mercury/mercurous sulfate electrode (MSE) was used as the reference electrode. An ac amplitude of 40 mV rms was used. After 200 s at which the steady current was reached, the impedance spectroscopy was started at 200 kHz and swept down to 0.2 Hz. Integration errors were observed at the low frequencies resulting from an insufficient signal to noise ratio and from drift of the dc current density during the dissolution [11]. Only those points at low frequency not affected by the integration errors were used. In a typical run initiated after 200 s, using an integration time of 10 s and a time delay at each frequency of 1 s the overall acquisition time for a complete diagram was less than 3 minutes. The EIS measurements were performed in various concentrations at both room temperature and –30^{o}C.

5.3 Results and discussions

5.3.1 EIS measured in the 3 M and 2 M sulfuric acid-methanol electrolytes

Figure 5.5 shows the influence of applied potential on the impedance diagram measured in the 3 M sulfuric acid-methanol electrolyte at both room temperature and -30^{o}C. The potential was varied from 8 V to 3 V in the limiting current region. The high frequency part of impedance diagram begins with 100 kHz because the higher frequency data was unreliable due to the integration limitation of the measurement circuit. In both diagrams shown in figure 5.5, the diameter of semicircle increases while R_s remains constant with increasing potential. All surfaces following the EIS measurements appeared polished to

the unaided eyes. For comparison, Nb dissolutions at the voltage of 1 V prior to the limiting current plateau were measured (figure 5.6). The impedance responses at 1 V in both diagrams of figure 5.6 are markedly different to those shown in figure 5.5. At room temperature the impedance at 1 V shows a very small loop. At -30^{o}C the loop increases in diameter and is comparable to that at 8 V. The surface after the potential hold at room temperature showed little change and the surface at -30^{o}C was dull.

Parameters of R_s, C_{dl}, and R_p were calculated form the impedance data of figures 5.5 and 5.6 using the model shown in figure 5.4 by using ZPlot software. The fit results are summarized in table 5.1. Matlosz and Grimn discussed the expected variation of R_s, C_{dl}, and R_p as a function of applied potential for a salt film model versus an acceptor model of EP as: 1) for the compact film model, R_s represents the resistance between the metal surface and the reference electrode and is potential-independent, R_p increases with increasing potential as the film thickness increases, C_{dl} is determined by R_p and decreases with increasing potential; 2) for the porous film model, ion transport occurs in the saturated electrolyte within the pores and R_s increases with increasing applied potential and the other two parameters remain constant; 3) for the adsorbate-acceptor model (no anodic film), R_p is only proportional to the steady-state current and therefore is independent on potential, the other parameters remain constant with increasing potential [7, 14, 15]. The descriptions of R_s, C_{dl}, and R_p as a function of applied potential are summarized by Tian and shown in table 5.2 [13, 16].

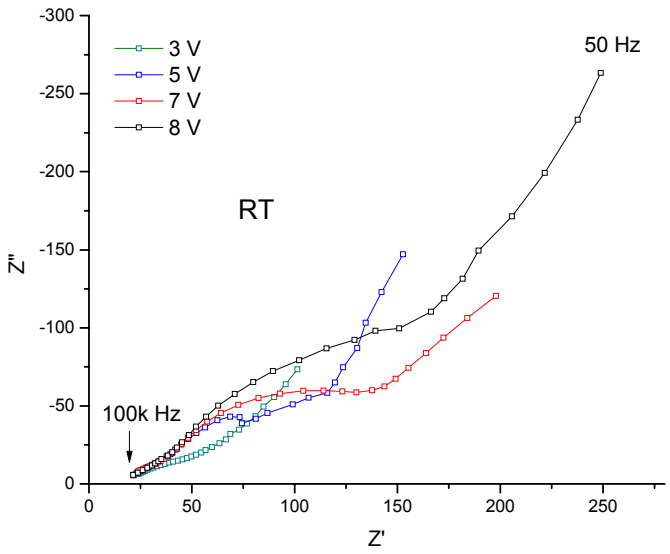

(a)

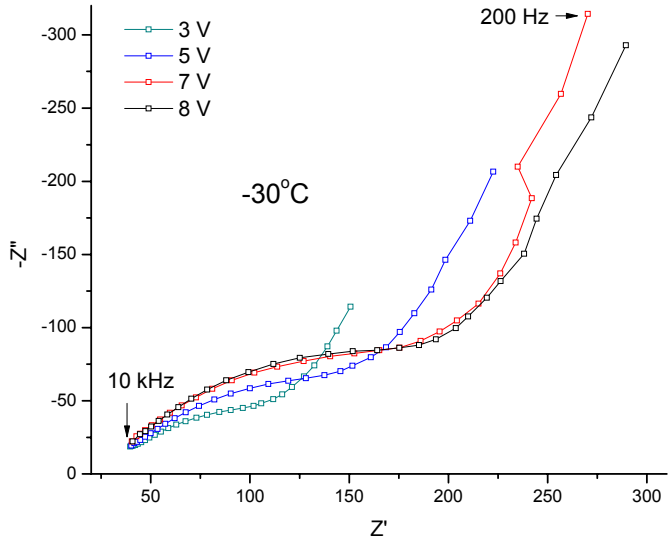

(b)

Figure 5.5: Nyquist diagram showing the effect of applied potential on the impedance measured in the 3 M electrolyte at (a) room temperature and (b) -30°C.

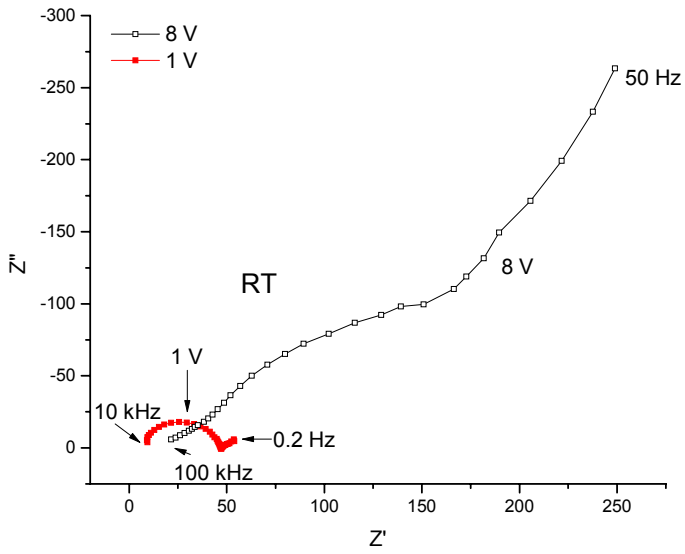

(a)

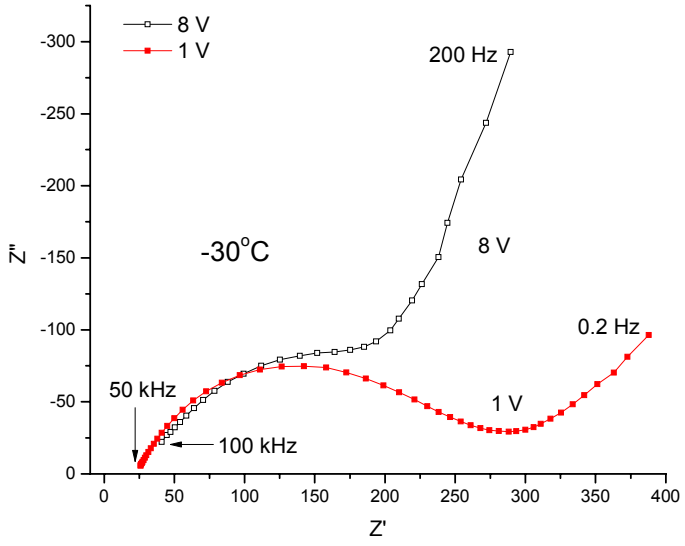

(b)

Figure 5.6: Impedance diagram measured at 1 V and 8 V in the 3 M electrolyte at (a) room temperature and (b) -30°C.

Table 5.1: Parameters estimated from the EIS measured in the 3 M and 2 M electrolytes at room temperature and -30°C.

Concentration (M)	Temperature (°C)	Potential (V)	R_s (Ω·cm^2)	C_{dl} (μF)	R_p(Ω·cm^2)
3	RT	8	21.7	1.183	116.7
		7	21.5	1.318	114.8
		5	21.6	1.608	82.34
		3	21.7	1.786	39.41
		1	9.40	2.872	39.09
	-30	8	40.9	0.164	163.0
		7	40.5	0.181	152.4
		5	40.3	0.285	118.5
		3	39.6	0.555	109.7
		1	31.7	1.269	244.1
2	RT	8	15.1	0.845	33.2
		7	14.9	1.260	26.6
		5	15.0	1.149	23.2
		3	15.0	1.678	7.92
		1	9.79	2.299	15.27
	-30	8	31.8	0.227	56.8
		7	31.8	0.246	55.3
		5	32.2	0.293	46.5
		3	32.3	0.438	29.7
		1	31.9	2.019	148.7

RT = room temperature

Figure 5.7 shows the changes in R_s, C_{dl}, and R_p as a function of applied potential in the 3 M electrolyte. At both temperatures, R_s remains constant, C_{dl} decreases with increasing potential, and R_p increases with increasing potential. The compact film model is the only model consistent with these results. The C_{dl} also decreases with decreasing temperature. This may explain the plateau extension and improved surface finish observed with decreasing temperature (chapter 4), because the smaller the capacitance the smaller the current necessary to establish a steady-state field [14]. In contrast, both R_s and R_p increase with decreasing temperature. This might be related to a thicker compact film at -30°C. However, the temperature-dependence of resistivity is still unknown and must be understood in order to discuss the thickness variation with temperature.

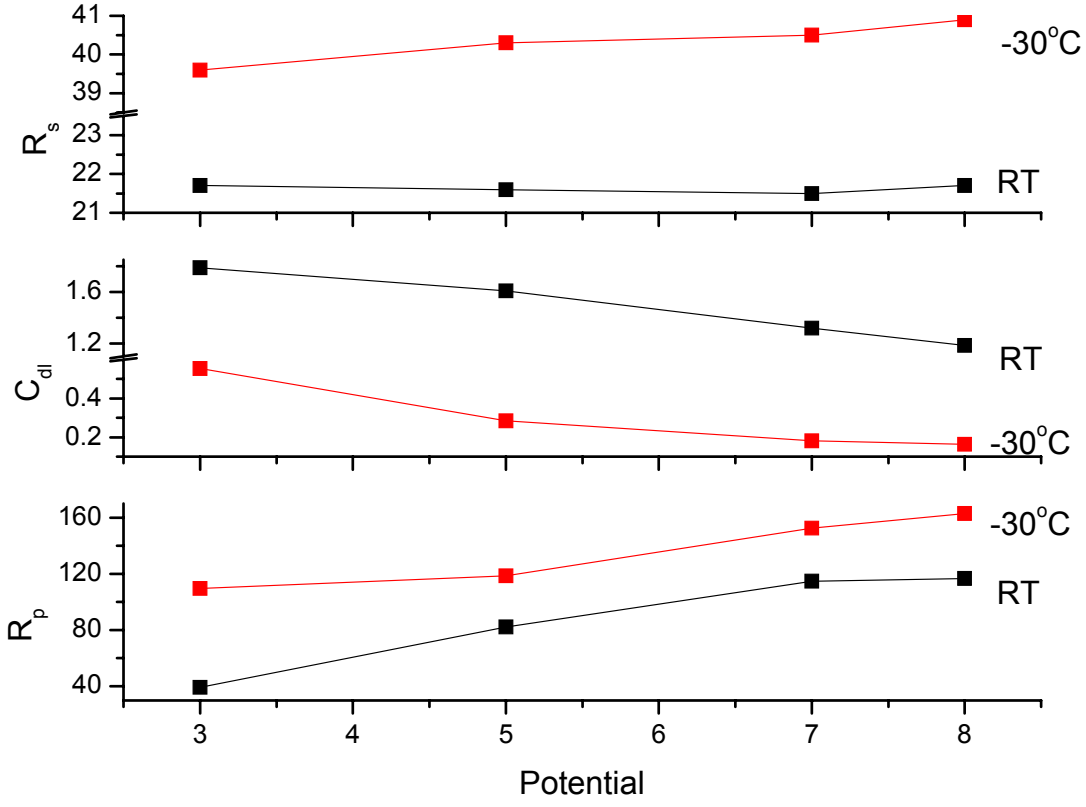

Figure 5.7: R_s, C_{dl}, and R_p as a function of applied potential in the 3 M electrolyte.

Table 5.2: Characteristic features of the Nyquist diagram expected for various EP methods obtained from

	Salt film models						Acceptor model		
	Porous film			Compact film			Adsorbate-aceptor		
Potential ↑	R_s ↑	C_{dl} C	R_p C	R_s C	C_{dl} ↓	R_p ↑	R_s C	C_{dl} C	R_p C
	↑ = increases, ↓ = decreases, C = keeps constant								

Figures 5.8 and 5.9 show the influence of applied potential—including 1 V—on the impedance diagram measured in the 2 M sulfuric acid-methanol electrolyte. The diagram behaves identically to that measured in the 3 M electrolyte. The fit results of R_s, C_{dl}, and R_p for the 2 M electrolyte are also summarized in table 5.1. Plotted as a function of applied potential (figure 5.10), R_s, C_{dl}, and R_p also changed consistent with the compact film model.

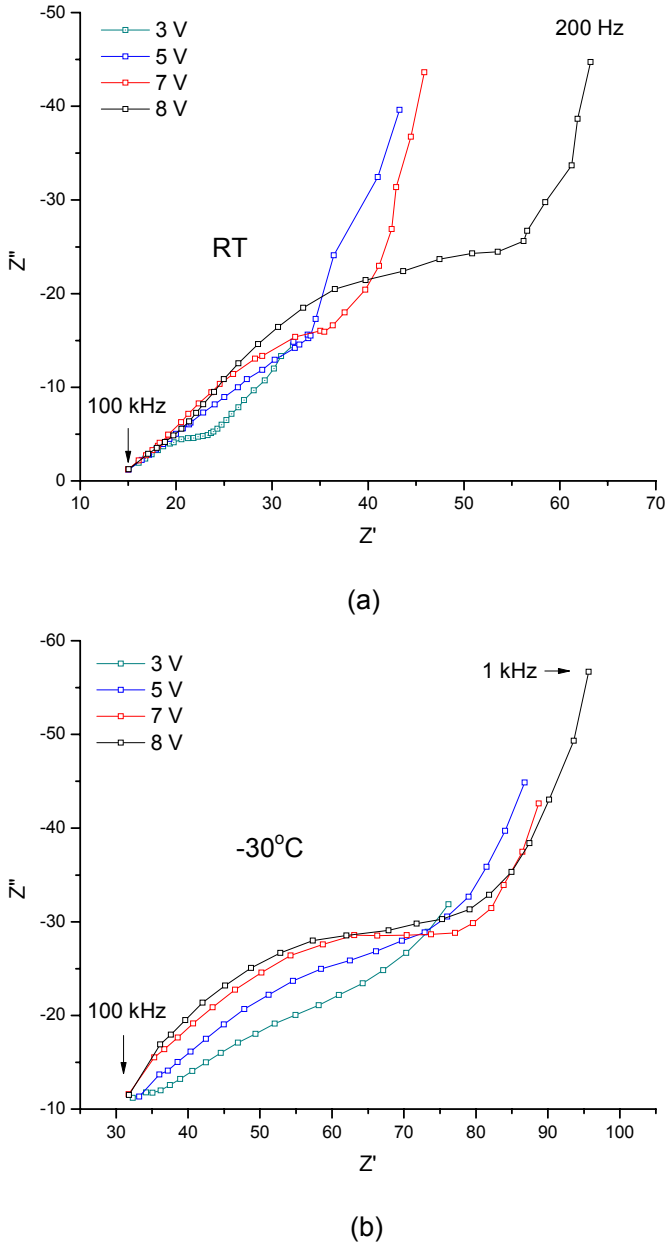

Figure 5.8: Nyquist diagram showing the effect of applied potential on the impedance measured in the 2 M electrolyte at (a) room temperature and (b) -30°C.

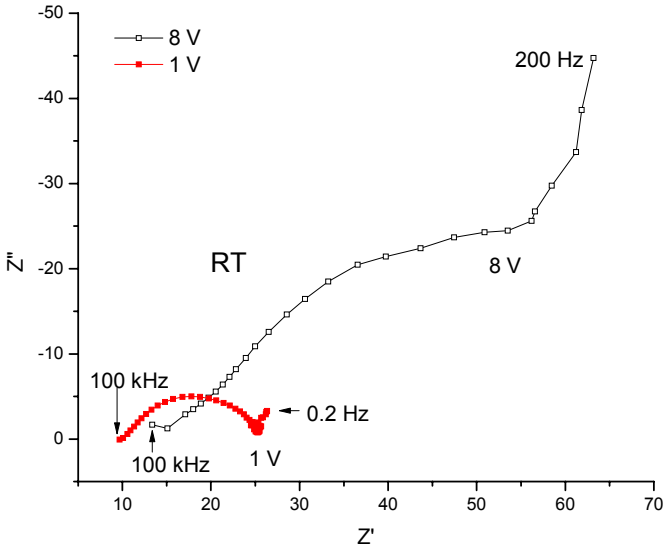

(a)

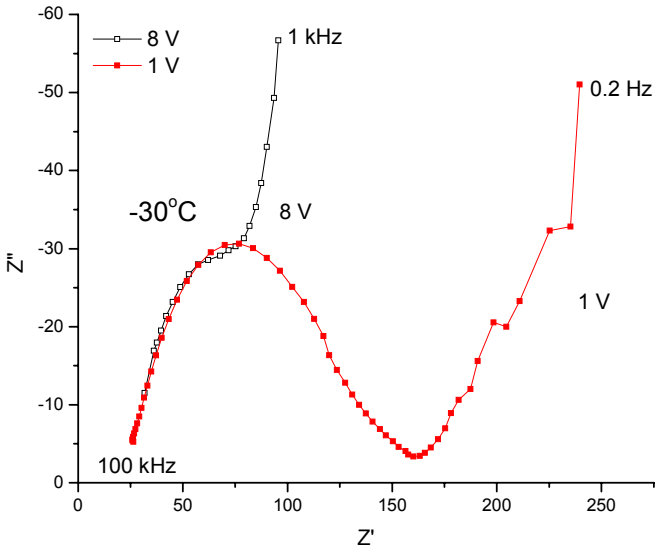

(b)

Figure 5.9: Impedance diagram measured at 1 V and 8 V in the 2 M electrolyte at (a) room temperature and (b) -30°C.

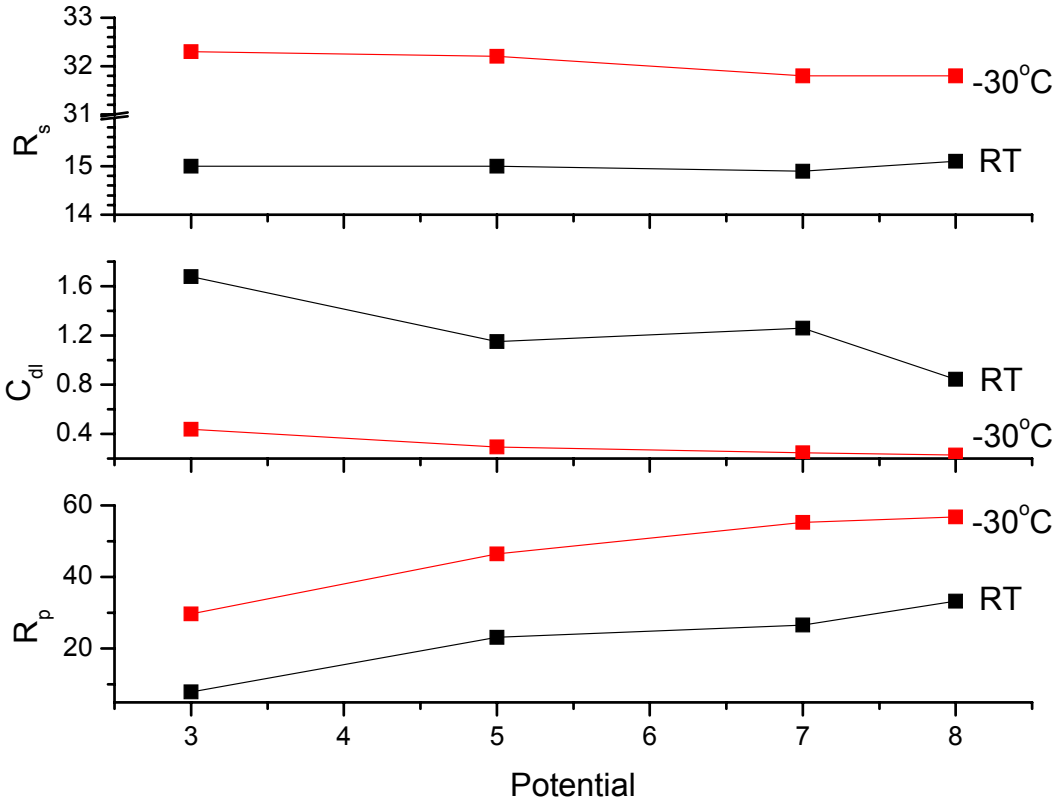

Figure 5.10: R_s, C_{dl}, and R_p as a function of applied potential in the 2 M electrolyte.

5.3.2 EIS measured in the 1 M and 0.5 M sulfuric acid-methanol electrolytes

Figure 5.11 shows the influence of applied potential on the impedance diagram measured in the 1 M sulfuric acid-methanol electrolyte. In contrast to the 3 M and 2 M electrolytes, the high frequency part of the impedance diagram lacks the semicircular feature. The high frequency part of the impedance diagram measured in the 1 M electrolyte at -30°C looks similar to those in the 3 M and 2 M electrolytes. However, its behavior follows

neither the salt film model nor the acceptor model, which is consistent with the lack of the EP under these conditions. The impedance diagram measured in the 0.5 M sulfuric

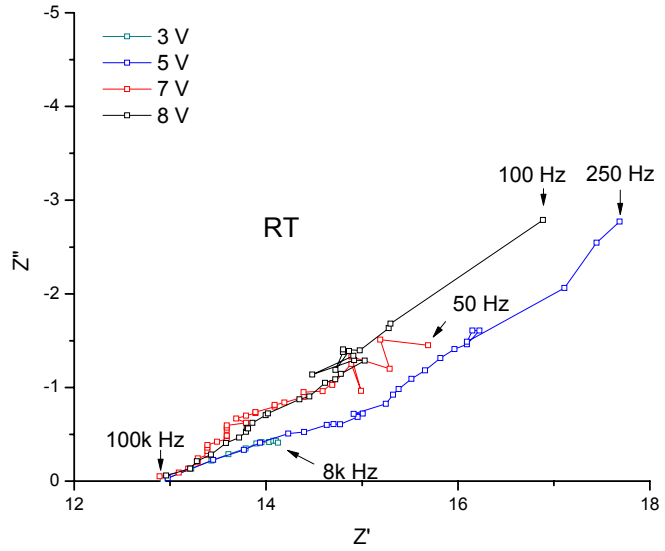

(a)

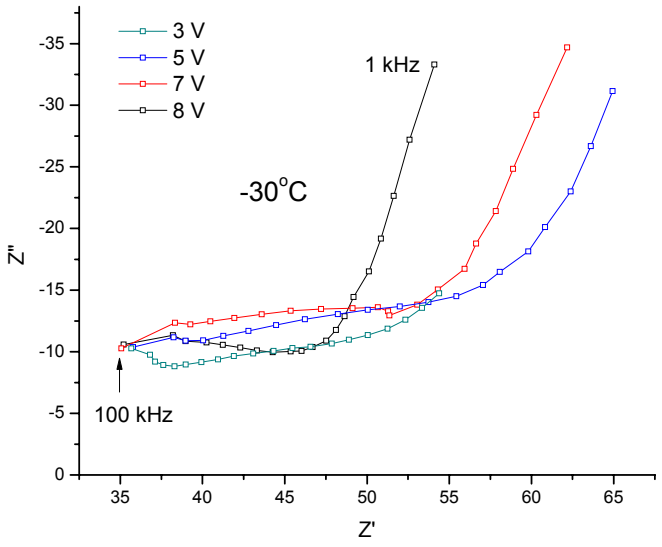

(b)

Figure 5.11: Nyquist diagram showing the effect of applied potential on the impedance measured in the 1 M electrolyte at (a) room temperature and (b) -30°C.

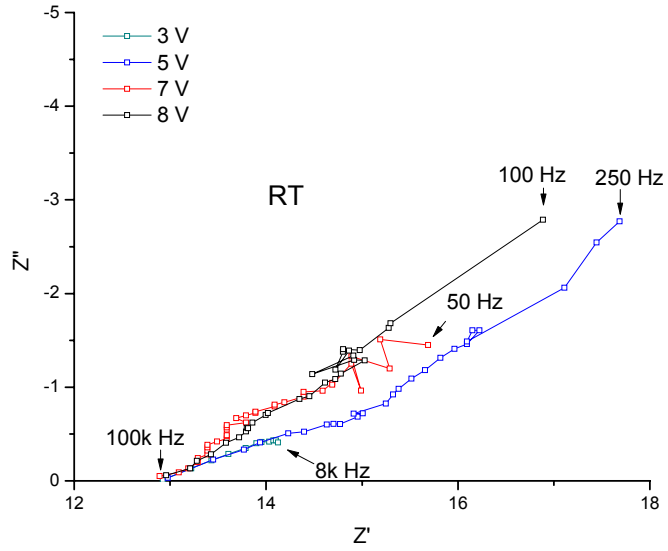

(a)

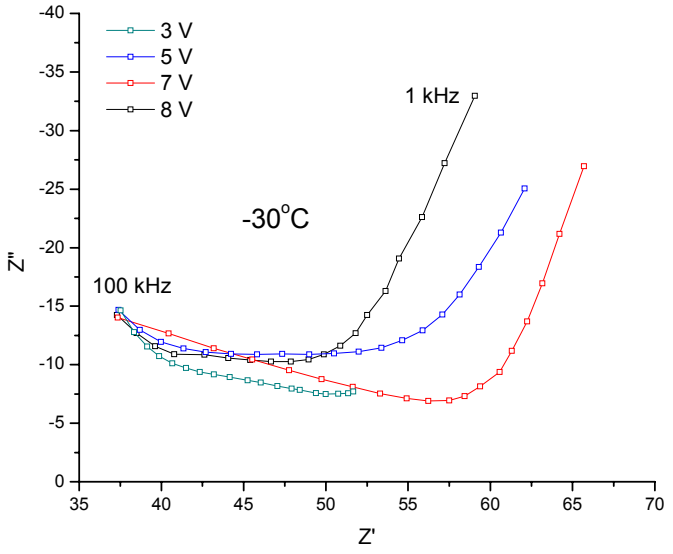

(b)

Figure 5.12: Nyquist diagram showing the effect of applied potential on the impedance measured in the 0.5 M electrolyte (a) room temperature and (b) -30°C.

acid-methanol electrolyte (figure 5.12) under the influence of applied potential shows the identical behaviors to that measured in the 1 M electrolyte at both room temperature and -30^{o}C. The surfaces after the potential hold in the 0.5 M and 1 M electrolytes appeared etched at room temperature and polished at -30^{o}C.

The lack of a semicircular feature indicates the absence of a surface anodic film in the 0.5 M and 1 M electrolytes. Table 5.3 summarizes the steady-state currents measured during EP under multiple conditions. Figure 5.13 shows the comparison of currents measured during EP in the 3 M and 0.5 M electrolytes at both room temperature and -30^{o}C. The current measured in the 3 M electrolytes at room temperature behaves identically to the C-V curve indicating a mass transport mechanism as shown in figure 4.1 (a). This current behavior is related to the mass transport through a compact film. The current measured in the 0.5 M electrolyte at room temperature shows linear current-potential behavior. This is also identical to the linear C-V curve presenting an ohmic mechanism as shown in figure 4.1 (a). In this case, no anodic film is present to influence the movement of charged species [1]. A film-free Nb surface is proposed during Nb dissolution in the 0.5 M electrolyte at room temperature.

The current measured in the 0.5 M electrolyte at -30^{o}C looks similar to that measured in the 3 M electrolyte. This is also identical to the plateau extension in the 0.5 M electrolyte at -30^{o}C (figure 4.1 (d)). The surface finish in the 0.5 M electrolyte at -30^{o}C resulted in microsmoothing as discussed in chapter 4. Since microsmoothing is only achieved under mass transport control, both the improvement of surface finish and the limiting current

plateau extension indicate a transition from ohmic control to mass transport control during EP in the 0.5 M electrolyte at -30°C. According to the discussion on mass transport limiting species in section 5.3.4, an acceptor mechanism is excluded. So the mechanism of EP in the 0.5 M electrolyte at -30°C is also related to the presence of a compact film through which the Nb ions transport.

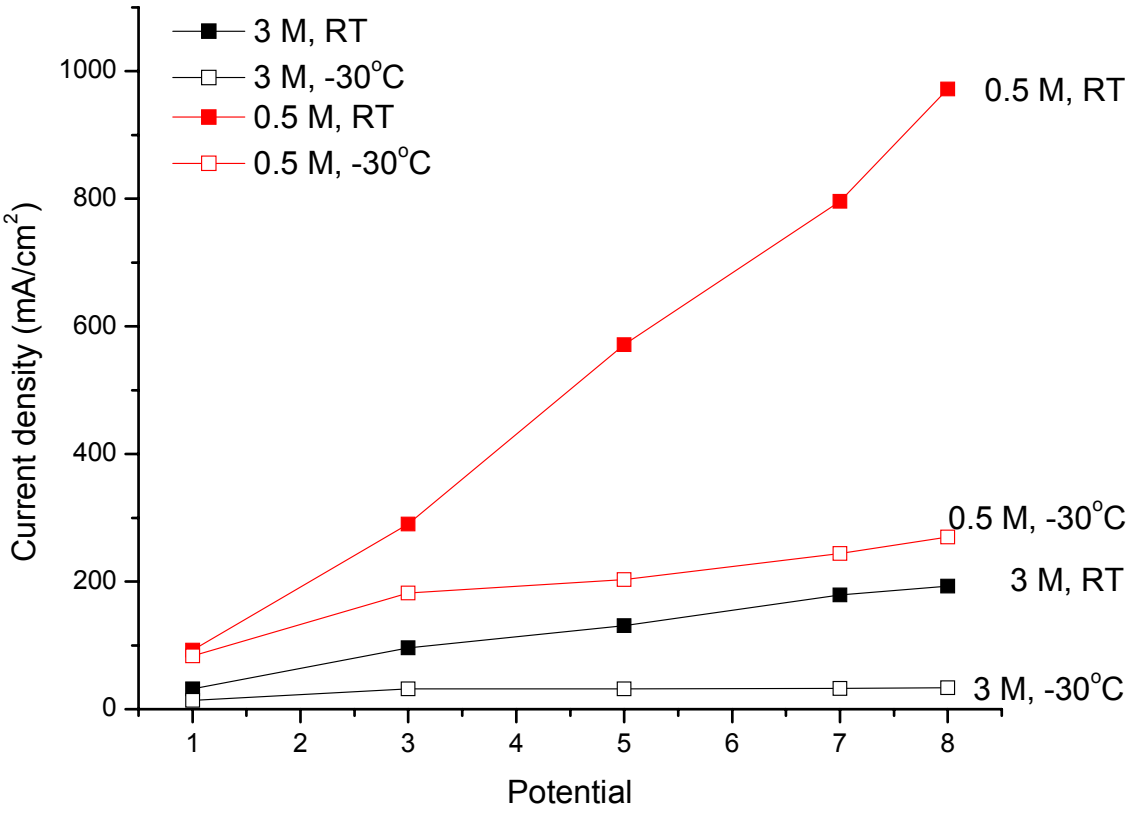

Figure 5.13: Current-voltage behavior measured in the 0.5 M and 3 M electrolytes at both room temperature (solid symbol) and -30°C (open symbol).

Table 5.3: Steady-state current measured during EP at multiple conditions.

Concentration (M)	Temperature (^{o}C)	Potential (V)	Steady-state current (mA/cm^2)
3	RT	8	192.8
		7	178.8
		5	131.2
		3	96.0
		1	31.6
	-30	8	33.9
		7	32.6
		5	31.9
		3	31.8
		1	14.0
2	RT	8	621.2
		7	572.8
		5	456.4
		3	298.4
		1	92.2
	-30	8	58.5
		7	55.2
		5	52.4
		3	51.0
		1	31.5
1	RT	8	1036.0
		7	924.0
		5	752.0
		3	451.6
		1	136.8
	-30	8	208.4
		7	118.4
		5	94.0
		3	74.8
		1	42.3
0.5	RT	8	972.0
		7	796.0
		5	571.2
		3	290.4
		1	92.4
	-30	8	269.6
		7	244.0
		5	203.2
		3	200.8
		1	133.8

RT = room temperature

The behavior of the impedance diagrams in the 0.5 M electrolyte at -30°C on the other hand is still difficult to interpret. It is likely that the high current level measured in the 0.5 M electrolyte may be one reason. The large current causes the electrolyte temperature to increase during the practical EP and EIS experiments in the 0.5 M electrolyte at -30°C, which show a temperature fluctuation of ±3 °C. The unstable temperature may introduce an unstable film precipitation. This explains why the EP process in the 2 M and 3 M electrolytes results in a better surface finish than that measured in the 0.5 M and 1 M electrolytes at -30°C. However, more experiments and observations are required.

5.3.3 Dissolution stoichiometry

The valence (n) of Nb dissolution during EP under multiple conditions was determined using Faraday's Law [8]:

$$n = \frac{Q \times M}{\Delta m \times F} = \frac{i \times t \times A \times M}{\Delta m \times F} \tag{5.1}$$

where Q is the total charge (C) passed in each EP process, Δm is the weight loss (g), i is the current density (A/cm^2), t is the EP duration (s), A is the anodic area (cm^2), M is the atomic weight of Nb (93 g/mol), and F is the Faraday constant (96500 s·A/mol). Table 5.4 lists a part of the calculation. The average of all calculations is n = 5.11, which is close to the theoretical value of n = 5 for production of Nb^{5+}. As proposed in chapter 4 that the current is contributed by dissolved Nb ions, the dissolution during EP is then believed to yield five valent Nb species.

Table 5.4: Calculated valence of dissolution for Nb electropolished under multiple conditions.

Electrode #	Concentration (M)	Temperature (^{o}C)	Duration (hr)	Valence
2	0.1	RT	1	5.36
		0		5.10
		10		5.00
		-30		4.49
	1	-30	0.5	4.72
	2	-30		5.48
3	0.5	RT		5.55
	1			5.38
	2			5.52
	3			6.07
		0		5.40
		-10		5.66
		-30		4.26
			3	4.41
			7	4.53

RT = room temperature

5.3.4 Discussion on mass transport limiting species

Results obtained in this chapter confirm that the dissolution of Nb in concentrated sulfuric acid-methanol electrolyte is mass transport controlled. Possible mass transport limiting species taking part directly or indirectly in the dissolution reaction are Nb ion

(Nb^{5+}), electrolyte anion (SO_4^{2-}), and water molecule. The SO_4^{2-} and water are suggested to act as acceptors during mass transport [14]. With increasing sulfuric acid concentration—for example from 2 M to 3 M—the water content listed in table 4.1 increases from 0.49 wt% to 0.66 wt%, but the current listed in table 5.3 decreases at both room temperature and -30°C. The current decreasing with increasing SO_4^{2-} and water content excludes the mechanism based on rate limited transport of sulfuric acid and water acceptor species [10]. Piotrowski et al discussed the anodic dissolutions of Ti and Ta in sulfuric-acid methanol electrolytes under EP conditions and determined Ti^{4+} and Ta^{5+} to be the species transport from anode to bulk electrolyte [8-10]. The decreasing current with increasing concentration is suggested to be due to the decreasing solubility of metal ion [10]. The result and discussion in the present study suggest the similar mechanism that the Nb^{5+} acts as the mass transport species.

5.4 Summaries

The EIS measured in the 3 and 2 M sulfuric acid-methanol electrolytes indicates the presence of a compact film between Nb surface and electrolyte at both room temperature and -30°C. The EIS also indicates a transfer in the 1 and 0.5 M from a film-free surface at room temperature to an anodic film precipitation at -30°C. The high current resulting in temperature increasing may cause an unstable anodic film deposition. Nb^{5+} is suggested to be the mass transport species during EP at limiting current.

References

1. D. Landolt, Electrochim. Acta **32**, 1 (1987).
2. D. Landolt, R. Muller, and C. Tobias, J. Electrochem. Soc. **116**, 1384 (1968).
3. D. Landolt, R. Muller, and C. Tobias, Fundamentals of Electrochemical Machining, The Electrochemical Soc. Princeton, NJ (1971).
4. M. Datta and D. Landolt, J. Electrochem. Soc. **122**, 1466 (1977).
5. M. Datta and D. Landolt, J. Appl. Electrochem. **7**, 247 (1977).
6. M. Datta and D. Landolt, Electrochim. Acta **25**, 1263 (1980).
7. M. Matlosz, S. Magaino, and D. Landolt, J. Electrochem. Soc. **141**, 410 (1994).
8. O. Piotrowski, C. Mafdore, and D. Landlt, Electrochim. Acta **44**, 3389 (1999).
9. O. Piotrowski, C. Mafdore, and D. Landlt, Plat. Surf. Finish. **85**, 115 (1998).
10. O. Piotrowski, C. Mafdore, and D. Landlt, J. Electrochem. Soc. **145**, 2362 (1998).
11. R. Grimn, and D. Landolt, Corro. Sci. **36**, 1847 (1994).
12. http://www.solartronanalytical.com/technicalsupport/technicalnotes/technote06.htm
13. H. Tian, Surface study of niobium for superconducting radio frequency (SRF) accelerators, PhD dissertation, College of William and Mary, (2008).
14. M. Matlosz, Electrochim. Acta **40**, 393 (1995).
15. R. Grimn, A. West, and D. Landolt, J. Electrochem. Soc. **139**, 1622 (1992).
16. H. Tian, S. Corcoran, C. Reece, and M. Kelley, J. Electrochem. Soc. **155**, D563 (2008).
17. S. Magaino, M. Maltosz, and D. Landolt, J. Electrochem. Soc. **140**, 1365 (1993).

Chapter 6

Conclusions and suggestions for future work

6.1 Conclusions

As a conclusion, in this dissertation project electropolishing (EP) of niobium (Nb) in sulfuric acid-methanol electrolytes was successfully performed in the electrochemical cell of both two-electrode setup and three-electrode setups. The surface finish is at least comparable to that obtained by HF-based BCP and EP. Nb surfaces electropolished under multiple conditions present a roughness of order of a few hundred nanometers at the macroscopic scale and a strong grain boundary elimination at microscopic scale. The surface characterization shows that temperature is the most critical parameter leading to condition of microsmoothing. Electrolyte concentration and EP duration also improve the Nb surface finish. Thickness etching of 100 μm is enough to remove the mechanically damaged layer and improves the Nb surface quality. The mechanism investigation indicates the presence of a compact film during EP. A transfer from a film-free surface to an anodic film deposition with decreasing temperature is also observed. Nb^{5+} ions are determined to be the mass transport limiting species. Microsmoothing of Nb surface is only achieved under the mass transport of Nb^{5+} through the compact film under the high-

field solid state conduction. So far it is still difficult to distinguish the two-electrode setup from the three-electrode setup only by surface finish, but the results indicate that EP is feasible in both types of setup. People may refer to the two-electrode setup for practical fabrication of Nb cavities and refer to the three-electrode setup for experimental understanding of HF-free EP

6.2 Suggested future work

Future works can be performed by focusing on the following directions:

Surface chemistry is an important characterization of the polished Nb surface, because oxides forming on the Nb surface strongly impact the cavity performance [1]. X-ray photonic spectroscopy (XPS) is a powerful technique to probe the near-surface composition and oxide depth. Application of XPS on surface chemistry characterization is easy to found in the literature [2-5]. The investigation of surface chemistry of electropolished Nb surface by XPS should be a complementary understanding of the methanol-based EP process of Nb.

Rotating disk electrode (RDE) modifies the material diffusion during EP. Many researchers have employed RDE in their examinations of EP process [6, 7]. Piotrowski observed that increasing rotation rate could result in improved surface finish [6]. Further, the Nb cavity is also rotated in practical fabrication [8, 9]. The linear relationship between the reciprocal of the limiting current density and the reciprocal of the square root

of the rotation rate indicates that the current plateau is mass transport controlled [6]. It would be promising to try a rotating Nb working electrode under proper rotating rate for a better surface finish than in static state.

Combined conditions may result in a better surface finish. The electrochemical experiments present the dependence of corrosion rate and surface finish on electrolyte concentration and temperature. Further, the mechanism investigations show the transfer from a film-free surface to an anodic film precipitation with decreasing temperature. Microsmoothing is only achieved under mass transport control. The mechanism study on successful microsmoothing of Nb indicates the precipitation of a compact film through which the mass transport limiting species pass. The most efficient surface finish may be: first, sufficient thickness etching to remove the mechanically damaged layer; second, EP process by potential hold under a condition resulting in microsmoothing.

To realize a better surface finish by the methanol-based EP is only a part of the task to develop the HF-free electrolytes. To finish an Nb SRF cavity by the methanol-based EP resulting in a cavity performance comparable to or better than that obtained by the HF-based finish techniques will be the final goal.

References

1. H. Tian, Surface study of niobium for superconducting radio frequency (SRF) accelerators, PhD thesis, College of William and Mary (2008).
2. J. Halbritter, Surf. Interf. Anal. **12**, 354 (1998).
3. Q. Ma, and R. Rosenberg, Appl. Surf. Sci. **206**, 209 (2003).
4. Q. Ma, and R. Rosenberg, J. Appl. Phys. **96**, 7675 (2004).
5. M. Grindner, and J. Halbritter, J. Appl. Phys. **51**, 397 (1980).
6. O. Piotrowski, C. Madore, and D. Landolt, Electrochim. Acta **44**, 2289 (1999).
7. O. Piotrowski, C. Madore, and D. Landolt, J. Electrochem. Soc. **145**, 2362 (1998).
8. H. Diepers, O. Schmidt, H. Martens, and F. Sun, Phys. Lett. **37(A)**, 139 (1971).
9. K. Satio, Y. Kojina, T. Furuya, S. Mitsunobu, S. Noguchi, K. Hosoyama, T. Nalazato, T. Tajima, K. Asano, K. Inoue, Y. Lino, H. Nomura, and K. Takeuchi, Proceeding of 4^{th} of RF superconductivity, KEK, Tsukuba, Japan, p635 (1989).

Appendix A

Water content calculation

The maximum water content in sulfuric acid-methanol electrolytes is calculated by

$$WaterContent = \frac{\sum WaterWeight}{ElectrolyteWeight} \times 100\% .$$

The water contents come from sulfuric acid (98wt%) and methanol (99.9wt%).

For 1 liter x M sulfuric acid-methanol electrolyte, the weight of sulfuric acid can be calculated by:

$$W_{SufuricAcid} = 1l \times xM \times 98.08g/mol(MoleculeWeight) = 98.08xg .$$

Then the volume of sulfuric acid is:

$$V_{SulfuricAcid} = \frac{98.08g}{1.84g/cm^3(Density)} \approx 53.3xml .$$

The volume of methanol is:

$$V_{Methanol} = (1000 - 53.3x)ml .$$

The weight of methanol is:

$$W_{Methanol} = 0.792g/cm^3(Density) \times (1000 - 53.3x)ml = (792 - 42.2x)g$$

The water content in sulfuric acid and methanol is:

$Water_{SulfuricAcid} = 0.0192 \times 98.08xg = 1.883xg$,

and

$Water_{Methanol} = 0.001 \times (792 - 42.2x)g = (0.792 - 0.0422x)g$.

The water content in electrolyte is:

$$WaterContent = \frac{1.883x + 0.792 - 0.0422x}{98.08x + 792 - 42.2x} \times 100\% = \frac{79.2 + 184.08x}{792 + 55.88x}\% .$$

For example, for 1 M electrolyte, x = 1, the water content is 0.31wt%. Table A.1 lists the water content calculated for the 0.1 M, 0.5 M, 1 M, 2 M, and 3 M sulfuric acid-methanol electrolytes.

Table A.1: Water content calculated for the 0.1 M, 0.5 M, 1 M, 2 M, and 3 M sulfuric acid-methanol electrolytes.

Concentration (M)	Water content (wt%)
0.1	0.05
0.5	0.21
1	0.31
2	0.49
3	0.66

Appendix B

Solution volume estimation

The total mole of electrons passing through the electrolyte during EP can be calculated by

$$Mol(e^-) = \frac{i \times A \times t}{96500},$$

where i is the current density (A/cm^2), A is the electrode area (cm^2), t is the EP duration (s), and 96500 is the Faraday constant (C/mol). By assuming i = 1 A/cm^2, A = 0.5 cm^2, and t = 3600 s, the totally consumed electrons is calculated to be 1.865×10^{-2} mol. The total hydrogen ion number is also1.865×10^{-2} mol, and the total H_2SO_4 number is 9.325×10^{-3} mol. The necessary volumes of electrolyte for the concentrations of 0.1 M, 0.5 M, 1 M, 2 M, and 3 M are listed in table B.1. In practical EP, the electrolyte volume was about 300 ml.

Table B.1: Calculated electrolyte volume necessary for EP in each concentration.

Concentration	Minimum volume
0.1 M	93.25 ml
0.5 M	18.65 ml
1 M	9.325 ml
2 M	4.662 ml
3 M	3.108 ml

Appendix C

Electrolyte consideration: The influence of sulfuric acid hydration

Niobium (Nb) has a large negative free energy and is highly reactive toward oxygen [1-3]. In an aqueous solution, it is easy for Nb to react with water molecules to form non-soluble niobium pentoxide (Nb_2O_5) during electropolishing (EP) [3, 4]. Sulfuric acid-methanol electrolyte has a much-decreased water content, which reduces the possibility to form Nb_2O_5. However, the surface finish is sensitive to the water content in sulfuric acid-methanol electrolytes. The water content increase markedly reduces the current during EP. Piotrowski et al observed the current decrease by adding water into electrolyte during EP of titanium (Ti) [5]. When they added water into the 3 M sulfuric acid-methanol, the current decreased approximately 75 percent from 0.8 to 0.2 A/cm^2 as the water content increased from 0.02wt% to 5wt%. When the water content reached 10wt%, the Ti anode became passive and the current decreased to a very low value. It is then important to guarantee the electrolyte fresh for each EP process and prevent the water condensing for air during low temperature experiment. Since the hydration of sulfuric acid is thermodynamically favorable, it is also critical to conserve the sulfuric acid from absorbing water in the air.

Present authors observed the Nb anode passivation due to sulfuric acid absorbing water. Figure C.1 shows the current-voltage (C-V) data measured in electrolytes prepared by different sulfuric acid. The 0.1 M electrolyte was prepared by fresh sulfuric acid from newly-opened bottle while the other concentrations (0.5 M and 3 M) were prepared by old sulfuric acid from a bottle opened half-year ago and conserved without any extra protection. The voltage was scanned from 57 to 0 V at a rate of -0.1 V/s. The C-V data measured in the electrolyte prepared by fresh sulfuric acid (0.1 M) shows a linear relationship between current and voltage. The linear C-V relationship is consistent with an "active" status of Nb anode resulting at least surface etching. The C-V data measured in other concentrations prepared by old sulfuric acid show a very low current across the whole voltage range. This current behavior is identical to that observed by Piotrowski on the Ti EP in a water contaminated sulfuric acid-methanol electrolyte and is consistent with the anodic passivation [5]. High voltage such as 57 V did not break the passive layer.

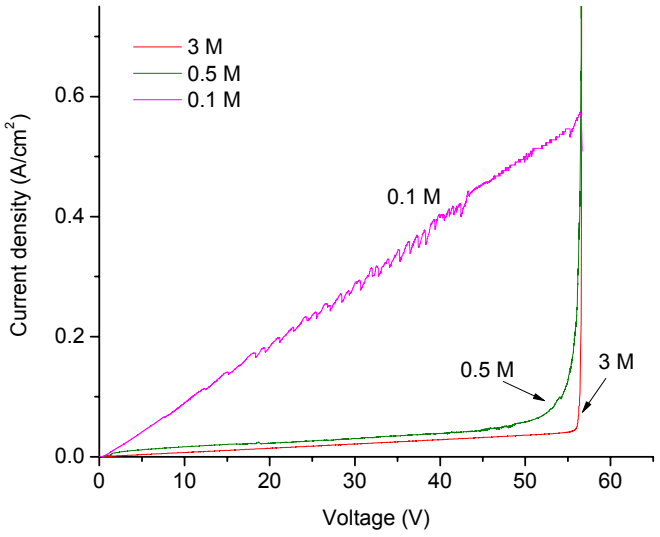

Figure C.1: Nb C-V data measured in the electrolytes prepared by fresh sulfuric acid (0.1 M) and old sulfuric acid (0.5 M and 3 M) at room temperature.

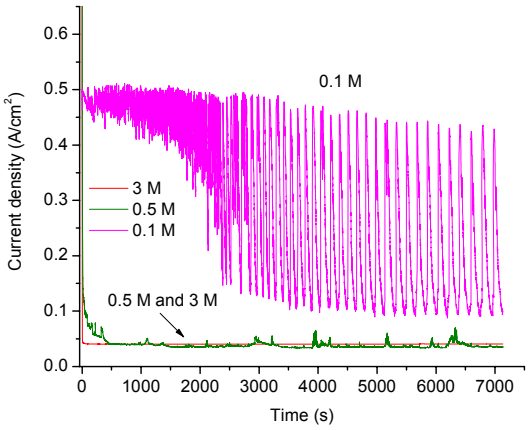

Figure C.2: Nb C-t curves measured during EP at 57 V for 2 h in the electrolytes prepared by fresh sulfuric acid (0.1 M) and old sulfuric acid (0.5 M and 3 M).

Figure C.2 shows the currents measured during the EP in all the concentrations at a voltage of 57 V for 2 h. The current measured during EP in the 0.1 M electrolyte has a high current value and shows a strong current oscillation. The current oscillation is related to the formation and dissolution of an anodic film [6]. The currents measured during EP in other concentrations are small and shows few oscillation. Furthermore, during the EP in electrolytes prepared by old sulfuric acid, white cover layers were observed to form on the anode. Figure C.3 (a) shows the optical image of the white cover layer after EP. The white cover layer is loss and easy to remove. Nb_2O_5 is the main composition as determined by x-ray photonic spectroscopy (XPS). Figures C.3 (b) and (c) show optical images of Nb surfaces under the white cover layer. The surface polished in the 3 M electrolyte (figure C.3 (b)) shows no surface etching and is covered by a compact passive film. The surface polished in the 0.5 M electrolyte (figure C.3 (c)) is also mainly passive, but pitting corrosion is observed as indicated by the arrow. In the contrast, the surface polished in the 0.1 M electrolyte (figure C.3 (d)) shows no cover layer but clean

grain faucets and clear boundaries. The anode polished in the 0.1 M electrolyte was "active" and finally resulted in a surface etching.

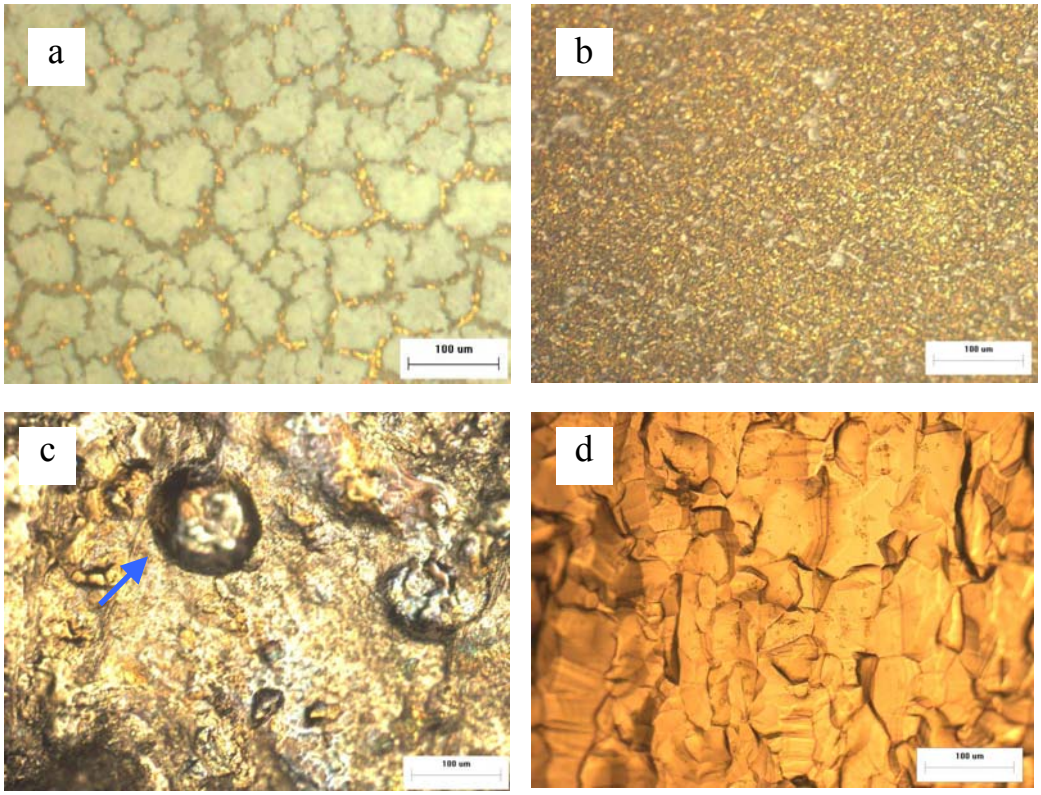

Figure C.3: Optical images of (a) white cover layer, (b) surface under the cover layer polished in the 3 M sulfuric acid-methanol electrolyte prepared by old sulfuric acid, (c) surface under the cover layer polished in the 0.5 M sulfuric acid-methanol electrolyte prepared by old sulfuric acid, and (d) surface under the cover layer polished in the 0.1 M sulfuric acid-methanol electrolyte prepared by fresh sulfuric acid.

The precise water content in the electrolytes causing passivation was not measured, but it is obvious that the water absorption occurred during the conservation. The increase of water molecules resulted in the formation of Nb_2O_5 preventing further polishing. To keep water content from electrolytes as much as possible is an essential requirement for successful EP. In this dissertation project, sulfuric acid of high concentration (98%) was

used. The bottle was small (500 ml) to reduce the conservation time. Each EP process was performed in a fresh electrolyte. A Teflon cover was fabricated to seal the cell during low temperature experiments. According the EP results, passivation due to the water contamination was no longer observed. High concentration resulted in a better surface finish.

Reference

1. Arsova, A. Prusi, T. Grcev, and L. Arsov, J. Serb. Chem, Soc. **71**, 177 (2006).
2. Q. Ma, and R. Rosenberg, Proceeding of the 2001 particle accelerator conference, Piscataway, NJ, 2, p1050 (2001).
3. A. Dacca, G. Gemme, L. Mattera, and R. Parodi, Appl. Surf. Sci. **126**, 219 (1998).
4. H. Tian, Surface study of niobium for superconducting radio frequency (SRF) accelerators, PhD thesis, College of William and Mary (2008).
5. O. Piotrowski, C. Madore, and D. Landolt, J. Electrochem. Soc. **145**, 2362 (1998).
6. K. Satio, Proceeding of the 2003 particle accelerator conference, Portland, OR USA, p462 (2002).